IOWA STATE UNIVERSITY
Digital Repository

1999

Inductively coupled plasma mass spectrometry for stable isotope metabolic tracer studies of living systems

Elise Tuy Luong
Iowa State University

Follow this and additional works at: https://lib.dr.iastate.edu/rtd

 Part of the Analytical Chemistry Commons, and the Biochemistry Commons

INFORMATION TO USERS

Inductively coupled plasma mass spectrometry for stable isotope metabolic

tracer studies of living systems

by

Elise Tuy Luong

A dissertation submitted to the graduate faculty

in partial fulfillment of the requirements for the degree of

DOCTOR OF PHILOSOPHY

Major: Analytical Chemistry

Major Professor: Robert S. Houk

Iowa State University

Ames, Iowa

1999

UMI Number: 9924742

UMI

300 North Zeeb Road
Ann Arbor, MI 48103

Graduate College

Iowa State University

This is to certify that the Doctoral dissertation of

Elise Tuy Luong

has met the dissertation requirements of Iowa State University

Signature was redacted for privacy.

Committee Member

Signature was redacted for privacy.

Committee Member

Signature was redacted for privacy.

Committee Member

Signature was redacted for privacy.

Committee Member

Signature was redacted for privacy.

Major Professor

Signature was redacted for privacy.

For the Major Program

Signature was redacted for privacy.

For the Graduate College

TABLE OF CONTENTS

CHAPTER 4. METHODS FOR IMPROVING ION TRANSMISSION AND PRECISION DURING ISOTOPE RATIO MEASUREMENTS WITH THE INDUCTIVELY COUPLED PLASMA TWIN QUADRUPOLE MASS SPECTROMETER 123

LIST OF FIGURES

CHAPTER 3. SIGNAL IMPROVEMENT AND ^{13}C : ^{12}C RATIO DETERMINATION IN AMINO ACIDS, PROTEINS, AND OLIGOSACCHARIDES WITH AN INDUCTIVELY COUPLED PLASMA TWIN QUADRUPOLE MASS SPECTROMETER

CHAPTER 4. METHODS FOR IMPROVING ION TRANSMISSION AND PRECISION DURING ISOTOPE RATIO MEASUREMENTS WITH THE INDUCTIVELY COUPLED PLASMA TWIN QUADRUPOLE MASS SPECTROMETER

LIST OF TABLES

CHAPTER 4. METHODS FOR IMPROVING ION TRANSMISSION AND PRECISION DURING ISOTOPE RATIO MEASUREMENTS WITH THE INDUCTIVELY COUPLED PLASMA TWIN QUADRUPOLE MASS SPECTROMETER

ABSTRACT

Sub-nanogram per gram levels of molybdenum (Mo) from human blood plasma are isolated by the use of anion exchange alumina microcolumns. Million-fold more concentrated spectral and matrix interferences such as sodium, chloride, sulfate, phosphate, etc. in the blood constituents are removed from the analyte. The recovery of Mo from the alumina column is $82 \pm 5\%$ (n = 5). Isotope dilution inductively coupled plasma mass spectrometry (ID-ICP-MS) is utilized for the quantitative ultra-trace concentration determination of Mo in bovine and human blood samples. The average Mo concentration in reference bovine serum determined by our method is 10.2 ± 0.4 ng/g, while the certified value is 11.5 ± 1.1 ng/g (95% confidence interval). The Mo concentration of one pool of human blood plasma from two healthy male donors is 0.5 ± 0.1 ng/g.

The inductively coupled plasma twin quadrupole mass spectrometer (ICP-TQMS) is used to measure the carbon isotope ratio from non-volatile organic compounds and bio-organic molecules to assess the ability as an alternative analytical method to gas chromatography combustion isotope ratio mass spectrometry (GC-combustion-IRMS). Trytophan, myoglobin, and β-cyclodextrin are chosen for the study, initial observation of spectral interference of $^{13}C^+$ with $^{12}C^1H^+$ comes from the incomplete dissociation of myoglobin and / or β-cyclodextrin. The interference species is most sensitive to the aerosol gas flow rate. Carefully decreasing this parameter can eliminate $^{12}C^1H^+$ interference. $^{13}C/^{12}C$ ratios in myoglobin and β-cyclodextrin can be determined precisely and quantitatively. The

best relative standard deviation (RSD%) obtained in the $^{13}C/^{12}C$ study is 0.91%, which is close to the limiting precision predicted by counting statistics (1.16%).

Many improvements have been made to the current ICP-TQMS device. A new skimmer interface together with the new ion optics arrangement improves the ion collection efficiency 19-fold. A second-generation ion beam splitter has been designed to reduce the background count rate and improve the ion transmission. A modified ion beam splitter transmits 5 times more ions while maintaining the performance characteristics of the ICP-TQMS system. The precision is further improved by measuring each data point for a longer dwell time (9s instead of 1.5s) and keeping the total ion collection time low ($\leq$ 50s instead of 150s).

CHAPTER 1. GENERAL INTRODUCTION

Historical perspective of the inductively coupled plasma

Science and technology are advancing ceaselessly since the creation of mankind. From the discovery of a simple element to deciphering the origin of the universe, chemistry today is scarcely recognizable as the subject that chemists knew a century ago. From the ancient gravimetric analysis of grams of sample to the modern spectrometric determination of 10^{-9} grams of unknown, what once seemed beyond reason now defines the frontier of science. Advancement in analytical chemistry has led to significant progression in biotechnology and vice versa. With the aid of the computer engineering today, biochemists are able to pinpoint the location of a mutant base pair of a gene. Scientists in all fields are working together for the ultimate goal of unlocking the secret of life. Traditionally, the analytical chemist is the one that carries the burden of constantly developing new and improving techniques for qualitative and quantitative determinations of substances that are found on our planet Earth and in outer space. One of the milestones of modern science is the development of the inductively coupled plasma mass spectrometry, the prime candidate for trace and ultra-trace analyses.

This dissertation focuses on the development of methods for stable isotope metabolic tracer studies in living systems using inductively coupled plasma single and dual quadrupole mass spectrometers.

The origin of the inductively coupled plasma (ICP) can be dated back as far as nearly 60 years ago. The first atmospheric pressure ICP was invented by a Russian Physicist who

resided in Leningrad (now Saint Petersburg) during the dark age of the human society [1]. During World War II, the ICP researches were hindered by the lack of electricity, which is the vital ingredient for generating the inductively coupled plasma. This infant ICP had stopped and remained undeveloped for nearly two decades. Not until the early 1960's, Reed continued the development of the atmospheric ICP [2, 3]. Reed also described many of the physical properties of this plasma and suggested its possible application as a spectral source for solids [4]. Later, a group of American and British scientists led by Fassel at Iowa State University in the United States, and by Greenfield at Albright and Wilson Ltd. in England studied the ICP as an analytical emission source [5-7]. It was Fassel and co-workers who were responsible for the complete development and maturing of this fiery plasma [8, 9].

Inductively coupled plasma spectrometry

At the time this new atomic emission ionization source was ready to be introduced to the world, ICP had to compete with the contemporary flame atomic absorption spectrometry (AAS) that was expanding exponentially and gaining worldwide acceptance as an analytical tool [10-15]. Meanwhile, the established arc source atomic emission spectrometry (AES) was declining in general usage. The combination of the growing AAS and the declining of AES had established the conditions for the ICP source being less accepted by the scientific community. Not until 1975 was the first commercial ICP spectrometer born. Since then, the ICP-AES has become the most common technique for routine multi-elemental analyses [9, 16, 17]. At the same time, the analytical capability of the ICP continued to be explored as an ionization source for mass spectrometry. Houk and co-workers obtained the first analytical

mass spectra from an ICP in 1978 [18]. Five years later, Sciex launched the first commercial quadrupole based ICP-MS instrument, which stimulated the growth of interest in the technique. Since then, ICP-MS has gained world wide recognition as one of the most complete and versatile analytical technique for elemental determinations and isotopic analyses in geochemistry [19, 20], semiconductor industry [21, 22], environmental chemistry [23, 24], clinical chemistry [25, 26], and nuclear chemistry [27].

ICP-MS system

In general, the ICP-MS system consists of five parts: the sample introduction system, the ICP ionization source, the ICP-MS interface, the mass analyzer, and the electronics (including the detector, computer and data collection and processing). Gas samples can be directly introduced into the ICP, whereas solution and solid samples are introduced as fine aerosols and fine particles. There are a variety of sample introduction techniques for both cases.

Solution samples

Solution samples are usually introduced to the ICP as aerosols. Several types of nebulizers have been used to produce the fine mists. The standard nebulizer is the pneumatic type [28], which produces aerosol by shattering the liquid stream as it leaving the tiny tip of the quartz tube with a fast flowing gas stream on the outer concentric tube. The pneumatic type nebulizer produces primary aerosols with a wide droplet size distribution (diameter from 2 to 40μm) [29]. The larger aerosol droplets are removed as they pass through the spray chamber. A double pass Scott type spray chamber is normally used for this purpose [30].

The secondary aerosols are then sent to the ICP for desolvation, vaporization, dissociation, atomization, ionization, and excitation. An ultrasonic nebulizer (USN) in conjunction with a conical spray chamber has also been widely used for generating solution aerosol [31]. In more recent times, the USN system is usually equipped with a desolvating and condensing system to remove most of the solvent. The tertiary aerosol produced by the USN has a narrow aerosol size distribution with 90% of the droplets with only 5 μm diameter [32, 33]. A Babington type nebulizer is designed specially for a solution with high solid contents to avoid clogging [34]. There are other types of nebulizers specifically used for low flow nebulization of effluent that comes out of a HPLC or CE column. These include the microconcentric nebulizer (MCN) [35], direct injection nebulization (DIN) [36, 37], microflow ultrasonic nebulization (m-USN) [38], high efficiency nebulization (HEN) [39], and electrospray nebulization (ESP) [40-42]. Recently, Brown developed a low flow nebulizer known as the oscillating capillary nebulizer (OCN) with nebulizer efficiency of 100% [43]. Other less commonly used nebulizers and spray chambers are discussed in reference 44-46.

Recently, the monodisperse dried microparticulate injector (MDMI) developed by French is used to inject a single liquid droplet with diameter of ~ 40 μm to the ionization source [47]. This type of sample introduction technique is used mainly for the study of matrix effects [48-50] and will be discussed later. Finally, electrothermal vaporization, which was developed for atomic absorption spectrometry, can also be used as an alternative sample introduction technique for ICP-MS [51, 52].

Solid samples

Solid sample can be introduced to the ICP by several techniques: laser ablation [53-55], arc or spark nebulization [56, 57], and direct sample insertion [58, 59]. Slurry nebulization of fine particles has recently been used for geological samples [60]. Solid sample introduction has several advantages, including the reduction in analysis time because of no need for sample dissolution. Furthermore, spatial information can be achieved if laser ablation is used. However, the major drawback of direct solid sample analysis is the lack of matrix matched standard materials, making quantification difficult.

ICP operation

An ICP is a weakly ionized plasma. Physicists have described plasma as the fourth state of matter. The simplest definition of plasma is gases of ionized atoms and molecules. More precisely, plasmas are ensembles of charged particles interacting with one another through coulombic forces. Strong electric forces attracting opposite charges in the plasma provide its quasineutrality. Plasmas behave like fluids. They can flow, they follow physical boundaries, they carry waves, and they react with electric and magnetic fields in many ways.

The inductively coupled argon plasma is energized by a high frequency electromagnetic field. The allowable operating frequency is 27 or 40 MHz with power output from 700 to 1500 Watts. Figure 1 shows the cross section of the ICP torch and the load coil surrounding it. The ICP torch consists of three concentric quartz tubes. The outer gas (usually argon) flows tangentially and spirals between the outer and the middle tubes with flow rate of ~ 15 L / min. This outer flow is the main supporting gas for the plasma and also acts as the cooling gas for the outer quartz tube. A second argon flow is known as the makeup
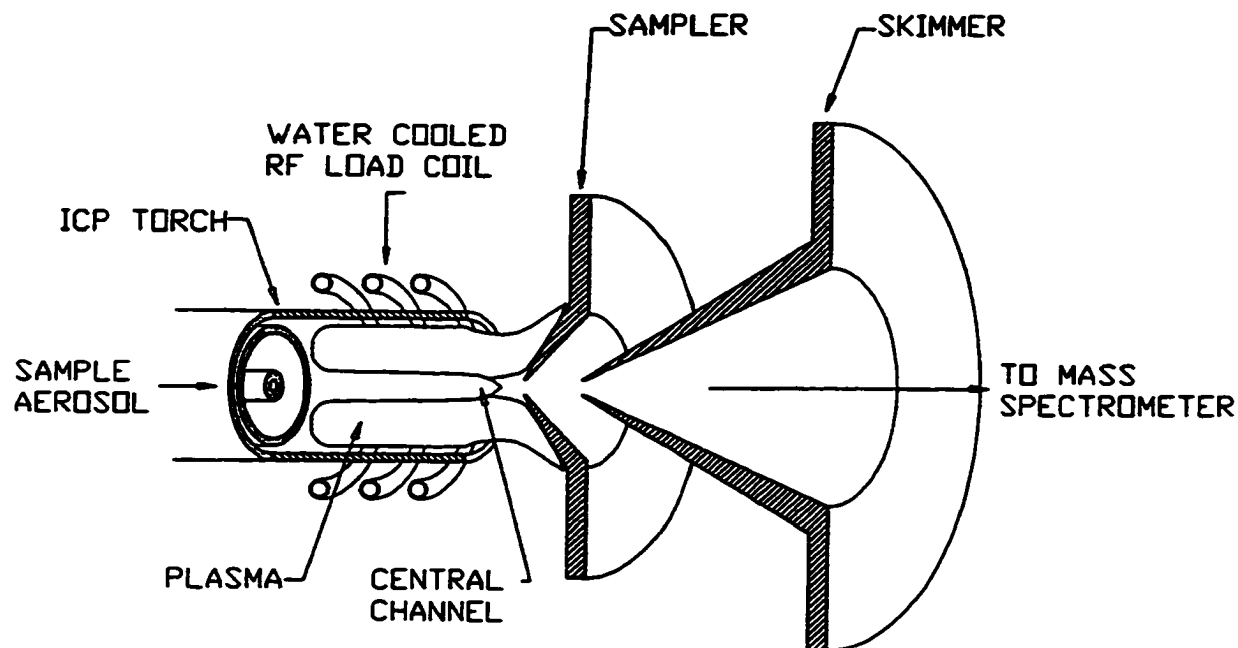
Figure 1. Schematic diagram of the ICP torch and ICP-MS interface [61].

or auxiliary flow with a flow rate of ~ 1 L / min. and flows between the outer and the middle tube. This makeup flow keeps the hot argon plasma away from the tip of the central tube known as the injection tube, and protects it from melting. A third argon flow called the nebulizer gas flow or aerosol gas flow, punches a hole through the hot plasma to form a relatively cool region known as the axial channel and carries aerosols from the sample introduction system to the ICP. The flow rate of this third flow is ~ 1 L / min. The relatively cool axial channel confines the sample aerosols in the central channel and improves the ion extraction efficiency at the ICP-MS interface [62-69]. Since the sample aerosols travel through the central channel well separated from the induction region, the basic electrical processes that sustain the plasma are not overly sensitive to the changes of sample composition.

The argon-ICP produces mostly singly charged species. The exact mechanism of ionization in the ICP is not known. However, there are at least three processes responsible for the ionization.

Electron impact

The most effective pathway for the production of charged particles is the result of collisions between electrons and atoms or molecules.

$$A + e^-_{fast} \rightarrow A^+ + 2e^-_{slow}$$
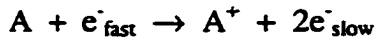
Penning ionization

The Penning process involves the production of a free electron via the collision of excited atom (A*) with atom or molecule (B) provided the excitation energy of A is greater than the ionization potential of B.

$$A^* + B \rightarrow A + B^+ + e^-$$

Non-resonant charge transfer reaction

The ionized species A^+ in a higher energy state collides with the species B in a lower energy state to produce the ionized excited B^{+*} and the neutral lower energy species A. Energy is thus transferred from A^+ to B. The process is highly selective, the two energy levels of the A^+ and the B^{+*} have to be closely matched ($\pm$ 0.5 eV), and the energy difference between B^{+*} and B should not be greater than the energy difference between A^+ and A [70]. The whole process can be summarized as follow.

$$A^+ + B \rightarrow A + B^{+*}$$
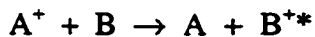
There are other reactions between atoms and ions occurring at the same time in the plasma such as resonance charge transfer, excitation of atomic level by electron impact, second ionization reactions.

ICP-MS interface

The ICP-MS interface provides the means of extracting the positive ions from the ICP into the mass analyzer. Differential pumping is used to reduce the pressure from 760 Torr to ~ 10^{-5} Torr. The sampler and skimmer serve as the first and second differential pumping orifices as well as the ion extraction media [71] [Figure 1]. The pressure behind the sampler is ~ 1 to 2 Torr. A supersonic free jet expansion is formed behind the sampler and terminated at the Mach disk as the extracted beam collides with the background gases. The skimmer is usually positioned at ~ 1/2 to 2/3 the distance downstream from the sampler orifice to the onset of the Mach disk for optimum ion extraction [72]. Somewhere behind the skimmer, the quasineutrality of the beam breaks down and electrons are lost. Now the beam is composed mainly of positive ions (detailed description of the ion extraction process is given in reference 73). The skimmed beam is then focused and guided by a series of ion optics to the third pressure stage (~ 10^{-5} Torr) that houses the mass analyzer which differentiates ions by their different m/z values.

Mass spectrometer

The quadrupole is the most widely used mass spectrometer in conjunction with the ICP owing to its strong focusing properties, robustness, simplicity, ease in operation, high performance to cost ratio, and tolerance to moderate pressure environments (~ 10^{-5}) [74-77].

A quadrupole mass analyzer is composed of four metal rods. Opposite pairs are connected together, and dc and rf potentials are applied to each pair in opposite sign and phase. For simplicity, the trajectory and stability of the ion motion inside the quadrupole can best be described with the stability diagram [Figure 2] where
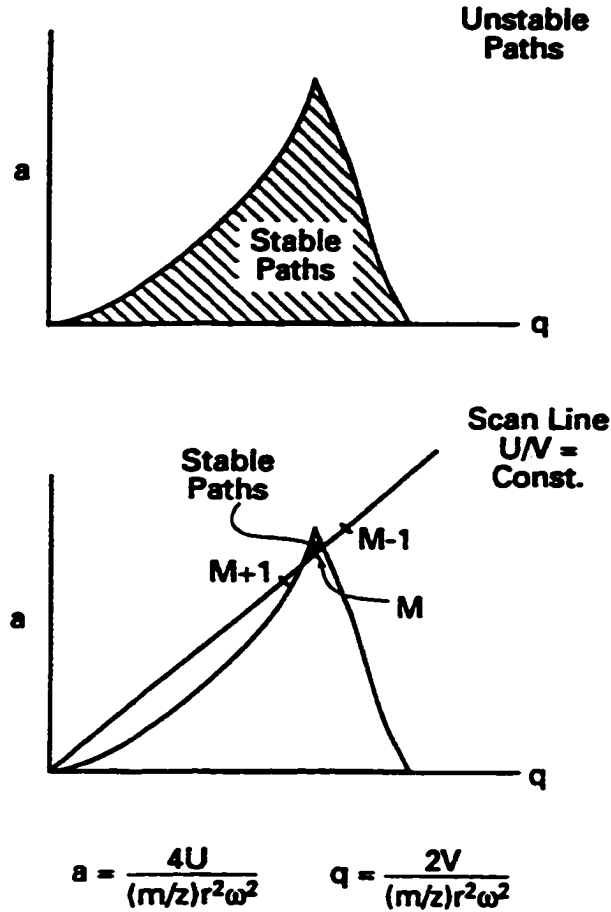
Figure 2. The a-q stability diagram [63].

$$a = 4zU/m\omega^2 r_0^2 \qquad (1)$$

$$q = 2zV/m\omega^2 r_0^2 \qquad (2)$$

U is the applied dc voltage, V is the applied rf amplitude and m is the mass of the ion. For a given set of rods, ω (angular frequency $2\pi f$) and r_0 (distance from the central axis to the rod) are constant, hence, $a \sim U/(m/z)$ and $q \sim V/(m/z)$. As seen from Figure 2, varying the slope of the scan line (changing the a/q ratio) changes the resolution, whereas changing the values of U and V while keeping the a/q ratio constant transmits ions of different m/z value. Scanning or changing the resolution is done solely electronically.

Other mass spectrometers have also been employed with ICP such as the ion trap [78, 79], time of flight [80, 81], double focusing magnetic sector [82-86], and the ion cyclotron resonance cell [87].

Ion detection

Different types of detectors have been used for ion detection in ICP-MS such as the Daly detector [88], Channeltron electron multiplier [89], and now the discrete dynode type detectors [90] are used in most instruments. The Faraday cup detector with no gain mechanism has also been used [91]. Recently, the active film discrete dynode electron multiplier is becoming popular for its better gain stability and longer operating life, larger linear dynamic range, and tolerance to higher-pressure environment than the other detectors [92].

Analytical applications of ICP-MS

ICP-MS offers outstanding linear dynamic range (at least 6 to 8 orders of magnitude), low concentration detection limits (sub-part per trillion) for a wide range of elements, fast multi-elemental determination, and good precision in isotope ratio measurements [63]. The analytical application of ICP-MS is immense, especially in trace and ultra-trace analyses of geological, clinical, environmental samples, as the result of the striking features of the technique. There are hundreds of publications using ICP-MS as an analytical tool for routine elemental determinations and isotopic analyses. It is not feasible to name them all, only a few representative reviews are included in the references at the end of this dissertation [63, 93, 94].

Problems of ICP-MS

Despite the numerous advantages offered by ICP-MS, it is somewhat susceptible to spectral interference and non-spectral interference or matrix effects.

Spectral interference

Spectral interference arises from the spectral overlap of two or more ions sharing the same nominal mass. For examples, $^{40}Ar^+$, $^{40}K^+$, and $^{24}Mg^{16}O^+$ interfere with $^{40}Ca^+$; $^{40}Ar^{35}Cl^+$, $^{150}Nd^{+2}$, $^{150}Sm^{+2}$ interfere with $^{75}As^+$; $^{40}Ar^{16}O^+$, $^{40}Ca^{16}O^+$ interfere with $^{56}Fe^+$. A complete list of possible spectral interferences can be found in references 95-97.

Methods for attenuating the formation of metal oxide (one of the interference species) include altering the plasma operating conditions (forward power, aerosol gas flow rate, sampling position, etc.) [63, 98, 99], and adding certain molecular (N_2, H_2) or noble gases (Xe) to the central channel [100, 101].

Another method includes the use of a high-resolution mass spectrometer to solve the spectral interference problems. For example, Begerow and Dunemann used a high-resolution ICP-MS to determine Pd and Rh from human blood [102]. The determination of Pd and Rh using a quadrupole at standard operating conditions is impaired by spectral interferences of Cd^+, Pb^{+2}, RbO^+, SrO^+, $CuAr^+$, and $ZnAr^+$. However, even when the magnetic sector was operating at a resolution of $m/\Delta m = 7500$, it is still not sufficient to separate Pd and Rh from all spectral overlaps. Jiang et al. [103], Nonose [104], Sakata [105] and Tanner [106] have explored the possibility of operating the plasma under a "cooler" condition to attenuate some of the polyatomic interferences. When the plasma is kept cooled by increasing the aerosol gas flow rate and decreasing the rf power, troublesome background ions Ar^+, ArH^+ and ArO^+

are removed, the background mass spectrum is simplified dramatically [105]. However, polyatomic ions NO^+, O_2^+ and/or H_3O^+ still remain in the background spectrum. Other researchers have explored the use of helium plasma instead of argon plasma [107-109]. For some reason, though, the He ICP is much harder to operate than the Ar ICP. Cryogenic removal of organic solvents to attenuate certain polyatomic ions has also been performed [110]. Lastly, the best way to eliminate the problem is to employ chromatographic separation techniques to isolate the analyte from the interference species.

Non-spectral interference or matrix effects

Matrix effects arise from the change in analyte signal caused by the change in concentration of matrix elements. Normally, as the concentration of the matrix element increases, the analyte signal decreases. This interference is known as matrix-induced signal suppression [101-115]. In some cases, matrix induced analyte signal enhancement is also observed [116]. ICP mass spectrometrists have come a long way in studying and understanding matrix effects [117]. A common conclusion is that matrix effects are most severe when the analyte is light (such as lithium) and the matrix is heavy (such as lead). Researchers are now convinced that many aspects of the observed matrix effects phenomenon are attributed mainly to the space charge effect. Space charge effect is the coulombic repulsion of like charges when the ion current exceeds the space charge limiting current [73, 98, 118, 119]. The contribution of space charge to matrix effects was first proposed by Gillson et al. in 1988 [118] and later by Tanner [98], Li et al. [119], and Chen and Houk [117]. Matrix effects have been studied by spatial-resolved and time-resolved methods. The former one involves the deposition of ions onto a target [117, 120], and the

later involves using monodisperse dried microparticlutate injector and laser fluorescence techniques to observe the temporal signal of the light analyte (Li^+) in the present of a heavy matrix (Pb^+) [48-50]. Allen et al. has also used the same sample introduction technique to study the matrix effect in their ICP-twin quadrupole system [121]. There are numerous ways to attenuate or correct for matrix effects. These are optimization of instrument parameters and ion optics, internal standardization, isotope dilution, other calibration methods, chromatographic separation of analyte from the matrix elements, and chemical vapor generation.

Optimization of instrumental parameters and ion optics

Wang and Caruso et al. [122, 123], and Marshall and Frank [124] successfully alleviated matrix effects by optimizing instrumental parameter such as rf forward power, aerosol gas flow rate, ICP sampling position, and etc. Evans and Caruso [125], Hu and Houk [126], Ross and Hieftje [127], Vaughan and Horlick [128], Chen and Houk [117], and Tanner [98] alleviated matrix effects by manipulating the ion lenses potentials. Beauchemin et al. added N_2 gas to the outer plasma flow to reduce the matrix suppression [129-131].

Internal standardization

An internal standard can compensate for matrix effects, instrumental instability and signal drift. Munro et al. first applied the technique to ICP-MS [132]. A variety of internal standard elements that span the whole periodic table are often employed [133-137]. For example, ^9Be, ^{59}Co, ^{115}In, and ^{205}Tl are common internal standards. This method requires the properties (both atomic mass and ionization potential) of the internal standard to closely match that of the analyte. This is often the limiting factor, which leads to a more sophisticated type of calibration method, which is discussed below.

Isotope dilution

Isotope dilution is the most powerful calibration method for elemental quantitative determination in conjunction with ICP-MS [138]. It is the ideal form of the internal standardization method. This technique is often used in the nuclear industry and isotope geology [139]. In 1969, the National Bureau of Standards (now the National Institute of Standards and Technology) first applied isotope dilution mass spectrometry (ID-MS) to certify a Standard Reference Material and to resolve a discrepancy between two analytical methods [140].

The isotope dilution method is based on the measurement of the change in ratio of two selected isotopes after one was enriched with a known amount of standard. If the element to be determined in the sample has two or more isotopes (e.g. vanadium-50 and vanadium-51), the more abundant isotope is often chosen to be the reference isotope (^{51}V), and the less abundant isotope is used as the spiked isotope (^{50}V). Assuming the vanadium in the sample is at natural abundance, then the ratio of $^{50}V / {}^{51}V$ in the original unspiked sample is the same as the natural abundance ratio (0.0025 / 0.9975). After the sample is spiked with a standard of known weight and known concentration of vanadium as well as known $^{50}V / {}^{51}V$ ratio (e.g. 0.56468) or known atom fraction, the altered $^{50}V / {}^{51}V$ ratio is measured by ICP-MS. The measured $^{50}V/{}^{51}V$ ratio can be expressed mathematically in terms of the weight (W), atom fraction (A for ^{50}V, B for ^{51}V), and concentration of the original (C_x) and spiked samples (C_s).

$$R_m = (A_x C_x W_x + A_s C_s W_s) / (B_x C_x W_x + B_s C_s W_s)$$

Since every term in the expression is known except C_x, the original concentration of vanadium can be calculated.

The advantages of isotope dilution are: First, it can compensate for partial loss of the analyte during sample preparation. Second, it is immune to a wide variety of physical and chemical interferences because the two selected isotopes are from the same element. Any physical or chemical interference on one will have to same effect on the other, causing the effects to be cancelled out in the ratio measurement.

The disadvantages of isotope dilution are: First, the method is not applicable to mono-isotopic elements. Second, not all of the enriched isotopes are available. Third, the enriched isotope is usually costly. Fourth, the method is very time consuming for routine analysis.

Other calibration methods

Chen and Houk utilized the strong polyatomic ions as internal standards for matrix corrections in ICP-MS [117]. This is based on the fact that the signals of the polyatomic ions are suppressed by the matrix to the same extent as the analyte ion signals at nearby m/z values. For example, $^{14}N_2^+$ can be used as internal standard for $^{24}Mg^+$, and similarly, $^{35}Cl^{16}O^+$ for $^{55}Mn^+$, $^{40}Ar^{16}O^+$ for $^{59}Co^+$, $^{32}S^{16}O^+$ for $^{45}Sc^+$, $^{40}Ar_2^+$ for $^{75}As^+$, and $^{89}Y^{16}O^+$ for $^{103}Rh^+$. Traditionally, the standard addition method has been used to overcome the matrix effects in ICP-MS [141-143].

Chromatographic separation of analyte from the matrix elements

This is by far the most effective way to separate the analyte from the matrix interferences in order to obtain accurate and precise quantitative information of the elements. Much of the emphasis has been placed on rapid and direct analysis with minimal sample preparation. The analytical capability of the ICP-MS is degraded as a result of untreated samples with high solid contents. Chemical separations can indeed improve the detection limit of the system. It can also improve the precision and accuracy of the measurements

[144-147]. The following are some examples of sample cleanup with the aid of liquid chromatography.

Beauchemin and McLaren et al. [141, 146, 148], and Orians [149] utilized silica-immobilized 8-hydroxyquinoline to preconcentrate trace metals from sea water to remove matrix interferences and improve the detection limit as great as 7-fold. Miyazaki used Chelex-100 to preconcentrate lead for isotope ratio determination [150]. Jarvis et al. employed a commercially available ion chelation system (cellulose-immobilized ethylenediaminetriacetic acid) for the separation of many transition and rare earth metals from a sea water matrix [151].

Size exclusion chromatography has also been used to separate proteins containing metals [152]. HPLC and supercritical fluid chromatography can also be coupled with ICP-MS to separate organometalic compounds [153-160]. Recently, online capillary electrophoresis (CE) coupled to the ICP-MS has been explored [161, 162]. The high resolution of CE offers significant advantages for the determination of chemical speciation in complex mixtures. Finally, cryofocusing GC-ICP-MS systems have been described by many workers for the determination of selenite, organometallic and organometalloid species in river and harbor sediments [163].

Chemical vapor generation

Hydride generation continues to dominate the field of chemical vaporization. Environmental analysis appears to be the primary motivation for the continuing development of hydride generation. Geological applications are the second motivation. Hydride generation is a very effective method to separate the analyte from the matrix components.

There are many publications in the field, but only some representative papers are given in the references [164-166].

Signal drift and instrumental instability in ICP-MS

Signal drift with time is another problem of the ICP-MS system at least for now. Several causes have been identified, which include temperature dependent fluctuations in the quadrupole power supply [93] and gradual solid deposition on the sampler orifice. By limiting the total solute levels < 0.1% the latter problem should be minimized. However, the former problem still remains. This indeed limits the analytical precision of the quadrupole instrument. Other factors limiting the precision are associated with the noise of the ICP-MS system. Because of instrumental instability and signal drift, fast peak hopping is preferred than mass scanning for isotope ratio measurements. Although the peak can be hopped for a very short time scale (~ 1 ms), the precision of isotope ratio measurement is still limited to ~ 0.05% to 0.1% relative standard deviation (RSD%) in the single quadrupole system.

Improving precision by simultaneous measurement of two signals

Warren and co-workers constructed an instrument several years ago called the inductively coupled plasma twin quadrupole mass spectrometer (ICP-TQMS) mainly for improving precision during isotope ratio measurement [167]. The extracted ion beam is split into two parts by an ion beam splitter (discussed in greater details in Chapter 3). Each part of the beam is sent to its own quadrupole for m/z filtering and its own detector. In this fashion, both beams experience nearly the same level of noise at any given time. Thus, the noise on

both sides is cancelled when the ratio of the two-m/z value is taken [168, 169]. In comparison with thermal ionization mass spectrometry (TIMS) [170-175], the long time champion in isotope ratio measurement, ICP-TQMS is attractive with its low operating cost, fast semi-quantitative multi-elemental determinations, and no time dependent isotopic fractionation. However, the peak profile generated by the quadrupole is far from "flat top" shape, which is always the case with the magnetic sector when operating at low resolution, whereas the problem associated with the TIMS method [165-170] mainly comes from the ionization source. Walder and co-workers has combined the best feature of ICP-TQMS and TIMS to generate a new instrument known as the multi-collector (MC) ICP-MS [83-85]. This instrument is capable of performing isotope ratio measurement with ultra high precision. In comparison with MC-ICP-MS, ICP-TQMS has the unique ability of measuring two m/z values far apart.

Dissertation objectives and organization

This dissertation consists of five chapters: The general introduction, three research manuscripts either published in or ready to submit to scientific journals, and the general conclusions. Each research manuscript has its own abstract, introduction, conclusion, acknowledgment, and references. The tables and figures in the manuscripts have their own numbering system. The references are formatted according to specifications of the corresponding journal.

Chapter 2 is a published scientific paper. This paper describes a novel chromatographic separation technique for the isolation and recovery of ultra-trace amounts of molybdenum

from human blood plasma for the quantitative concentration determination of Mo using isotope dilution ICP-MS. This method can be used for isotope tracer study and Mo in complex organic matrixes can be quantified.

Chapter 3 introduces to the world a future alternative analytical method to gas chromatography combustion mass spectrometry for carbon isotope ratio determination in non-volatile bio-organic molecules (amino acid, protein, and carbohydrate) with an inductively coupled plasma twin quadrupole mass spectrometer device. To the best of our knowledge, we are the pioneers in determining the ^{13}C / ^{12}C ratio using ICP as the ionization source. Chapter 3 also presents the ion collection efficiency of our home-built ICP-TQMS device which can be increased 14-fold if the first ion extraction lens is positioned ~ 1/2 to 2/3 from the skimmer orifice to the onset of the second Mach disk.

Chapter 4 provides several instrumental approaches for improving the ion collection efficiency of our elemental ICP-TQMS system. This includes designing a new ion beam splitter, the component responsible for splitting the ion beam into two parts to achieve simultaneous measurement of two individual m/z values. This chapter also contains the first detailed statistical report on the relationship between dwell time and total ion collection time and their influences on the precision of isotope ratio measurements of the ICP-TQMS system.

References

1.   Greefield, S. *Talanta*, 1976, *23*, 1-14.

2.   Reed, T. B. *Appl. Phys.* 1961, *32*, 821.

3. Reed, T. B. *Idem, ibid.* **1961**, *32*, 2534.

4. Reed, T. B. *Idem, International Science and Technology*, **1962**, 42.

5. Wendt, R. H. and Fassel, V. A. *Anal. Chem.* **1965**, *37*, 920-922.

6. Dickinson,G. W. and Fassel V. A. *Anal. Chem.* **1978**, *41*, 1021-1024.

7. Greenfield, S.; Jones, J. L. and Berry, C. T. *Analyst.* **1964**, *89*, 713-720.

8. Fassel, V. A. *Science.* **1978**, *202*, 183.

9. Fassel, V. A. and Kniseley, R. N. *Anal. Chem.* **1974**, *46*, 1110A.

10. Robinson, J. W. *Atomic Absorption Spectroscopy in Treatise on Analytical Chemistry*: Elving, P. J. and Kolthoff, I. M, eds, Wiley Interscience, New York, **1981**.

11. Pinta, M. *Atomic Absorption Spectrometry, Vol 2. Application to Chemical Analysis* 2nd *ed.*: Masson, Paris, **1980**.

12. Asha, A. *CRC Handbook of Atomic Absorption Analysis*: CRC Press, Boca Ratio, Fla., **1984**.

13. Walsh, A. *Anal. Chem.* **1977**, *49*, 1269A.

14. Cantle, J. E. *Atomic Absorption Spectrometry*: Elsevier, Amsterdam, **1982**.

15. Salvin, M. *Atomic Absorption Spectroscopy*: 2nd ed., wiley, New York, **1979**.

16. Fassel, V. A. *Anal. Chem.* **1979**, *51*, 1290A.

17. Wing, R. K.; Fassel, V. A.; Peterson, V. J. and Floyd, M. A. *Inductively Coupled Plasma-Atomic Emission Spectroscopy*: An Atlas of Spectral Information, Elsevier, New York, **1985**.

18. Houk, R. S.; Fassel, V. A.; Flesch, G. D.; Svec, H. J.; Gray, A. L.; Taylor, C. E. *Anal. Chem.* **1980**, *52*, 2283.

19. Jarvis, K. E. *Chem. Geol.* **1988**, *68*, 31.

20. Feng, R.; Machado, N. and Ludden, J. *Geochim. Cosmochim. Acta.* **1993**, *57*, 3479.

21. Tan, S. H. Nucl. Inst. and Meth. *In Phys. Res. B.* **1995**, *99*, 458.

22. Fucsko, J.; Tan, S. H. and Balazs, M. K. *J. Electrochem. Soc.* **1993**, *140*, 1105.

23. Dolan, R.; Van Loon, J.; Templeton, D. and Paudy, A. Fresenius' *J. Anal. Chem.* **1990**, *336*, 99.

24. Takunori, K.; Nakamura, S. and Morita, M. *Anal. Sci.* **1990**, *6*, 623.

25. Mulligan, K. J.; Davidson, T. M. and Caruso, J. A. *J. anal. At. Spectrom.* **1990**, *5*, 301.

26. Ting, B. T. G. and Janghorbani, M. *Spectrochim. Acta, Part B,* **1987**, *42*, 21.

27. *Applications of Inductively Coupled Plasma Mass Spectrometry to Radionuclide Determinations*: Morrow, R. W. and Crain, J. S., eds, American Society of Testing and Materials, Philladelphia, P. A. **1995**.

28. Meinhard, J. E. *ICP Inform. Newslett,* **1976**, *2*, 163.

29. Canals, A.; Wagner, J. and Browner, R. F. *Spectrochim. Acta,* **1988**, *43B*, 1321.

30. Scott, R. H.; Fassel, V. A.; Kniseley, R. N. and Nixon, D. E. *Anal. Chem.* **1974**, *6*, 76-80.

31. Fassel, V. A. and Bear, B. R. *Spectrochim. Acta.* **1986**, *41B*, 1089-1113.

32. Clifford, R. H.; Sohal, P.; Liu, H.; Montaser, A. *Spectrochim. Acta,* **1992**, *47B*, 1107-1122.

33. Matthew, A. T.; Guangxuan, Z. and Browner, R. F. *Appl. Spectros.* **1991**, *45*, 1424-1432.

34. Babington, R. S. *Popular Sci.* **1973**, *May*, 102-104.

35. Lofthouse, S. D.; Greenway, G. M. and Stephen, S. C. *J. Anal. At. Spectrom.* **1997**, *12*, 1373-1376.

36. LaFreniere, K. E.; Fassel, V. A. and Eckels, D. E. *Anal. Chem.* **1987**, *59*, 879-887.

37. Wiederin, D. R.; Smith, F. G. and Houk, R. S. *Anal. Chem.* **1991**, *63*, 219-225.

38. Tarr, M. A.; Zhu, G. and Browner, R. F. *Anal. Chem.* **1993**, *65*, 1689-1695.

39. Liu, H. and Montaser, A. *Anal. Chem.* **1994**, *66*, 3233-3242.

40. Dole, M.; Mach, L. L.; Hines, R. L.; Mobley, R. C.; Ferguson, L. P. and Alice, M. B. *J. Chem. Phys.* **1968**, *49*, 2240.

41. Yamashita M. and Fenn, J. B. *Phys. Chem.* **1984**, *88*, 4451.

42. Van Holderbeke, M.; Zhao Y.; Vanhaecke, F.; Moen S. L.; Dams, R. and Sandra, P. *J. Anal. At. Spectrom.* **1999**, *14*, 229-234.

43. Wang, L.; May, S. W. and Browner, R. *J. Anal. At. Spectrom.***1996**, *11*, 1137-1146.

44. Kniseley, R. H.; Amenson, H.; Butler, C. C. and Fassel, V. A. *Appl. spectrosc.* **1974**, *28*, 285-286.

45. Anderson, H.; Kaiser, H. and Meddings, B. *Developments in Atomic Spectrochemical Analysis, Proc. Int. Winter Conf.*: Barnes, R. M., ed., Heyden, Philadelphia, **1981**, pp255-277.

46. Layman, R. R. and Lichte, F. E. *Anal. Chem.* **1982**, *54*, 683-641.

47. French, J. B. Etkin, B. and Jong, R. *Anal. Chem.* **1994**, *66*, 685.

48. Dziewatkowski, M. P.; Daniels, L. b. and Olesik, J. W. *Anal. Chem.* **1996**, *68*, 101.

49. Olesik, J. W. and Dziewatkowski, M. P. *J. Am. Soc. Mass Spectrom.* **1996**, *7*, 362.

50. Olesik, J. W.; Stewart, I. *Unpublished results*, **1997**.

51. Park, C. J. and Hall, G. E. M. *J. anal. At. Spectrom.* **1987**, *2*, 473.

52. Vollkopf, U.; Paul, M. and Denoyer, E. R. Fresenuis' *J. Anal. Chem.* **1992**, *342*, 1421.

53. Gray, A. L. *Analyst*, **1985**, *110*, 551.

54. Kogan, V. V.; Hinds, M. W. and Ramendik, G. I. *Spectrochim. Acta, Part B*, **1994**, *49*, 205.

55. Chenery, S. and Cook, J. M. *J. Anal. At. Spectrom.* **1993**, *8*, 299.

56. Jiang, S. J. and Houk, R. S. *Anal. Chem.* **1986**, *58*, 1736.

57. Jiang, S. J. and Houk, R. S. *Spectrochim. Acta, Part B*, **1987**, *42*, 9312.

58. Bloomer, D. W.; Powell, M.; Sing, R. L. A. and Salin, E. D. *Anal. Chem.* **1986**, *58*, 975.

59. Karanassios, V. and Horlick, G. *Spectrochim. Acta. Rev.* **1990**, *13*, 89.

60. Ebdon L.; Foulkes M. and Sutton K. *J. Anal. At. Spectrom.* **1997**, *12*, 213-229.

61. Chen, X. *Ph.D. Thesis:* Iowa State University, **1995**, p111.

62. Houk, R. S. *in Handbook of the Physics and Chemistry of Rare Earths*: Gschneidner, K. A., Jr.; and Eyring, L., Elsevier, New York, **1990**, *vol 13*, ch. 89.

63. Jarvis, K. E. Gray, A. L. and Houk, R. S. *Handbook of Inductively Coupled Plasma Mass Spectrometry*: Blackie & Son, Glasgow, **1992**.

64. Barnes, R. M. CRC Crit. Rev. *Anal. Chem.* **1978**, *7*, 203.

65. *Inductively Coupled plasma in Analytical Atomic Spectrometry: 2nd ed.*: Montaser, A. and Golightly, D. W., eds., VCH Publishers, New York, **1992**.

66. Olesik, J. W. *Anal. Chem.* **1991**, *63*, 12A.

67. Meyer, G. A. *Anal. Chem.* **1987**, *59*, 1345A.

68. Blades, M. W. and weir, D. G. *Spectroscopy.* **1994**, *9*, 14.

69. Ingle, J. D. and Crouch, S. R. *Spectrochemical Analysis*: Prentice Hall, Englewood Cliffs, New Jersey, **1988**.

70. Phillips, H. A. *Optical Spectrosc. Instrum. & Tech.* **1990**, *1318*, 160.

71. Begley, I. S. and Sharp, B. L. *J. Anal. At. Spectrom.* **1984,** *9,* 171.

72. Douglas, D. J.; French, J. B. *J. Anal. At. Spectrom.* **1988,** *3,* 743.

73. Niu, H.; Houk, R. S. *Spectrochim. Acta, Part B* **1996,** *51,* 779-815.

74. Miller, P. E. and Denton, M. B. *J. Chem. Education* **1986,** *63,* 617.

75. McEwen, C. N. and Larsen, B. S. *Electrospray Ionization on Quadrupole and Magnetic Sector Mass Spectrometers in Electrospray Ionization Mass Spectrometry Fundamentals, Instrumentation, and Applications*: Cole, R. B., Wiley, New York, **1997,** pp 177.

76. Dawson, P. H. *Quadrupole Mass Spectrometry and its applications*: Elsevier, Amsterdam, **1976.**

77. Dawson, P. H. *Mass Spectrom. Rev.* **1986,** *5,* 1.

78. Vanhaecke, F.; Moens, L.; Dams, R. and Taylor, P. *Anal. Chem.* **1996,** *68,* 567.

79. Barinaga, C. J. and Koppenaal, d. W. *Rapid Commun. Mass Spectrom.* **1994,** *8,* 71.

80. Koppenaal, D. W.; barinaga, C. J. and Smith, M. R. *J. Anal. At. Spectrom.* **1994,** *9,* 1053.

81. Meyers, D. P.; Li, G.; Mahoney, P. P. and Hieftje, G. M. *J. Am. Soc. Mass Spectrom.* **1995,** *6,* 400.

82. Thirlwall, M. F. and Walder, A. *J. Chemical Geol.* **1995,** *122,* 241-247.

83. Walder, A. J. and Freedman, P. A. *J. Anal. At. Spectrom.* **1992,** *7,* 571-575.

84. Walder, A. J.; Platzner, A. I. and Freedman, P. A. *Spectrochim. Acta.* **1993,** *48B,* 397-402.

85. Walder, A. J.and Platzner, I. *J. Anal. At. Spectrom.* **1993,** *8,* 19-23.

86. Lee, D. and Halliday, A. N. Inter. *J. Mass Spectrom. Ion Processes.* **1995**, *146/147*, 35-46.

87. Milgram, K. E.; Watson, C. H.; White, F. H.; Kappenaal D. W.; Goodner, K. L.; Barinaga, C. J.; Smith, B. H.; Winefordner, J. D.; Marshall, A. G.; Houk, R. S. and Eyler, J. R. *Anal. Chem.* **1997**, *69*, 3714-3721.

88. Huang, L. Q.; Jing, S.-L. and Houk, R. S. *Anal. Chem.* **1987**, *59*, 2316-2320.

89. Kurz, E. A. *Am. Lab.* **1979**, *11*, 67-82.

90. Russ, G. P. Isotope ratio measurements using ICP-MS. In *Applications of Inductively Coupled Plasma Mass Spectrometry:* eds. Date, A. R. and Gray, A. L., Blackie, Glasgow, **1989**, pp90-114.

91. McKenna, C. M. *Springer Ser. Electrophys.* **1982**, *10*, 73-103.

92. ETP Scientific, *Unpublished results.* **1997**.

93. Houk, R. S. *Anal. Chem.* **1986**, *58*, 97A-105A.

94. Bacon, J. R.; Crain, J.; McMahon, A. W. and Williams, J. G. *J. Anal. At. Spectrom.* **1997**, *12*, 407R-448R.

95. Vaughan, M. and Horlick, G. *Appl. Spec.* **1986**, *40*, 434.

96. Alves, L. C. *Ph. D. Thesis*, Iowa State University, Appendix I, **1993**.

97. Krushevska, A.; Kotrebai, M.; Laszitiy, A.; Barnes, R. M. and Amarasiriwardena, D. Fresenius' J. *Anal. Chem.* **1996**, *355*, 793.

98. Tanner, S. D. *Spectrochim. Acta, Part B*, **1992**, *47*, 809.

99. Tanner, S. D. *J. Anal. At. Spectrom.* **1993**, *8*, 891.

100. Evan, E. H. and Ebdon, L. J. *J. Anal. At. Spectrom.* **1990**, *5*, 425.

101. Smith, F. G.; Weiderin, D. R. and Houk, R. S. *Anal. Chem.* **1991**, *63*, 1458.

102. Begerow, J. and Dunemann, L. *J Anal. At. Spectrom.* **1996**, *11*, 303.

103. Jiang, S. J.; Steven, M. A. and Houk, R. S. *Anal. Chem.* **1988**, *60*, 1217.

104. Nonose, N. S.; Matsuda, N.; Fudagawa, N. and Kubota, M. *Spectrochim. Acta. Part B.* **1994**, *49*, 955.

105. Sakata, K. and Kawabata, K. *Spcectrochim. Acta Part B.* **1994**, *49*, 1027.

106. Tanner, S. D. *J. Anal. At. Spectrom.* **1995**, *10*, 905.

107. Evans, E. H.; Giglio, J. J.; Castillano T. M. and Caruso, J. A. *Inductively Coupled and Microwave Induced Plasma Source for Mass Spectrometry: Royal Society of Chemistry:* Cambridge, UK, **1995**, Chap.2, and pp. 29, 51, 89.

108. Olson, L. K. and Caruso, J. A. *Spectrochim. Acta. Part B.* **1994**, *49*, 7.

109. Montaser, A.; Zhang, H.; Caruso, J. A.; Vela, N. P.; Sheppard, B. and Montaser, A. *Mass Spectrometry with sources other than argon ICPs, in A. Montaser (Ed.), Inductively Coupled Plasma Mass Spectrometry:* VCH, New York, **1996**, Chaps. 10 and 11.

110. Alves, L. C.; Wiederin, D. R. and Houk, R. S. *Anal. Chem.* **1992**, *64*, 1164.

111. Olivares, J. A. and Houk, R. S. *Anal. Chem.* **1986**, *58*, 20.

112. Gregorie, D. C. *Appl. Spectrosc.* **1987**, *41*, 467.

113. Vandecasteele, C.; Nagels, M.; Vanhoe, H. and Dams, R. *Anal. Chim. Acta.* **1988**, *211*, 91.

114. Kawaguchi, H.; Tanaka, T.; Nakamura, T.; Morishita, M. and Mizuike, A. *Anal. Sci.* **1987**, *3*, 305.

115. Hobbs, S. E. and Olesik, J. W. *Appl. Spectrosc.* **1991**, *45*, 1395.

116. Beauchemin, D.; McLaren, J. W.; and Berman, S.S. *Spectrochim. Acta. Part B.* **1987**, *42*, 467.

117. Chen, X. C. and Houk, R. S. *Spectrochim. Acta. Part B.* **1996**, *51*, 41.

118. Gillson, G. R.; Douglas, D. J.; Fulford, J. E.; Halligan, K. W.; Tanner, S. D. *Anal. Chem.* **1988**, *60*, 1472.

119. Li, G.; Duan, Y.; Hieftje, G. M. *J. Mass Spectrom.* **1995**, *30*, 841.

120. Farnsworth, P. B.; Chen, Y. and Wu, M. *XXI FACSS Conference*, St. Louis, MO, September **1994**, Paper No. 773.

121. Lloyd, A. A.; Leach, J. J. and Houk, R. S. *Anal. Chem.* **1997**, *69*, 2384-2391.

122. Wang, J.; Shen, W. L.; Sheppard, B. S.; Evans, E. H.; Caruso, J. A. and Fricke, F. L. *J. Anal. At. Spectrom.* **1990**, *5*, 445-449.

123. Wang, J.; Evans, E. H.; Caruso, J. A. *J. Anal. At. Spectrom.* **1991**, *6*, 605-608.

124. Marshall, J. and Franks, J., *J. Anal. At. Spectrom.* **1991**, *6*, 591-600.

125. Evans, E. H. and Caruso, J. A. *Spectrochim. Acta. Part B.* **1992**, *47*, 1001-1012.

126. Hu, K.; Houk R. S. *J. Am. Soc. Mass Spectrom.* **1993**, *4*, 28-37.

127. Ross, B. S. and Hieftje, G. M. *Spectrochim. Acta. Part B.* **1991**, *46*, 1263-1273.

128. Vaughan, M. A. and Horlick, G. *Spectrochim. Acta Part B.* **1990**, *45*, 1301-1311.

129. Beauchemin, D. and Craig, J. M. *Spectrochim. Acta Part B.* **1991**, *46*, 603-614.

130. Craig, J. M. and Beauchemin, D. J. Anal. At. Spectrom. **1992**, *7*, 937-942.

131. Xiao, G. and Beauchemin, D. *J. Anal. At. Spectrom.* **1994**, *9*, 509-518.

132. Munro, S.; Ebdon, L. and McWeeny, D. J. *J. Anal. At. Spectrom.* **1986**, *1*, 211-219.

133. Hall, G. E.M.; Park, C. J. and Pelchat, J. C. *J. Anal. At. Spectrom.* **1987**, *2*, 189.

134. Litchte, F. E.; Meier, A. L. and Crock J. G. *Anal. Chem.* **1987**, *59*, 1150.

135. Doherty, W. *Spectrochim. Acta Part B.* **1989**, *44*, 263.

136. Garbarino, J. R. and Taylor, H. E. *Anal. Chem.* **1987**, *59*, 1568.

137. Vandecasteele, C.; Nagels, M.; Vanhoe, H. and Dams, R. *J. Anal. At. Spectrom.* **1993**, *8*, 781.

138. Fassett, J. D. and Paulsen, P. J. *Anal. Chem.* **1989**, *61*, 643A-648A.

139. Faure, G. *Principles of Isotope Geology*: 2nd edition, John Wiley and Son, New York, **1986**.

140. Shield, W. R. Ed. *Analytical Mass spectrometry Section: Summary of Activities*; *National Bureau of Standard*: Washing D. C, **1970**, NBS Tech. Note (U.S) 506.

141. Mclaren, J. W.; Mykytiuk, A. P.; Willie, S. N. and Berman, S. S. *Anal. Chem.* **1985**, *57*, 2907-2911.

142. Mclaren, J.; Beauchemin, D. and Berman, S. S. *J. Anal. At. Spectrom.* **1987**, *2*, 277-281.

143. Mclaren, J.; Beauchemin, D. and Berman, S. S. *Anal. Chem.* **1987**, *59*, 610-613.

144. Kawabata, K.; Kishi, Y.; Kawaguchi, O.; Watanabe, Y. and Inoue, Y. *Anal. Chem.* **1991**, *63*, 2137-2140.

145. Ketterer, M. E. *Anal. Chem.* **1990**, *62*, 2522-2526.

146. Beauchemin, D. and Berman, S. S. *Anal. Chem.* **1989**, *61*, 1857-1862.

147. Liu, Y. and Ingle, J. D. Jr. *Anal. Chem.* **1989**, *61*, 520-524.

148. Beauchemin, D.; Mclaren, J. W.; Mykytiuk, A. P. and Berman, S. S. *J. Anal. At. Spectrom.* **1988**, *3*, 305.

149. Orians, K. J. and Boyle, E. A. *Spectrochim. Acta.* **1983**, *282*, 63-74.

150. Miyazaki, A. and Reimer, R. A. *J. Anal. At. Spectrom.* **1993**, *8*, 449-452.

151. Jarvis, K. E.; Williams, J. G.; Alcantara, E. and Wills, J. D. *J. Anal. At. Spectrom.* **1996**, *11*, 917.

152. Shum, S. C. K. and Houk, R. S. *Anal. Chem.* **1993**, *65*, 2972-2976.

153. Shen, W. L.; Vela, N. P.; sheppard, B. S. and Caruso, J. A. *Anal. Chem.* **1991**, *63*, 1491-1496.

154. Vela, N. P and Caruso, J. A. *J. Anal. At. Spectrom.* **1992**, *7*, 971-977.

155. Alrashdan, A.; Vela, N. P.; Caruso, J. A. and Hietkemper, D. T. *J. Anal. At. Spectrom.* **1992**, *7*, 551-555.

156. Carey, J. M.; Vela, N. P. and Caruso, J. A. *J. Anal. At. Spectrom.* **1992**, *7*, 1173-1181.

157. Vela, N. P.; Olson, L. K. and Caruso, J. A. *Anal. Chem.* **1993**, *65*, 585A.

158. Vela, N. P and Caruso, J. A. *J. Chromatogr.* **1993**, *641*, 337-345.

159. Kumar, U. T.; Vela, N.; Dorsey, J. G. and Caruso, J. *J. Chromatogr. A.* **1993**, *655*, 340-345.

160. Carey, J. M.; Vela, N. P. and Caruso, J. A. *J. Chromatogr. A.* **1994**, *662*, 329-340.

161. Michallke, B. and Schramel. P. *J. Chromatogr. A.* **1996**, *750*, 51.

162. Lu, Q. H. and Barnes, R. M. *Microchem. J.* **1996**, *54*, 129.

163. Krupp, E. M.; Gruemping, R. Furchtbar, U. R. R. and Hirner, A. V. Fresenius' *J. Anal. Chem.* **1996**, *354*, 546.

164. Narasaki, H. and Cao, J. Y. *Anal. Sci.* **1996**, *12*, 623.

165. Bowman, J.; Fairman, B. and Catterick. T. *J. Anal. At. Spectrom.* **1997**, *12*, 313.

166. Hall, G. E. M. and Pelchat, J. C. *J. Anal. At. Spectrom.* **1997**, *12*, 103.

167. Warren, A. R.; Allen, L. A.; Pang, H. M.; Houk, R. S.; Janghorbani, M. *Appl. Spectrosc.* **1994**, *48*, 1360-1366.

168. Lloyd, A. A.; Pang, H.; Warren, A. R. and Houk, R. S. *J. Anal. At. Spectrom.* **1995**, *10*, 267-271.

169. Lloyd, A. A.; Leach, J. J.; Pang, H. and Houk, R. S. *J. Anal. At. Spectrom.* **1997**, *12*, 171-176.

170. Walder, A. J.; Koller, D.; Reed, N. M.; Hutton, R. C.; Freedman, P. A. *J. Anal. At. Spectrom.* **1993**, *8*, 1037.

171. Walder, A. J.; Furuta, N. *Anal. Sci.* (Japan) **1993**, *9*, 675.

172. Walder, A. J.; Abell, I. D.; Platzner, I.; Freedman, P. A. *Spectrochim. Acta*, Part B **1993**, *48B*, 397.

173. Esat, T. M. *Int. J. Mass Spectrom. Ion Processes* **1995**, *148*, 159.

174. Swihart, G. H. *Rev. Mineral.* **1996**, *33*, 845.

175. De Lacter, J. R.; Rosman, K. J. R.; Loss, R. D. *At. Energy Can. Ltd. AECL 1996* (AECL-11342), **1996**, *8*, 8.

CHAPTER 2. CHROMATOGRAPHIC ISOLATION OF MOLYBDENUM FROM HUMAN BLOOD PLASMA AND DETERMINATION BY INDUCTIVELY COUPLED PLASMA MASS SPECTROMETRY WITH ISOTOPE DILUTION

Elise T. Luong[2], R. S. Houk, and Robert S. Serfass[3]

ABSTRACT

A method is developed for the determination of Mo in human blood plasma by ion exchange chromatography and inductively coupled plasma mass spectrometry (ICP-MS). Molybdenum is isolated from the plasma matrix by microwave digestion and anion exchange on an alumina column. Recoveries are a) $88 \pm 10\%$ ($\pm$ 1 standard deviation, n = 4) from a solution that contains 5 ppb Mo and 92 ppm phosphate, and b) $82 \pm 5\%$ (n = 5) for a solution containing 0.5 ppb Mo and 92 ppm phosphate. The relative standard deviation (RSD) of the count rate for $^{98}Mo^+$ at 0.5 ppb is 5 to 10%, while the ratio $^{94}Mo/^{98}Mo$ has a precision of 0.5 to 2.0% RSD. The detection limit for Mo is 1 ng L^{-1}. The average Mo concentration in

reference bovine serum determined by our method is 10.2 ± 0.4 ng g^{-1}, while the certified

value is 11.5 ± 1.1 ng g^{-1} (95% confidence interval). The Mo concentration of pooled human

blood plasma is 0.5 ± 0.1 ng g^{-1}.

Keywords: Molybdenum, isotope dilution, inductively coupled plasma mass spectrometry, human blood plasma, ultra-trace analysis.

INTRODUCTION

Molybdenum is an essential trace element for plants, animals and microorganisms. The concentration of Mo in the diet and tissues of humans is generally below 1 μg g^{-1} (reference 1). Mo contributes to the function of 11 known enzymes. The first tracer study of Mo metabolism in humans was reported in 1964[2] using the only available radioisotope ^{99}Mo, which has a radioactive half life too short (69 hours) for metabolic studies. Thus, the study of Mo metabolism in humans has progressed slowly[3]. A method for determining of Mo concentration and isotopes in human blood plasma is needed for further progress in studies of the metabolism, functions, and distribution of this element.

Atomic absorption spectrometry is the main method used to determine trace metals in biological samples[4]. Neutron activation analysis is a valuable confirmatory method. For isotope tracer studies, thermal ionization mass spectrometry (TI-MS) has been used to some extent. The precision of TI-MS is very good, typically ± 0.01% relative standard deviation or

better. Unfortunately, TI-MS requires at least 1 μg of Mo, which corresponds to at least 1 L of human blood[5].

There are two general strategies for trace element analysis of biological fluids by ICP-MS. In some cases, the elements of interest can be determined by simply diluting the sample without removing the matrix[6]. The advantages of such a direct procedure are speed and minimization of sample handling steps and contamination. Dilution to a typical total solute level (0.1%) reduces the concentration, which is not tolerable for elements like Mo that are already at concentration $< \sim 1$ ng g^{-1}. Even if the Mo signal remains detectable, spectral interferences become problematical, and it is difficult to obtain the desired precision for isotope ratio measurements if the signal level is too low.

For these reasons, this paper describes a chromatographic isolation and preconcentration procedure for Mo. Although the determination of Mo concentration by isotope dilution is emphasized here, the same procedure could be readily used for isotope tracer studies. In the latter application, the samples come from clinical feeding protocols and are very valuable; isolation of the analyte helps ensure the success of the analysis and is well worth the extra time and effort. In this paper, we first describe procedures for control of contamination and loss of Mo during sample preparation. This area is neglected in recent literature but is often the limiting factor in accuracy of analysis by ICP-MS. A procedure for isolation of Mo from human blood plasma and the use of isotope dilution for quantification of Mo are then described. Finally, results for the determination of Mo concentration in a standard reference material and in pooled human blood plasma are presented.

EXPERIMENTAL

Instrumentation

The ICP-MS was the TS Sola (Finnigan Ltd, Hemel Hempstead, United Kingdom). The ultrasonic nebulizer with desolvating system was purchased from CETAC Technologies (Model U-5000AT, Omaha, Nebraska). Instrumental operating conditions are listed in Table 1. The Milestone microwave digestion apparatus with ten 100 mL capacity flouropolymer vessels was from Buck Scientific (Model MLS 1200 MEGA, Norwalk, Connecticut). A class 100 clean room with a class 10 polypropylene fume cabinet was installed by Controlled Environmental Services Inc.(Mansfield, Massachusetts). The laser particle counter used to monitor the particulate level in the clean room was obtained from Met One, (Model 1506, Grants Pass, Oregon). Barnstead Thermolyne Corporation (Model Nanopure II, Dubuque, Iowa) furnished the clean room with two analytical grade ultra-pure cartridges and one organic free cartridge, which supplied 18 MΩ de-ionized water. Empty polyethylene chromatographic microcolumns with frits (1 mL capacity) were obtained from J. T. Baker.

Materials and reagents

Ultra-pure reagents (concentrated HNO_3, 30% H_2O_2) containing less than 0.005 ng mL^{-1} Mo and 30% NH_4OH containing < 0.02 ng mL^{-1} Mo (indicated on the certificates) were purchased from Fisher Scientific and J. T. Baker and were used without further purification. Trace metal grade HNO_3 used for cleaning plasticware was also obtained from Fisher. Molybdenum standard stock solutions (1.000 g L^{-1}) were from Fisher Scientific. Enriched

stable isotopic ^{94}Mo (Lot 134191, Oak Ridge National Laboratory) was used to prepare a stock solution in which the ^{94}Mo concentration was 10.8 ± 0.1 µg g^{-1}. Fused quartz crucibles were purchased from Fisher Scientific. The activated alumina powder column packing material (Activity Grade Super I, type WA-4) and ammonium heparin (porcine) were from Sigma Chemical, St. Louis. Bovine serum standard reference material 1598 containing Mo certified at 11.5 ± 1.1 ng g^{-1} (95% confidence interval) was purchased from the National Institute of Standard and Technology (NIST). Human blood samples were provided by two healthy male donors.

Contamination control

Except for centrifugation and microwave digestion, the samples were prepared in the clean room described earlier. In ultra-trace analyses, control of contamination and loss remains a major challenge, especially when the sample is subjected to several purification stages. Therefore, the procedures for providing Mo-free containers and utensils are described here.

Closed microwave digestion vessels with polytetrafluoroetheimide liners that contain 5 ml ultrapure concentrated HNO_3 are heated at 230 °C for 30 minutes (step 1), rinsed with a large volume of 18 MΩ de-ionized water (d-H$_2$O for short), replaced with 80 mL d-H$_2$O, heated again under the same conditions (step 2), followed by rinsing with a large volume of d-H$_2$O. Two mL of 0.15 moles L^{-1} HNO_3 (ultrapure acid) is added to each vessel, which is heated again under the same conditions as in step 1. The vessels are cooled to room

temperature, then the solutions are analyzed by ICP-MS. If the Mo concentration of the 0.15 moles L^{-1} HNO_3 measured at m/z = 94 and m/z = 98 is greater than 0.025 ng mL^{-1}, steps 1 and 2 are repeated. When the blank is below this value, each Mo-free vessel is filled with d-H_2O, cover and stored in the clean room.

Fused quartz crucibles are soaked in hot conc. HNO_3 (trace metal grade) in an acid washed polypropylene container for 24 hours, rinsed copiously with d-H_2O, then boiled in a large volume of d-H_2O, rinsed again with d-H_2O, and soaked in hot conc. HNO_3 (ultra-pure acid) for another 24 hours. The sequence is repeated until the background Mo is below 0.010 ng mL^{-1} when measured in 0.15 moles L^{-1} HNO_3 with ICP-MS. The cleaned quartz crucibles are stored in d-H_2O in the clean room.

Polypropylene bottles are soaked in 3 moles L^{-1} HCl for 7 days, then rinsed copiously with d-H_2O. Bottles are filled with 1 mole L^{-1} HNO_3 (ultrapure acid), and leached for 2 more days. In the final rinse, bottles are filled with d-H_2O, capped and stored inside the clean room. Polypropylene vials and centrifuge tubes are also acid washed in the same manner. Pipette tips and polyethylene transfer pipettes are rinsed up and down twice, first with 1 mole L^{-1} HNO_3 (ultrapure acid), then with d-H_2O rinsing right before use. Molybdenum-free alumina powders are prepared by soaking in 3.75 moles L^{-1} NH_4OH (ultrapure base) for 7 days with 3 changes per day. These powders are then washed thoroughly and stored in 18 $M\Omega$ d-H_2O. The cleaned alumina powders are checked by analyzing column blanks by the procedure described in the section on ion-exchange chromatography. Results are presented in Table 2 and explained under the section on background investigation.

Sample preparation

Microwave digestion

Blood from the donor is drawn into a polypropylene syringe with a stainless steel needle that contains 5-10 μL ammonium heparin stock solution (24 mg mL^{-1}) in 0.9% NaCl aqueous, transferred and pooled into a 50-mL polypropylene centrifuge tube. These samples are spun at 1,100 x gravity for 25 minutes. Plasma is separated from the formed elements and divided into ~ 2 mL aliquots in quartz crucibles. Each weighed aliquot of plasma is spiked with a known mass of ^{94}Mo working solution. The quartz crucibles are warmed at 50 to 60 °C on a hot plate until most of the liquid has evaporated. The samples are cooled to room temperature and pre-digested with 1 mL conc. HNO_3 for 45 minutes. A booster of 1 mL conc. HNO_3 plus 40 μL 30% H_2O_2 is added to each sample (called B). To each empty microwave vessel (called C), 5 mL conc. HNO_3 are added. Sample B is added to C, then microwave digestion is performed in a closed system under pressure of 4 to 5 bars, with temperature programming from 90 to 230 °C in 20 minutes, then digested 25 more minutes at 230 °C (45 min. total). Organic materials are removed as CO_2 (g) and N_xO_y (g). The resultant solutions in the crucibles are evaporated to dryness at 50 to 60 °C on a hot plate and reconstituted in 1 mL 0.01 mole L^{-1} HNO_3 (called D).

Ion exchange chromatography

The use of alumina to isolate Mo from potential interferences such as Na^+, Cl^-, $H_2PO_4^-$ was adapted from McLeod et al.[7], who used alumina columns to separate phosphorus in steel.

Human blood plasma, standard bovine serum, or blank samples were all processed by the same anion exchange procedure as follows:

1. Prepare Mo-free alumina microcolumns 0.5 cm long, one column per sample.

2. Rinse each column once with 1 mL 3.75 moles L^{-1} NH_4OH and collect effluent.

3. Rinse each column twice with 1 mL 18 MΩ d-H_2O, twice with 1 mL 0.01 moles L^{-1} HNO_3, then add sample digest (D).

4. Discard the initial column effluent containing cations Na^+, etc.

5. Wash with 1 mL 0.01 moles L^{-1} HNO_3 and discard the effluent containing weakly bound anions such as Cl^-, I^-, etc.

6. Elute Mo off the columns as MoO_4^{2-} with 1 mL 3.75 moles L^{-1} NH_4OH. Collect into 2-mL polypropylene vials.

7. Evaporate to dryness by heating at 90 °C in a heating block.

8. Re-dissolve the solid in 2 mL 0.15 moles L^{-1} HNO_3 for analysis.

9. Discard the column and packing after use.

RESULTS AND DISCUSSION

Isotope dilution

Molybdenum has seven stable isotopes of nominal masses 92, 94, 95, 96, 97, 98 and 100. The natural abundances are 14.84%, 9.25, 15.92, 16.68, 9.55, 24.13 and 9.63, respectively. Figure 1 shows a low resolution mass spectrum of a 0.25 ppb Mo standard solution. The most abundant isotope (^{98}Mo, 24.13%) was chosen as the reference isotope and

^{94}Mo as the spike isotope. ^{100}Mo might be preferred over ^{94}Mo, but we plan to analyze samples from a metabolic study in which ^{100}Mo is used as a label, so ^{94}Mo and ^{98}Mo are the only appropriate Mo isotopes at natural abundance in the samples.

If we assume, the isotope distribution of Mo in blood is natural, the concentration (C_x) of Mo in the sample can be calculated from the isotope dilution formula[8]:

$$C_x = (C_s W_s / W_x) [(A_s - R_m B_s) / (R_m B_x - A_x)]$$

C_s: Mo concentration in spike (nmoles g^{-1})

W_x: mass of sample (g)

W_s: mass of spike (g)

A_x: atom fraction of ^{94}Mo in sample (0.0925)

B_x: atom fraction of ^{98}Mo in sample (0.2413)

A_s: atom fraction of ^{94}Mo in spike (0.93808)

B_s: atom fraction of ^{98}Mo in spike (0.00764)

R_m: altered ^{94}Mo/^{98}Mo abundance ratio, measured by ICP-MS

Isotope dilution is based on ratio measurements, which can compensate for many sources of error such as signal drift and matrix effects. Indium internal standard has been used previously in blood serum[6], but our experience has been that matrix components suppress Mo and In intensities to different extents, affecting accuracy of analysis. As shown in Figure 2, the Mo$^+$ signal drifts substantially with time, but the isotope ratio drifts only slightly. In addition, moderate losses of analyte during the chromatographic isolation step do not affect the accuracy of the measured concentration. However, isotope dilution does not

compensate for spectral overlap interference or contamination. Therefore, keeping the background at m/z = 94 and 98 as low as possible is critical. The cleaning procedures described in the Experimental Section were helpful in this respect.

Effect of Solvent

The solvent used for the analytical solutions is also important. Figure 3 shows that the count rate for $^{98}Mo^+$ does not increase linearly with Mo concentration when the solvent is d-H_2O. A similar curve shape is seen in electrothermal vaporization ICP-MS when the sample is dilute and no carrier is used to provide condensation nuclei for proper transport of analyte to the plasma[9]. Molybdate probably suffers transport losses in the desolvation system, as further indicated by the following result. After 1 ppb Mo in d-H_2O was nebulized, the Mo signal rinsed out to 500 counts s^{-1} in three minutes. Nebulization of Mo-free, aqueous HNO_3 at 0.15 moles L^{-1} produced an immediate rise in $^{98}Mo^+$ signal to 20,000 counts s^{-1}. This Mo came from somewhere in the sample introduction system. Under neutral or basic conditions, MoO_4^{2-} should be the main molybdenum species[10]. If Cl^- is present, however, Mo can form various compounds with the general formula MoO_xCl_y (x = 1 to 3, and y = 2 to 5). For examples, $MoOCl_4$, MoO_2Cl_2, and $Mo_2O_3Cl_5$ species are highly volatile[11] and could sublime in the desolvation system, which causes transport losses. The extent of loss is related to the amount of complex formed. It is related to the Mo/Cl^- ratio, other anions present, and especially pH. What is the source of Cl^-? The 1000 ppm Mo stock solution is in diluted aqua regia, a solvent mixture containing 3 parts of HCl for each part of HNO_3. When a 1

ppb Mo solution is prepared by 10^6 dilution of the 1000 ppm stock Mo with d-H_2O , the ratio

of Mo : Cl⁻ : NO_3^- is unchanged. However, if a 1 ppb Mo solution is prepared by diluting the

same stock with 0.15 moles L^{-1} HNO_3, the Cl⁻ : NO_3^- ratio changes substantially, and this

solution is much more acidic. These conditions keep Mo as $[Mo_7O_{24}]^{6-}$ or $[Mo_6O_{21}]^{6-}$

species,[10,12] rather than the MoO_xCl_y compounds. Thus, the calibration curve becomes linear

and the sensitivity increases by a factor of ten when the samples are reconstituted in aqueous

HNO_3 (Figure 4).

The dependence of Mo⁺ signal on HNO_3 concentration was also investigated. Figure 5

shows that the optimum count rate at the reference isotope (^{98}Mo) is between 0.07 and 0.33

moles L^{-1} HNO_3. For this reason, all samples were dissolved in 0.15 moles L^{-1} HNO_3 before

ICP-MS analyses.

Background

The average background measured at m/z = 98 from 0.15 moles L^{-1} HNO_3 varies

between 0.004 ppb and 0.012 ppb total Mo from day to day. The detection limit for Mo of

our instrument (defined as the Mo concentration necessary to provide a net signal equal to 3

times the standard deviation of the background from 0.15 moles L^{-1} HNO_3) is ~ 0.001 ppb.

Column blanks are 0.010 ± 0.004 ppb Mo (Table 2). This level is very close to the Mo

background from the 0.15 moles L^{-1} HNO_3, which indicates that contamination of Mo from

the alumina column is insignificant. The composite background (everything but sample)

shows 0.035 ± 0.009 ppb Mo, which is 15 times below the typical analyte concentration in blood (~ 0.5 ppb).

Table 3 shows the composite background measurement for the ratio $^{94}Mo/^{98}Mo$. The mean ratio value is 0.4918 (RSD = 14.01%, n = 14). This is higher than the natural abundance ratio of ^{94}Mo to ^{98}Mo (0.3833). This background ratio (0.4918) increases the measured value of $^{94}Mo/^{98}Mo$ ratios in the samples, which causes low concentration values. Unfortunately, correction for this problem is difficult because different losses or contamination of analyte can occur in different stages of sample preparation. The current composite background level causes ~ 5% error on the analysis of a sample that contains 0.5 ppb Mo. This error becomes smaller as the Mo concentration in the sample increases.

Recovery of Mo from alumina column

Major inorganic species of blood plasma such as sodium (3.1 to 3.4 mg mL^{-1}), potassium (0.16 to 0.20 mg mL^{-1} and chloride (3.6 to 3.8 mg mL^{-1}) are removed by the anion exchange alumina column, as described in the Experimental section. Our current work is focused on the separation of phosphate (78 to 132 g μL^{-1}) and sulfate (25 to 50 μL^{-1}) from Mo because these two anions are the fourth and fifth major inorganic constituents in human blood[13]. This amount of phosphate alters the $^{94}Mo/^{98}Mo$ ratio measurements slightly (Table 4). The source of interference is not clear. The measured ratio $^{94}Mo/^{98}Mo$ decreases as the anion concentration increases, which is the direction expected from a matrix effect. Alternatively, spectral interferences from $^1H^{31}P^{18}O^{16}O_3^+$ and or $^{34}S^{16}O_4^+$ are possible.

Solutions of different Mo concentrations with and without phosphate or sulfate were tested for Mo recovery. The percentage recoveries and isotope ratio measurements of ^{94}Mo/^{98}Mo are summarized in Table 5. Percentage recovery is defined as the ratio of (^{98}Mo* signal for the solution containing phosphate, sulfate or both that has passed through the column) / (^{98}Mo* signal for the solution containing Mo alone that has not passed through the column) x 100%. Molybdenum recoveries vary between 68 to 100%, which is attributed to the variation of flow rate of the effluent. In spite of these differences in recoveries, the ^{94}Mo/^{98}Mo ratios are very close to the natural abundance ratio (0.3833). Analysis of the mass spectra of eluates at m/z = 31 revealed that 86% of the P was removed; the remaining P has no effect on the Mo ratio measurement of ^{94}Mo/^{98}Mo (Table 5).

The separation of S from Mo cannot be examined by analysis of the mass spectrum of eluates at m/z = 32 because of the background ion O_2^*. Detection of sulfate in column eluates is positive upon addition of a barium chloride solution. However, analysis of a standard solution of 5.0 ppb Mo containing 0.234 mmole L^{-1} (23 ppm) sulfates shows the ^{94}Mo/^{98}Mo ratio measurement shifts negatively by only 0.013% (Table 4), which is insignificant in comparison with to other sources of error.

Results from standard reference material and human blood plasma

The measured ^{94}Mo/^{98}Mo ratio for a known concentration of Mo standard solution is slightly different from the natural abundance ratio. This comes from two causes: Small and variable amounts of Zr and Mo in the nitric acid background, and the mass bias of the ICP-

MS. A normalization factor K is used to correct for this difference; K is defined as the natural abundance ratio (0.3833) divided by the measured ratio from a solution of known Mo concentration. The measured $^{94}Mo/^{98}Mo$ ratio from the spiked samples is then multiplied by this K factor to yield a new $^{94}Mo/^{98}Mo$ ratio (called R_m'). R_m' is used in place of R_m for the calculation of Mo concentration in the original samples from the isotope dilution formula.

Table 6 shows measured results for Mo concentration from 9 replicate bovine serum samples analyzed by our newly developed method. The measured Mo concentration is 10.2 ± 0.4 ng g^{-1} (one SD) of serum; the NIST value is 11.5 ± 1.1 ng g^{-1}. Our result is a little lower than the NIST value but is still within the 95% confidence limit. A plausible explanation verified by spectral scans of blanks (Figure 6) is that some contamination with ^{94}Zr occurs from the walls of the flouropolymer vessels during microwave digestion, even though the sample was isolated from the flouropolymer vessel wall by the quartz crucible ($^{94}Zr^+$ is most likely responsible for the elevated composite background $^{94}Mo/^{98}Mo$ ratio as discussed earlier). Nonetheless, replacement of these vessels with quartz vessels should eliminate this problem. The precision of the measured ratios is still good (~ 1.4 %RSD) even though the Mo concentration is only 10 ppb in the original sample.

The Mo concentration in pooled blood from two healthy male donors is 0.5 ± 0.1 ng g^{-1} (n=6) (Table 7). The RSDs of the $^{94}Mo/^{98}Mo$ ratio measurements range from 0.7 to 1.2%, whereas the RSDs expected from counting statistics are ~ 0.7%. The RSDs of the determined concentrations are ~ 1.4%, largely because of the fluctuation of the analytical balance as the spike isotope is weighed in the clean room. This problem can be solved by putting the balance on a marble weighing table.

CONCLUSION

Subnanogram amounts of Mo in human blood plasma are determined quantitatively by combining anion exchange chromatography with isotope dilution ICP-MS. Currently, our method can be applied to the analyses of blood from adults only, because 12 mL of blood is required for triplicate measurements. Improvements are expected to reduce the required sample volume to one mL per replicate by recycling the unnebulized sample from the spray chamber of the USN, by using a microscale nebulizer, or by changing software sequences. Other areas we would like to improve are lowering the composite background at m/z = 94 and 98 and modifying the microwave digestion vessels. These improvements would lower the detection limit.

ACKNOWLEDGMENT

REFERENCES

1. Rajagopalan, K. V., *Ann. Rev. Nutr.*, 1988, **8**, 401.

2. Rosoff, B., and Spencer, H., *Nature*, 1964, **202**, 410.

3. Turnlund, J. R., Keyes, W. R., and Peiffer, G. L., *Am. J. Clin. Nutr.*, 1995, **62**, 790.

4. Versieck, J., and Cornelis, R., *Anal. Chim. Acta*, 1980, **116**, 217.

5. Turnlund, J. R., Keyes, W. R., and Peiffer, G. L., *Anal. Chem.*, 1993, **65**, 1717.

6. Vanhoe, H., Vandecasteele, C., Versieck, J., and Dams, R., *Anal. Chem.*, 1989, **61**, 1851.

7. McLeod, C. W., Cook, I. G., Worsfold, P. J., Davies, J. E., and Queay, J., *Spectrochimica Acta*, 1985, **40B**, 57.

8. Fassett, J. D., and Paulsen, P. J., *Anal. Chem.*, 1989, **61**, 634A.

9. Ediger, R. D., and Beres, S. A., *Spect. Acta Part B*, 1992, **47B**, 907.

10. Busev, A. I., *Analytical Chemistry of Molybdenum*, Israel Program for Scientific Translations, Jerusalem, 1964.

11. Weast, R. C., and Astle, M. J., *CRC Handbook of Chemistry and Physics*, CRC Press, Inc., Boca Raton, 1982-1983, B-122.

12. Emeleus, H. J., and Anderson, J. S., *Modern Aspects of Inorganic Chemistry*, D. Van Nostrand Co., New York, 1973, 215.

13. Thiele, V. F., *Clinical Nutrition*, The C. V. Mosby Company, Saint Louis, 1976, 194.

Table 1. Standard operating conditions of ICP-MS

Radio frequency: 27.18 MHz

Forward power: 1.3 kW

Reflected power: < 2 W

Vacuum: 2.3 x 10^{-5} to 2.5 x 10^{-5} Torr

Argon gas flow rate:

Outer gas	15 L/min
Intermediate gas	1.0 L/min
Nebulizer gas 1.0 L/min[a]	

Solution uptake rate: 1.04 mL/min

Desolvating system: 140 °C

Condenser: 0 °C

Sampling position: 14 mm from load coil

Peak hopping parameters: Three points per peak, 8 channels, 16 ms
dwell time, 60 passes per scan, 15 scans

---

[a] Selected on daily basis to maximize signal for $^{98}Mo^{+}$

Table 2. Alumina column background

Mo concentration using	
$^{98}Mo^+$ (ppb)	$^{94}Mo^+$ (ppb)
0.015	0.011
0.009	0.006
0.013	0.005
0.011	0.006
0.010	0.007
0.010	0.008
0.014	0.009
0.008	0.005

0.010 ± 0.004 (ppb)   0.007 ± 0.002 (ppb)

Table 3. Composite background

Mo conc. (ppb)	$^{94}Mo/^{98}Mo$,	RSD%
0.045 ± 0.002	0.6700	4.92
0.036 ± 0.001	0.4425	4.95
0.031 ± 0.001	0.5712	3.52
0.028 ± 0.001	0.5585	4.95
0.029 ± 0.001	0.6308	4.79
0.052 ± 0.004	0.4316	3.42
0.029 ± 0.003	0.4460	5.01
0.045 ± 0.003	0.4444	3.30
0.022 ± 0.003	0.4826	5.97
0.036 ± 0.002	0.4526	4.68
0.045 ± 0.002	0.4588	3.10
0.024 ± 0.002	0.4278	3.34
0.036 ± 0.002	0.4728	3.29
0.029 ± 0.002	0.4591	7.89
0.090 ± 0.004	0.4090	3.50
0.035 ± 0.009 (ppb)	0.4918	14.01%

Table 4. Influence of H_3PO_4 or H_2SO_4 on measured $^{94}Mo/^{98}Mo$ ratios for a 5.0 ppb Mo standard solution in 0.7% HNO_3

[H_2SO_4] or [H_3PO_4] (mmoles L^{-1})	% change in $^{94}Mo/^{98}Mo$ ratios	
	Influence of H_3PO_4	Influence of H_2SO_4
0	0	0
0.234[a]	-0.90	-0.013
0.937[b]	-0.93	-0.18
3.75	-1.50	-0.74

[a]Typical sulfate level in human serum

[b]Typical phosphate level in human serum

Table 5. Recovery of molybdenum from alumina column

Condition	Conc. of Mo (ppb)	%recovery	$^{94}Mo/^{98}Mo$,	RSD%
92 ppm	5.00	96 ± 4	0.3886	1.68
H_3PO_4		85 ± 4	0.3804	2.47
		97 ± 3	0.3849	2.00
		75 ± 3	0.3855	3.05
92 ppm	0.50	82 ± 2	0.3808	1.45
H_3PO_4		73 ± 3	0.3838	1.22
		87 ± 3	*	*
		84 ± 3	*	*
		85 ± 4	*	*
92 ppm	0.50	97 ± 4	0.3883	0.81
H_3PO_4		100 ± 4	0.3930	0.60
and				
23 ppm	0.25	68 ± 4	*	*
H_2SO_4		68 ± 4	*	*
		100 ± 2	*	*

*Scan only

Table 6. Results of SRM 1598 from NIST by ICP-MS. K = 0.961

Sample number	$^{98}Mo^+$ signal (counts s^{-1})	RSD%	$^{94}Mo/^{98}Mo$ (R_m')	RSD%	Conc. of Mo (ng g^{-1})
1	237,000	12.50	1.0594	1.29	9.5 ± 0.1
2	295,000	3.47	1.0489	1.25	9.7 ± 0.1
3	292,000	3.72	1.0398	1.27	9.9 ± 0.1
4	256,000	1.47	1.0087	1.29	10.5 ± 0.1
5	257,000	2.58	1.0212	1.37	10.2 ± 0.1
6	245,000	2.43	1.0192	1.28	10.4 ± 0.1
7	256,000	5.35	0.9896	1.78	10.8 ± 0.1
8	243,000	5.41	0.9901	2.19	10.6 ± 0.1
9	301,000	3.34	1.0075	1.39	10.4 ± 0.1

mean: 10.2 ± 0.4 ng g^{-1}

NIST value: 11.5 ± 1.1 ng g^{-1}

Table 7. Results of blood pooled from two male donors. K = 0.928

Sample number	$^{98}Mo^+$ signal (counts s^{-1})	RSD%	Spike (pmoles)	$^{94}Mo/^{98}Mo$ (R_m')	RSD%	Conc. of Mo (ng g^{-1})
1	36,900	4.11	2.4141	1.2850	1.20	0.488 ± 0.007
2	29,700	2.10	2.4569	1.2800	1.09	0.501 ± 0.007
3	32,100	1.62	2.5447	1.5315	0.92	0.406 ± 0.005
4	30,500	5.61	4.9566	1.6852	0.73	0.696 ± 0.007
5	35,200	2.32	4.9543	1.9699	1.14	0.581 ± 0.008
6	34,200	2.30	4.9408	2.5000	0.95	0.424 ± 0.006

mean: 0.5 ± 0.1 ng g^{-1}
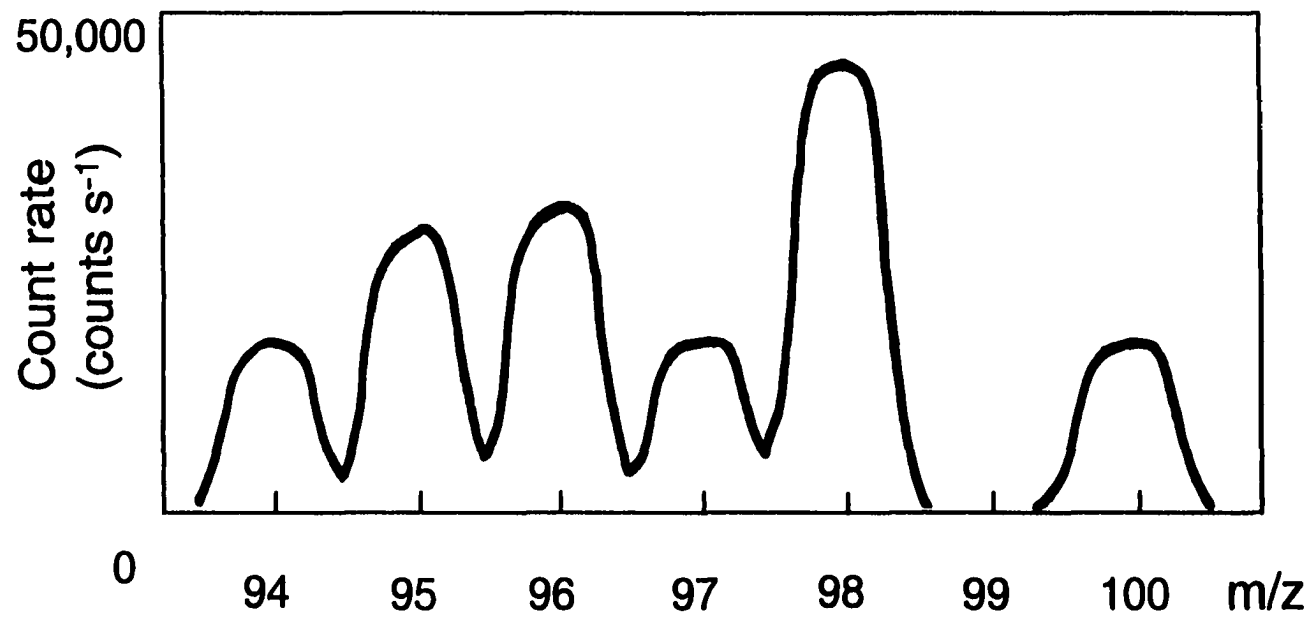
Figure 1. A low-resolution mass spectrum of 0.25 ppb molybdenum standard solution showing 6 stable Mo isotopes, ^{98}Mo was chosen as the reference isotope, and ^{94}Mo was the spike isotope. The natural abundance ^{94}Mo/^{98}Mo ratio is 0.3833. Conditions: 8 channels per m/z value, dwell time 16 ms per channel, 14 passes, full scale = 50,000 counts s^{-1}.
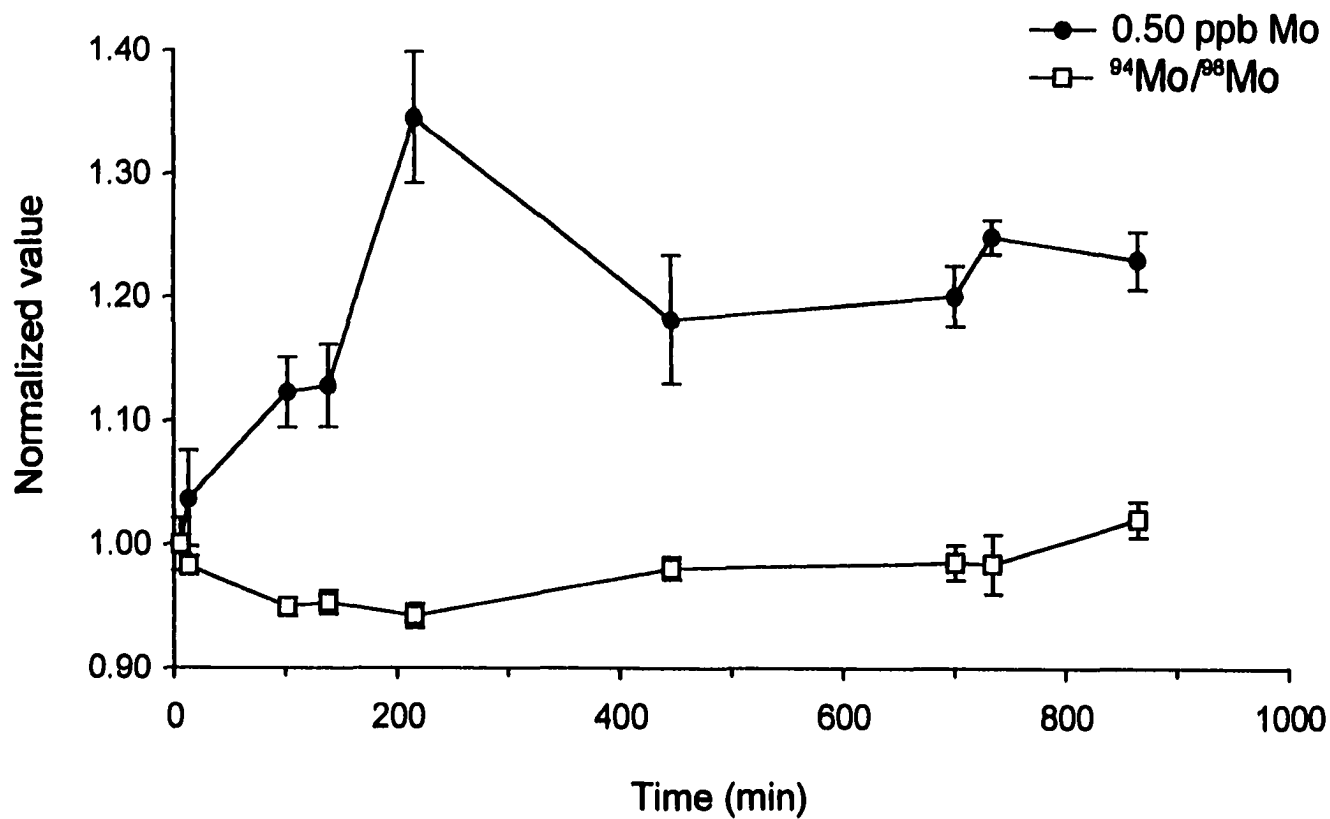
Figure 2. Instrumental stability. Count rate for ^{98}Mo' and ratio for ^{94}Mo/^{98}Mo of a

0.50 ppb Mo solution monitored over 15 hours of continuous operation. The value

1.00 for the normalized ratio corresponds to an actual measured ratio of 0.3957.

$$y = 1.35e^{4.2634x}$$
$$R^2 = 0.9608$$

Y-axis: Count rate $\times$ 10^2 (counts s^{-1})

X-axis: Concentration of Mo in H_2O (ppb)
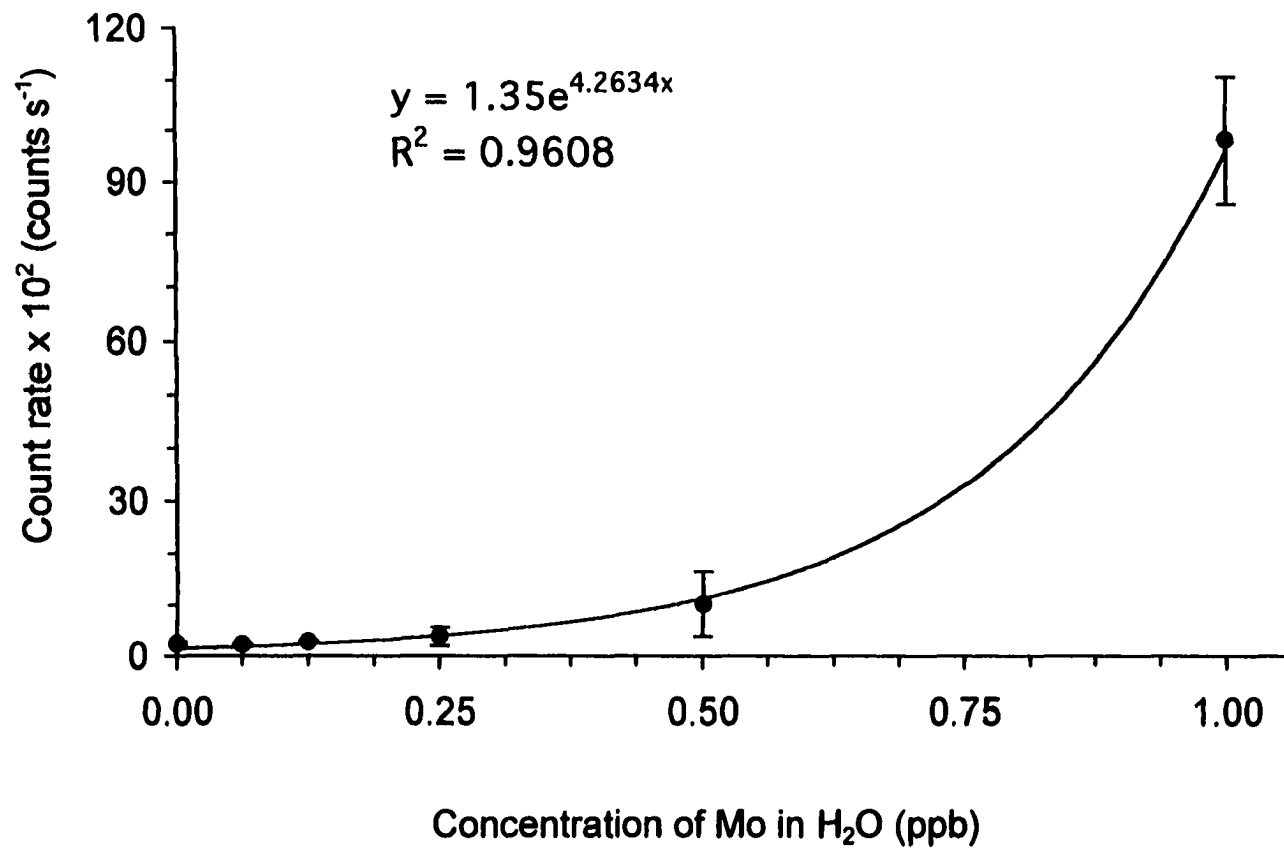
Figure 3. Calibration curve of ^{98}Mo' count rate versus Mo concentration in H_2O.

y = 113.14x + 0.6853
R² = 0.9996

Count rate x 10³ (counts s⁻¹)

Concentration of Mo (ppb) in 0.15 moles L⁻¹ HNO₃

57
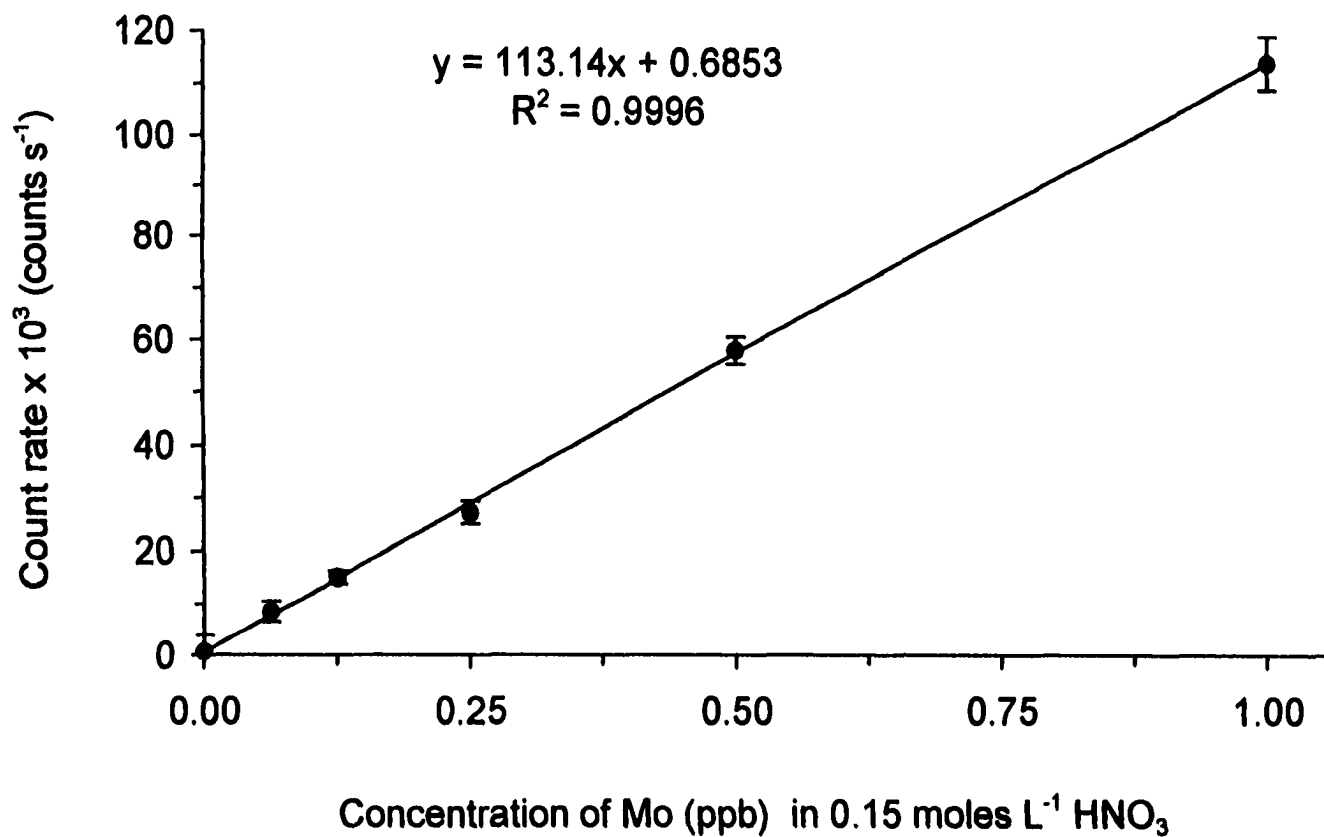
Figure 4. Calibration curve of ⁹⁸Mo⁺ count rate versus Mo concentration in 0.15 moles L⁻¹ HNO₃.
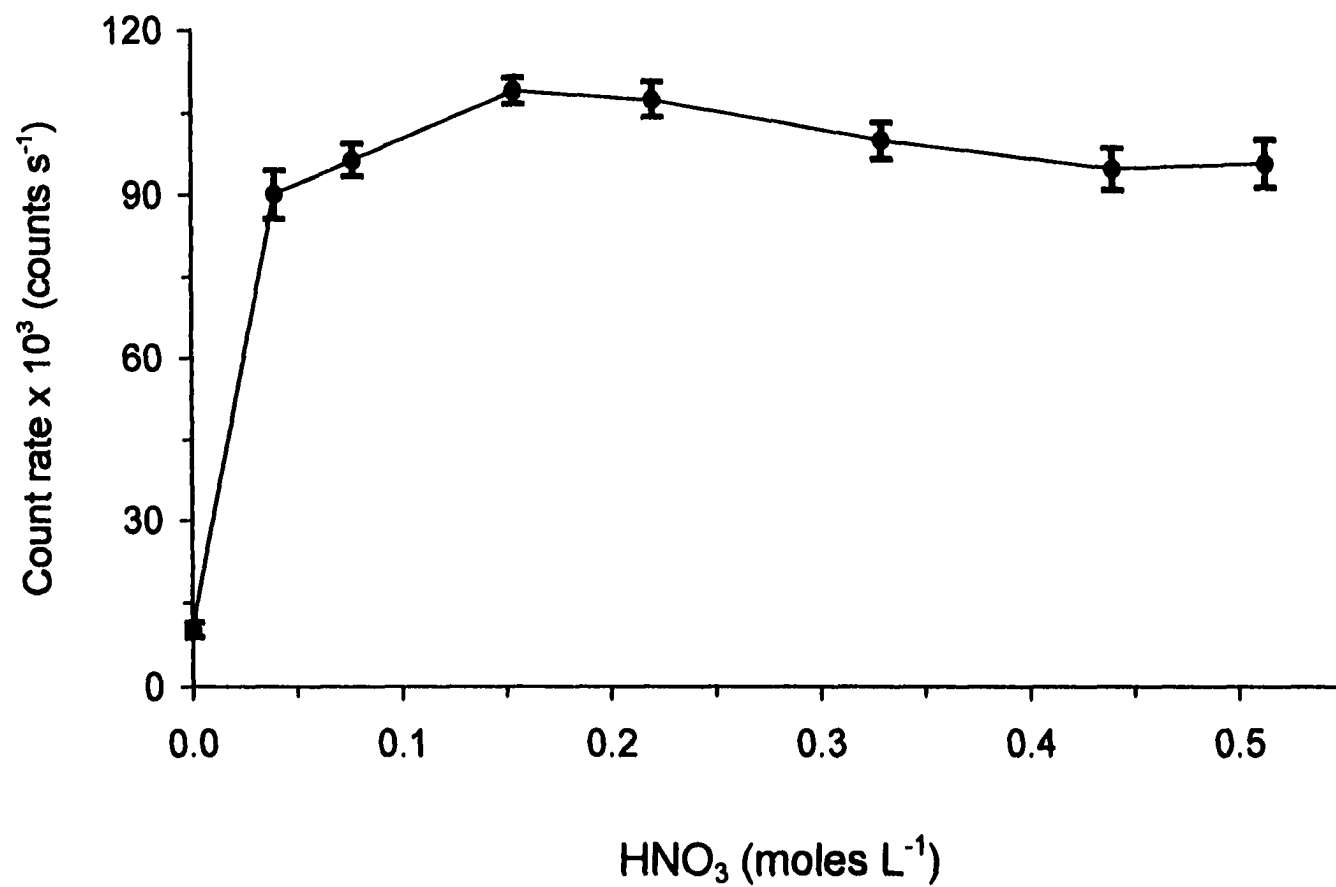
Figure 5. Count rate for a 0.5 ppb Mo standard solution as a function of HNO_3 concentration (moles L^{-1}).
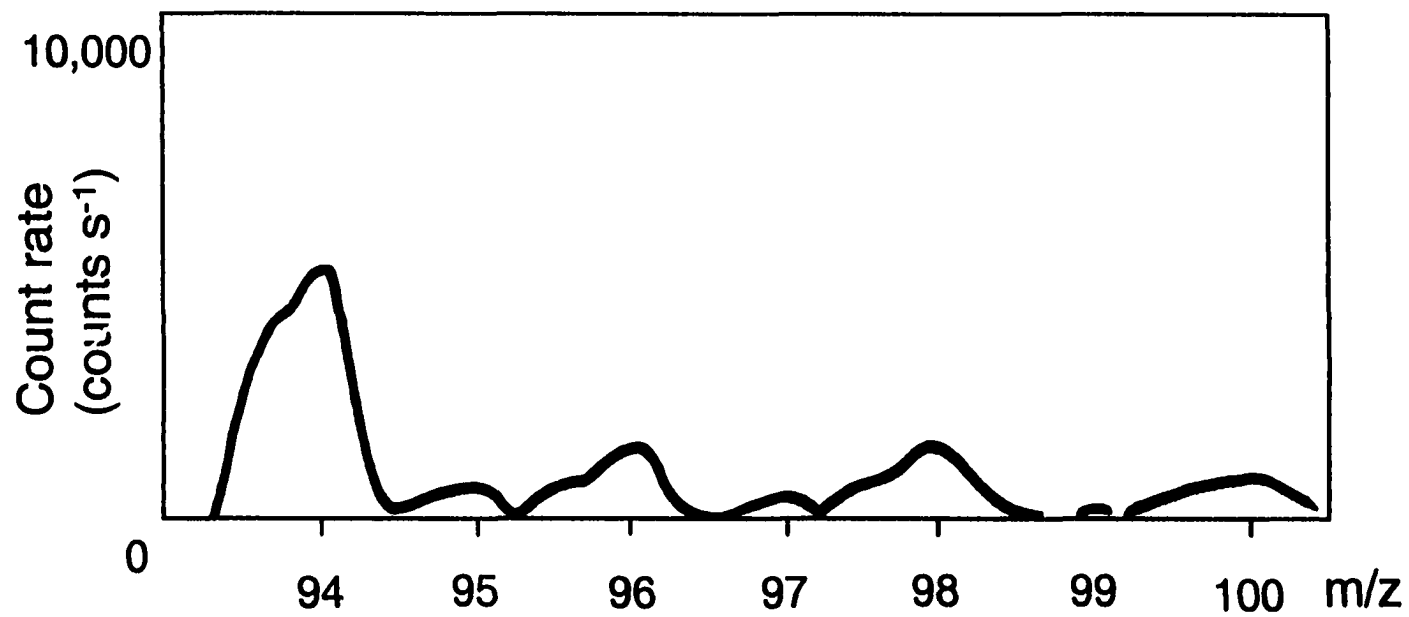
Figure 6. Spectral scan of a blank microwave digestion vessel. Signal at m/z = 94 is mainly

from $^{94}Zr^+$, partly from $^{94}Mo^+$. Conditions: 8 channels per m/z value, 16 ms dwell time per

channel, 15 passes, full scale = 10,000 counts s^{-1}.

CHAPTER 3. SIGNAL IMPROVEMENT AND ^{13}C : ^{12}C RATIO DETERMINATION IN AMINO ACIDS, PROTEINS, AND OLIGOSACCHARIDES WITH AN INDUCTIVELY COUPLED PLASMA TWIN QUADRUPOLE MASS SPECTROMETER

A paper to be submitted to the Journal of the American Society of Mass Spectrometry

Elise T. Luong[1] and R. S. Houk[2]

ABSTRACT

The position of the first extraction lens behind the skimmer is very important and greatly influences the ion collection efficiency. Experimental results show that when the skimmer-first extraction lens separation changes from 4.75 to 3.50 cm, at least 14 fold signal improvement for Li$^+$ is observed. An additional 5-fold improvement (total 19) is observed when a commercial skimmer is employed. Theoretical calculation shows that a skimmer-first extraction lens separation of 3.50 cm corresponds to ~ 1/2 or 2/3 the distance from the skimmer orifice to the onset of the second Mach disk depending on the type of skimmer used. In the ^{13}C : ^{12}C ratio measurements, one mass spectrometer monitors m/z = 13, and the other mass spectrometer monitors at m/z = 12 during a continuous flow of sample aerosol

from the ultrasonic nebulizer to the inductively coupled plasma (ICP). Carbon isotope ratios have been measured for tryptophan, myoglobin, and β-cyclodextrin using a prototype twin quadrupole mass spectrometer (TQMS). Spectral interference on $^{13}C^+$, presumably from $^{12}C^1H^+$, comes from the incomplete dissociation of myoglobin and / or β-cyclodextrin. Decreasing the aerosol gas flow rate slightly can eliminate $^{12}C^1H^+$ interference. $^{13}C : {}^{12}C$ ratios in myoglobin and β-cyclodextrin can be determined precisely and quantitatively. There was no $^{12}C^1H^+$ interference observed in the tryptophan analyses. The best relative standard deviation (RSD%) obtained in the $^{13}C : {}^{12}C$ study is 0.91%, which is close to the limiting precision predicted by counting statistics (1.16%). The count rate of the minor isotope (^{13}C) can be artificially enhanced by increasing the voltage of the detector that detects ^{13}C, and / or by shifting the ion beam splitter offset from the central axis.

Key words: Inductively coupled plasma mass spectrometry, twin quadrupole mass spectrometer, carbon isotope ratio, protein, amino acid, carbohydrate, non-volatile organic compound.

INTRODUCTION

Inductively coupled plasma mass spectrometry (ICP-MS) is a versatile analytical technique with a variety of applications, ranging from elemental determinations to isotopic analyses in nutrition, clinical studies, geochemistry, environmental studies, and nuclear chemistry [1-7]. Attractive features of ICP-MS include wide linear dynamic range (6 to 8 orders of magnitude) and low concentration detection limit (sub part per trillion). Single

quadrupole mass spectrometer is the most commonly used instrument owing to its low cost, compactness, robustness, ease in operation, minimum maintenance, and fast multi-elemental analyses [8-15]. The imperfection is that, single quadrupole ICP-MS usually provides only moderate to good precision in isotope ratio measurements (~ 0.5% to 0.1% RSD, relative standard deviation) [8-15], which is attributed to plasma fluctuation and instrumental instability. Signal drift with time has long been a problem. Instrumental drift in a homemade device is usually worse than the commercial device. The identified sources of drift include solid deposition on the orifice, temperature-dependent fluctuations in the quadrupole power supply, and gain of the detector [11]. The precision is still worse when the measured isotopic ratio is very large or very small. It is hard to get good counting statistics on minor isotope without counting loss on major isotope. The detector must have a very fast response time (low dead time) to distinguish separate pulses at very high-count rates.

Thermal ionization mass spectrometry (TIMS) has long been the method of choice for ultra-high precision in isotope ratio measurements (from 0.01 to 0.1 RSD%) for elements with low first ionization potentials [16-21]. Others are detected as negative ions (e.g. OsO_3^-, TcO_4^-, ReO_4^-, etc.) using negative thermal ionization mass spectrometry (NTIMS) [22, 23]. Recently, Schwieters and Bach have described an improved system, high abundance sensitivity TIMS with a retarding potential quadrupole (RPQ) filter lens. In the new system, the ion optical stability is from 0.5% per 10 minutes to as good as 0.1% per hour, ion counting stability and linearity to as good as 0.2% per hour, and the abundance sensitivity is 2×10^{-9} [24]. In the absence of molecular interference, the ultimate precision and accuracy of the measurement is only determined by the ion beam statistics.

In single detector ICP-MS the precision is limited by flicker noise at long dwell time. Fast peak hopping in isotope ratio measurements can compensate for some of the noise from the plasma and sample introduction system. Although peaks can be switched over a very short time scale (milli-seconds), peak hopping is still not a true simultaneous measurement. Warren et al. have built an instrument called the ICP twin quadrupole mass spectrometer (ICP-TQMS) several years ago [25], which was based on the idea of simultaneous measurements of signal ratios in ICP atomic emission spectrometry done by Tracy and others [26-31]. The ICP-TQMS device measures ion signals at two m/z values truly simultaneously by splitting the ion beam into two beams prior to the entrances of the quadrupole mass analyzers. Allen had performed solid analyses on copper and steel samples using laser ablation with this twin quadrupole device. The best RSD% reported by Allen for $^{63}Cu : {}^{65}Cu$ was 0.26%, and for $^{52}Cr : {}^{53}Cr$ was 0.06% to 0.1% depending on the dwell time and averaging method used [32, 33].

This newly developed twin quadrupole device has the ability of improving precision of ion ratio measurements; although the sensitivity is rather poor. It is poorer than the commercial single quadrupole ICP-MS. For example, 1 ppm Li in H_2O gives ~ 2 x 10^5 counts per second (cps) with our instrument, whereas the same count rate can easily be obtained from a 10 ppb Li solution when measured with the Micromass platform ICP-MS instrument [34]. Our immediate goal of following Warren and Allen's work was to improve the sensitivity of the ICP-TQMS. The first part of this manuscript focuses on the signal improvement technique. The second part demonstrates the ability of this ICP-TQMS to measure stable isotope ratios of carbon from organic compounds at their natural abundance. Our ultimate goal is to offer the world a future analytical method for carbon isotopic analyses

in bioorganic molecules. This is an ambitious goal, since carbon is no more than 5% ionized in the ICP [8], and carbon-13 is only ~ 1% of carbon-12.

As mentioned earlier, the precision generally obtained in isotope ratio measurement by an ICP with single quadrupole mass spectrometry is only from moderate to good. The precision is usually worse if the element is not sufficiently ionized in the ICP (i.e. the first ionization potential of the element is greater than 10 eV) [11]. This is because the precision is limited by low count rate. In order to obtain reasonable count rate, a large sample is used. For these reasons, analysis of isotopic composition requiring superior precision such as the determination of ^{13}C : ^{12}C isotope ratio in fossils or bioorganic molecules is generally not performed with ICP-MS. Up until now, gas chromatography combustion isotope ratio mass spectrometry (GC-combustion-IRMS) is the most widely used analytical method dedicated to the determination of carbon isotopic composition in organic compounds [35-43].

GC-combustion-IRMS is a hybridization of the conventional dual inlet, dual collector mass spectrometric and the selected ion monitoring gas chromatography mass spectrometry (SIM-GCMS) techniques [44], the first technique being developed by McKinney et al. in 1950, and the latter by Sweeley et al. in 1966 [45, 46]. The precision in isotopic analysis has improved from ~ 0.1‰ to 0.01‰ versus standard carbonate Pee Dee Belemnite (PDB) in the last 40 years. Nevertheless, this powerful GC-combustion-IRMS technique is most suitable for the analysis of compounds that are volatile and thermally stabile, in order to take full advantage of the speed that is offered by the GC column for on-line separation of mixtures of compounds. For isotopic analysis of non-volatile organic compounds, the off-line sealed tube combustion conventional dual inlet, dual collector MS method is still widely used.

The conventional sealed tube method involves several steps. First, a Pyrex tube and a few grams of combustion catalyst (e.g. copper oxide wire) are preheated to several hundred degrees (°C). Then both are cooled to room temperature and the purified non-volatile organic sample is added immediately to the tube containing the combustion catalyst. The tube is evacuated, sealed, and combusted at ~ 600 °C for at least two hours. The resultant CO_2 gas from the combusted sample is purified and analyzed for its stable carbon isotope composition [47]. Wong has described the sealed tube combustion method as tedious, labor intensive, and time consuming [48].

One option in the determination of isotope ratios of non-volatile substances is through derivatization [49]. However, the derivatization process is not problem-free, for it requires a large sample, increases risk of contamination, and possibly introduces additional carbon atoms and potential isotopic fractionation during the derivatization processes. Consequently, the process also alters the original stable carbon isotopic composition of the compounds. As an example, Engel et al. described the analysis of ^{13}C : ^{12}C ratio in amino acid enantiomers through derivatization [49]. They reported that isotopic fractionation during the esterification and acylation steps lowered the ^{13}C : ^{12}C ratio. Fortunately, the derivatization process introduces a distinct, reproducible isotopic fractionation that is constant for each amino acid type. Therefore, an empirical correction can be made to deduce the original ^{13}C : ^{12}C ratio from the altered ^{13}C : ^{12}C ratio by means of derivatization of a standard with a known ^{13}C : ^{12}C ratio together with the natural sample. They also reported that incomplete derivatization of the amino acids resulted in a bigger absolute difference in the ^{13}C : ^{12}C values between the derivatization and the conventional IRMS methods when compared with complete derivatization. Furthermore, not all the non-volatile compounds can be derivatized.

Caimi and Brenna have described an alternative method for isotope ratio analysis of non-volatile bioorganic compounds [50]. Their method involved a moving wire interface to couple a high-performance liquid chromatograph to a combustion interface of a dynamic IRMS. The aqueous protein solution was injected directly into a water stream passed through a pneumatic nebulizer and sprayed onto a moving wire. The wire passed through a drying oven and then a combustion interface. Though this system extends the type and number of compounds that can be analyzed, it suffers from transfer loss; only 0.1% of the compound is transferred to the wire and 2% of that reaches the IRMS.

Luke and Schoeller have designed an online combustion system for carbon isotopic analysis of previously isolated, non-volatile organic compounds [51]. Their system involved loading the sample onto a tungsten filament, sealing in a helium / oxygen carrier gas stream, and heating to combustion by passing an electrical current through the filament. The product of the combustion, CO_2, is then carried into the electron impact ion source of the IRMS. This online combustion system still requires the frequent replacement of the Pyrex tube enclosing the filament for accurate isotope ratio measurements. A memory of 30% was observed for the first enriched glucose sample but it did not follow a simple first order model, as the analysis of subsequent samples did not reduce the isotopic effect.

The second part of this paper describes an alternative to GC-combustion-IRMS for rapid determination of carbon isotope ratios from non-volatile organic compounds. We have extended the application of ICP-TQMS to measure isotope ratios of ^6Li : ^7Li (from Li ICP standard) and ^{13}C : ^{12}C (from α-D-glucose) [52]. Despite the tremendous differences in count rates between ^6Li and ^7Li, ^{13}C and ^{12}C, the ICP-TQMS is capable of measuring ^6Li : ^7Li and ^{13}C : ^{12}C ratios with precision (RSD%) as good as that expected from counting statistics.

To the best of our knowledge, this is the first attempt to determine the ^{13}C : ^{12}C ratios of a complicated non-volatile organic compound like β-cyclodextrin, and bioorganic molecules like tryptophan and myoglobin with ICP-MS.

The fundamental difference of ^{13}C : ^{12}C measurements between ICP-TQMS and GC-combustion-IRMS is the entities that are detected at the end run. In GC-combustion-IRMS, the success in carbon isotope ratio measurements relies on the combustion of the organic compound to CO_2 , N_2 and H_2O, followed by the purification of CO_2 (cryogenically or chemically), electron impact ionization of CO_2 and the detection of CO_2^+ molecular ions. Carbon isotope ratios are determined by measurement of the ion currents at masses 45 ($^{13}C^{16}O_2$ + $^{12}C^{16}O^{17}O$) and 44 ($^{12}C^{16}O_2$), and correction for ^{17}O is performed during data processing [53-55]. Complete combustion of the organic compound is imposed because non-quantitative combustion could be accompanied by isotopic fractionation and spectral interference from fragment ions arising from residual materials appearing at masses 44 and 45, thus causing serious errors in isotope ratio measurements as discussed by Matthews and Hayes [45]. In ICP-TQMS, the organic species is first dissolved in aqueous solution and then nebulized to form fine aerosols. The aerosols are then subjected to desolvation, the dried aerosols are sent to the ICP for vaporization, dissociation, atomization, excitation, and ionization. The detected entities are $^{13}C^+$ and $^{12}C^+$ atomic ions. This technique offers minimum sample preparation, less severe memory effect, no isotopic fractionation, and no need for ^{17}O correction.

EXPERIMENTAL

INSTRUMENTATION

Components of the homebuilt inductively coupled plasma twin quadrupole mass spectrometer (ICP-TQMS) and the standard operating conditions are listed in Tables 1 and 2 respectively. The three-dimensional structure and the exact dimensions of the ion beam splitter have been previously described [25]. The heart of this instrument is the ion beam splitter (Figure 1). It is two toroidal electrostatic analyzers back to back. The ion beam from ICP is extracted through the sampler and skimmer. The beam passes through a series of ion lenses and beam shift plates, is then split into two parts at the entrance of the splitter, each part travels on each side of the splitter to its own quadrupole mass analyzer and detector. Two individual m/z values can be measured separately and simultaneously. Most of the flicker noise from the ICP and sample introduction system cancels when the ratio is calculated. Consequently, the RSD% of isotope ratio measurements is greatly improved.

Typical ion lens voltages are also listed in Figure 1. The first extraction lens and the beam shift plates are the two most important lenses. The left and right beam shift plate voltages dictate the fraction of the ion beam to be sent to each channel. The voltages of the three electrodes of the splitter and the alignment of the splitter also influence the portion of the beam being sent to each channel. These relative potentials are optimized daily to achieve the best RSD% for isotope ratio measurements. As a result, the ion beam is not always split equally between the two channels. Sometimes, the ion beam is split more to channel A than channel B and vice versa. Consequently, the measured isotopic ratio is different from the natural abundance ratio, and thus, a daily ion beam splitter calibration curve is needed for

isotope ratio determinations. This will be discussed more in detail in the Results and Discussion section. Throughout this paper, the words channel A and channel B refer to quadrupole A and quadrupole B, or mass analyzer A and mass analyzer B as shown in Figure 1.

MODIFICATIONS SINCE LAST PUBLISHED PAPER

The sampler-skimmer separation has changed from 8 mm to 10 mm for normal operation. The second stage differential pumping orifice (Figure 1) has enlarged from 1.5 mm to 2 mm in diameter. An additional ion lens (1.5 mm long) was placed behind the second extraction lens and in front of the differential pumping plate. A series of extension lenses with different lengths (0.5, 0.75 and 1.25 cm) but with the same inner diameter of 1.5 cm were made of stainless steel and used to adjust the skimmer-first extraction lens separation. The skimmer interface was also modified to accommodate the Sciex 6000 nickel-skimmer. Finally, the discrete dynode electron multipliers (Model AF 562A, ETP Scientific, Auburn, Massachusetts, U.S.A.) replaced the Galileo 4870 for ion detection.

MATERIALS AND REAGENTS

A 5-mL Teflon sample loop was purchased from Alltech (Deerfield, Illinois, U.S.A.) and was installed in between the peristaltic pump and the ultrasonic nebulizer. This sample loop was necessary for the protein or carbohydrate solutions to bypass the peristaltic pump, in order to reduce the background noise and rinse out time of the system. A double layer tubing (formulation SE 200) composed of Tygon on the exterior wall with a thin Teflon

coating in the interior wall was purchased from Norton Performance Plastic (Akron, Ohio, U.S.A.). The inner thin Teflon provided a smooth and chemically inert surface, which minimized precipitation of protein or sugar during the transit. A Millipore Laboratory Water System (Bedford, Massachusetts, U.S.A.) furnished the laboratory with an organics pyrogen-free system, consisting of one super-C carbon cartridge, two ion-exchange cartridges, two organex-Q cartridges, which supplied 18 MΩ de-ionized water (H_2O). Standard stock and working solutions were stored in 15-mL or 50-mL polypropylene tubes that were obtained from Fisher Scientific (Pittsburgh, Pennsylvania, U.S.A.). 5-mL syringes and filters with 0.45 μm pore size were used for filtering the amino acid and protein solutions from particulates, also supplied by Fisher Scientific.

Ultrex II ultra-pure concentrated nitric acid was purchased from J. T. Baker (Phillipsburg, New Jersey, U.S.A.). Lithium working solutions were diluted from the stock 1000 ppm ICP standard that was obtained from Plasmachem (Farmingdale, New Jersey, U.S.A.). Standard 10000 ppm stock α-D-glucose solution was prepared by dissolving the α-D-glucose crystals (Aldrich, Milwaukee, Wisconsin, U.S.A.) in H_2O. Enriched [13]C α-D-glucose was purchased from Cambridge Isotope Lab (Andover, Massachusetts). Working solutions of 1000 ppm β-cyclodextrin were prepared by dissolution of the solid β-cyclodextrin, supplied by Fluka (Ronkonkoma, New York, U.S.A.). Lyophilized tryptophan and horse heart myoglobin were obtained from Sigma (St. Louis, Missouri, U.S.A.). All working solutions were prepared prior to use by diluting the stock solutions with H_2O, except for tryptophan, which was dissolved in HNO_3 at pH = 4.0.

RESULTS AND DISCUSSION

SIGNAL IMPROVEMENT

It has been known that ions made in the ICP are lost during the extraction process. Approximately 98% of the ions are lost after extraction through the sampling orifice, and approximately another 99% of the ions are lost after they are extracted through the skimmer [56-62]. For the first approximation, for every 10^6 to 10^8 ions that were made in the ICP, only a few ions successfully survive to the detector, thereby, making the overall efficiency ~ 5×10^{-6} [63, 64]. This wasteful extraction process is attributed to the substantial pressure difference of where the ions were made (760 Torr) to where the ions were detected (10^{-5} Torr) in the ICP-MS system. Signal was further reduced gradually through deposition of solids on the sampler orifice. This accounts for approximately 50% loss of signal.

Sampler orifice plugging can be avoided or minimized by using < 0.1% solid content in the sample solution and enlarging the sampler orifice [65, 66]. In this fashion, the sampler can extract a bigger portion of the central gas flow from the ICP. Vanghan and Horlik found that signal increased 10 times for metal ions when the sampler orifice was enlarged from 0.51 mm to 0.94 mm [67]. Hu and Houk also observed that signal of $^{59}Co^+$ and $^{209}Bi^+$ was improved ~ 8 times when the sampler orifice changed from 0.79 mm to 1.31 mm in their homebuilt ICP-MS system [68]. Although enlarging the sampler orifice is one way to improve the ion signal, the maximum orifice diameter is determined by the capacity of the pumping system in the expansion chamber. There is a limit to how large the orifice can be enlarged without destroying the pressure in the quadrupole chamber. Another way of improving the ion signal is to apply a potential to either sampler or skimmer cone as

described in reference 69. On doing this, Hu and Houk reported that the ion transmission had increased 4 to 6 fold.

Obviously, the ion extraction process plays a major role in the sensitivity of an ICP-MS device. Some manufacturers have tried to improve the signal by innovating a variety of shapes of the skimmer cones for a smoother gas flow [70]. A smoother gas flow can minimize the turbulence behind the skimmer and thus lose fewer ions. For example, Chilton innovates at least two types of skimmer cones that can increase the ion transmission between 2 to 4 fold. One type of skimmer has a compound curvature (flute like) on the outer surface and cylindrical shape at the tip of the inner surface. The other has the same fluted outer surface but conical shape at the tip of the inner surface [70]. Another researcher put the third differential pumping orifice close to the skimmer to improve the sensitivity. For example, Turner found that when a third metal cone was employed behind the skimmer and biased at a very high negative potential (-2 kV) to accelerate the ions to high kinetic energy, the sensitivity is increased (especially for the low m/z ions) [71].

Douglas and French have made theoretical calculations of the optimum sampler-skimmer separation that enables the skimmer to extract as many ions as possible behind the sampler. As a rule of thumb, the optimum skimmer position is approximately one half to two third the distance from the sampler orifice to the onset of the Mach disk [72]. In other words, the skimmer tip is actually inside the zone of silence that is created by the supersonic jet when the gas flows through the sampler orifice [72, 73-75].

The rule of thumb for the optimum skimmer position immediately brings to our attention the question as to why the same rule cannot be applied to the first extraction lens. Much of the attention has been paid to the sampler-skimmer extraction process. The

skimmer-first extraction lens separation is also important to a certain extent [76]. In the original design of this ICP-TQMS, the entrance to the first extraction lens was placed 4.75 cm downstream from the skimmer orifice. According to gas dynamics alone, gas flux is inversely proportional to the square of the distance [61, 62]. As a result, gas flux at distance 4.75 cm downstream is only about 4 % of the gas flux at the skimmer orifice. In reality, somewhere behind the skimmer charge separation occurs, electrons are lost and the remaining positive ions repel each other because the ion current exceeds the space charge limiting current [56, 60, 77-79]. This is known as space charge effect [56, 80, 81]. According to Chen and Houk, Tanner, and Gillson space charge effect is the cause of the major loss of the ions behind the skimmer. Under space charge limiting flow, the loss of the ions is exceeded by what can be calculated using the gas dynamics equation [82-84]. It makes perfect sense that reducing the distance between the skimmer and the first extraction lens in the original design should increase the ion collection efficiency. Unfortunately, there is no rule or clue of where the first extraction lens should be placed. It probably varies from instrument to instrument. The optimum position is thereby determined experimentally.

In an attempt to improve the ion transmission further, the existing skimmer interface was replaced by a new copper interface (made in house) to accommodate the Sciex 6000 nickel skimmer. It has a normal cone shape with interior and exterior angles of 52 and 61 degrees respectively. The orifice diameter is 0.82 mm. In the present investigation, the easily ionized element lithium was used. We made efforts to operate the instrument under similar conditions, as possible, from day to day during this study. Data were collected immediately after the instrument had optimized and before the drift in signals took place. Figure 2 shows a low-resolution mass spectrum of lithium obtained simultaneously from

channel A and channel B. A typical lithium standard curve is shown in Figure 3. Count rate of both channels was measured at m/z 7. Irregardless of solvent used, H_2O or 0.7% HNO_3 (data not shown), the instrument gives about the same sensitivity. The average detection limit (i.e., solution concentration that gives a net signal 3 times standard deviation of the background) measured over different ICP-MS operating conditions with different split ratios for Li is 2 ± 1 ppb (n = 14) on both channels. A typical rinse out curve of lithium observed simultaneously on both channels is shown in Figure 4a.

Signals from both channel A and B were rinsed out at the same time, and it appeared that there was memory effect in the system. After 4 minutes of rinsing, the remaining count rate on both channels was ~ 1% of the original count rate. A correlation plot (plot of normalized count rate of ^7Li measured at quadrupole A versus the normalized count rate of ^7Li measured at quadrupole B) from signals obtained during the entire rinse out curve is linear with $r^2 = 0.9998$, which indicates that flicker noise cancels (Figure 4b) when the ratios are computed. In the present study, the total count rate (sum of count rate from channel A and channel B measured at m/z 7) was used in the comparison of signal improvement. Despite our efforts to keep constant operating conditions, the total count rate does vary from ± 5 to 10% from day to day, therefore, the results listed under the column of factor of improvement in Table 3 are only semi-quantitative. Nevertheless, in spite of the type of skimmer employed (the original homemade stainless steel or the commercial Sciex 6000 nickel), a clear and substantial enhancement in ion collection efficiency was observed when the first extraction lens was brought closer and closer to the skimmer orifice (Table 3). When the homemade skimmer-first extraction lens separation is 3.50 cm [Figure 5, extension B], i.e. ~ 2/3 the distance from the skimmer tip to the onset of the second Mach disk (this will

be discussed in greater detail in the next section), 14 fold of signal enhancement was observed. An additional 5-fold signal improvement was observed when the commercial Sciex 6000 nickel skimmer replaced the homemade skimmer. A similar finding has been reported by the independent work of Hu and Houk, who found that a ~ 5-fold signal enhancement was observed when the skimmer-first extraction lens separation is 2.4 cm in their homebuilt ICP-MS [76]. However, they did not address the fact that signal enhancement might be related to the mouth of the first extraction lens inside the zone of silence, before the onset of the second Mach disk.

Existence of the second Mach disk (?)

There are lots of collisions as gas passes through the sampler. Ten or more Mach disks can in succession in the first stage if no skimmer is present [77]. It has long been suspected that there is a shock wave at the skimmer tip. Niu and Houk measured the electron density (n_e) with axial spatial resolution throughout the sampling interface by the Langmuir probe method. They found that the electron density was significantly higher than expected near the skimmer tip, and n_e was lower than expected behind the skimmer [86]. According to Niu and Houk, the higher value of n_e just in front of the skimmer, coupled with lower than expected value behind the skimmer, could indicate the presence of a shock wave or other disturbance at the skimmer tip. This disturbance interferes with the direct gas flow and essentially causes a new expansion originating at the skimmer orifice.

Another method of assessing the possibility of the existence of a second expansion is through the calculation of Knudsen number (Kn). Kn is defined as the ratio of the mean free

path (λ) to the skimmer aperture (D_s). The value of Kn can be used to characterize the flow

regimes of gas dynamics [87].

Continuum flow (gas-gas collision dominating):   Kn < 0.01

Slip flow: 0.01 < Kn < 0.1

Transition flow (intermediate flow):   0.1 < Kn < 10

Free molecule flow (gas-surface collision dominating):   10 < Kn

We can estimate Kn for our ICP-TQMS system by the following equation:

$$Kn = \frac{\lambda}{D_s} = \frac{1}{\sqrt{2}\, \pi \, \sigma \, n \, D_s} \approx 0.3 \qquad (1)$$

where λ has unit of cm, σ is the gas kinetic cross section for Ar (4.1×10^{-15} cm^2) [77], D_s is

the diameter of the skimmer orifice (0.082 cm), and n is the number density of Ar atoms at

the skimmer entrance, which can be estimated from equation 2 [88]:

$$n = 0.161 n_0 \left(\frac{D_s}{x}\right)^2 \qquad (2)$$

Here x is the sampler-skimmer separation (1 cm), and n_0 is the Ar density in the ICP

($\sim 1.5 \times 10^{18}$ cm^{-3}), calculated from the ideal gas law at 1 atm and 5000 °K. From equation 2,

$n = 2.0 \times 10^{15}$ cm^{-3}. Using n substitutes in equation 1, Kn is equal to 0.3, and that is if there

is no disturbance at the skimmer tip. If there is a disturbance at the skimmer tip, n could be

much higher. This value is in agreement with the estimation of Kn for ICP-MS systems by

Douglas and French [87]. Because Kn = 0.3 is at the border of the intermediate gas flow

regime and the slip flow regime, whether the second expansion exists is questionable. On the

other hand, Kn would have to be > 10 ($\lambda \gg D_s$) for the beam to expand through the skimmer

with no collisions at all. Thus, some disturbance around the skimmer entrance would be

expected from collisions (there is an error in reference 79 page 796, the author inadvertently wrote that Kn has to be much less than unity for the beam to expand through the skimmer without collisions). The first extraction lens should not be placed near, at, or after the onset of the second Mach disk. For the first approximation, this onset of the second Mach disk can be calculated from the same equation used for the calculation of the first Mach disk [89]:

$$X_{m2} = 0.67 \, D_s \left(\frac{P_i}{P_2} \right)^{\frac{1}{2}} \tag{3}$$

$$P_i = 0.6595 \left(\frac{D_o}{X_s} \right)^2 P_o \tag{4}$$

where X_{m2} is the distance from the skimmer orifice to the onset of the second Mach disk, P_i is the impact pressure at skimmer orifice [78]. P_i varies from 2.85 to 5.40 Torr depending on the sampler-skimmer separation X_s (from 1.46 to 1.06 cm). D_o is the sampler orifice diameter (0.11 cm), P_o is the ICP pressure (760 Torr), and P_2 is the second stage pressure which depends on the type of skimmer used (homemade $D_s = 1.1$ cm, Sciex 6000 $D_s = 0.082$ cm), and varies between 1.9×10^{-5} and 5.3×10^{-5} Torr. Equation 3 has been confirmed experimentally by optical measurements of emission excited in the first Mach disk [90-93] for pressure ratios from 15 up to 17,000 [94]. X_{m2} calculated from equation 3 equals 5.48 cm for the homemade skimmer (Table 3). Apparently, the position of the first extraction lens measured from the skimmer tip in the original design (4.75 cm) is near but inside the region where the second Mach disk is formed. Extension A in Figure 5 would bring the first extraction lens deeper inside the zone of silence, and extension B would place the extraction lens ~ 2/3 = 3.50 / 5.48 the distance from the skimmer tip to the onset of the second Mach disk. This probably explains the 14-fold increased in sensitivity. If a Sciex 6000 skimmer

was installed, a total of 19-fold increase in sensitivity was observed (Table 3). Please note that the theoretical calculations are based on if there were no ion lenses behind the skimmer.

The argument of placing the first extraction lens inside the zone of silence of the second Mach disk preferably ~ 1/2 to 2/3 downstream the skimmer tip influencing the ion collection efficiency is illustrated by the results summarized in the bottom half of Table 3. Replacing the homemade skimmer (D_s = 1.1 cm) with the Sciex skimmer (D_s = 0.082 cm) lowered the second stage pressure significantly. The second expansion was pushed much farther downstream than before (9.08 versus 5.48 cm). The relative position of the first extraction lens to the second Mach disk measured from the skimmer tip had changed from near the onset of the second Mach disk (0.86) to deep inside the zone of silence (0.52). Therefore, the count rate of Li had increased from 2.2 x 10^5 to 10.6 x 10^5 cps (~ 4.8 fold) without actually changing the sampler-first extraction lens distance. Changing the sampler-skimmer separation from 1.06 to 1.31 cm lowered the impact pressure at skimmer tip and shrank the second expansion. If we were to keep the relative position of the first extraction lens to the onset of the second Mach disk the same, we would have to bring the extraction lens closer to the skimmer. Now the Li count rate increased from 10.6 x 10^5 to 27.7 x 10^5 cps (~ 2.6 fold). Similarly, further increasing the sampler-skimmer separation and keeping the first extraction lens inside the zone of silence, the count rate of Li increased 1.5 fold. The fact that even if we shifted the skimmer such that the skimming position is outside the optimum position (~ 1/2 to 2/3 to the onset of the first Mach disk), we could still observe signal enhancement because of three factors. First, the extraction lens remained inside the zone of silence; second, the impact pressure at skimmer tip decreased, which decreased the degree of ion collision and scattering; third, the new commercial skimmer transmitted

smoother gas flow than our aged homemade skimmer. The signal did not increase by the same factor as in the case of the homemade skimmer. This is because the skimmer position was outside the optimum skimming position with respect to the onset of the first Mach disk.

CARBON ISOTOPE RATIO MEASUREMENTS

Optimization

The ICP-TQMS device is optimized daily first with lithium (the closest convenient element near the molar mass of carbon) after the ICP is ignited and all electronics have warmed up for at least one hour. The instrument is then fine-tuned with standard α-D-glucose. The nebulizer gas flow rate is normally adjusted to achieve maximum count rate of ^{12}C on both channels A and B. Lastly, the voltages of the beam shift plates are adjusted for the best precision obtained in $^{13}C : ^{12}C$ isotope ratio measurements. A typical low-resolution mass spectrum of carbon is shown in Figure 6a, in the normal scale, the peak at m/z 13 is just noticeable. But on the expanded scale (Figure 6b), the peak at m/z 13 shows up clearly and is baseline resolved from m/z 12 and m/z 14. Notice the count rate differences between m/z = 12 and m/z = 13. Although carbon is only < 5% ionized in the ICP [2, 8], a plot of count rate versus concentration still shows linearity with $r^2 = 0.9997$ as illustrated in Figure 7. Figure 8a shows a typical carbon rinse out curve. Signals from both channels rinse out simultaneously in less than 2 minutes. The correlation plot of the entire rinse out curves is linear with $r^2 = 0.9989$ (Figure 8b).

Table 4 summarizes the results of $^{13}C : ^{12}C$ isotope ratio measurements of α-D-glucose at natural abundance from five different days. Each value is the average of 100 data

points of the same day with one quadrupole at m/z = 13, and the other quadrupole at m/z = 12. In general, the RSD% of the ratios is better than the RSD% of the individual signal. To be fair, the RSD% should always be compared to the best RSD% achievable at shot noise limit. Although carbon-13 is only ~ 1% of carbon-12, our ICP-TQMS can measure isotope ratios with count rate differences as great as 1 : 58 with precision only 1.5 times above the precision expected from counting statistics. This performance is attributed to two individual m/z values measured simultaneously and most of the flicker noise cancels when the ratio is calculated.

Calibration curve for isotope ratio

The measured ^{13}C : ^{12}C ratios in Table 4 are different from each other and from the natural abundance ratio (0.0111). This is mainly attributed to the reasons mentioned in the experimental section. Other causes of the bias originate from the ion beam splitter itself. The beam splitter is merely rested but not permanently mounted to the base inside the expansion chamber. It was intended to provide the flexibility of adjusting the splitter position to enhance the count rate of the minor isotope in ratio measurement. This is actually one of the inherent features of this device. Unfortunately, this in-born advantage causes some inconvenience to the operator. The ion beam splitter could be shifted slightly from its original position unintentionally, for example, opening or closing the diffusion pump gate valve located outside the chamber could shift the beam splitter a little despite the operator's efforts to minimize his or her movements. Other reasons are attributed to the quadrupole mass analyzers and detectors, which are not exactly identical, and have different mass bias,

transmission, and drift. Nevertheless, the measured isotope ratios can be related to the actual ratios with an external calibration curve such as the one shown in Figure 9. The least squares fit of these 8 points of the calibration curve shows the square of the correlation coefficient is essentially unity. The intercept approaches to zero and the slope reflex the split ratio of the system. The steeper the slope, the greater the deviation of the measured ratio from the actual ratio. Figure 9a illustrates the calibration curve split ratio approximately equal to 1 : 2.5. Even in an extreme case where the split ratio is ~ 1 : 12 (Figure 9b), meaning 12 parts of the ion beam were directed to one channel, and only 1 part of the beam was sent to the other channel, the calibration curve is still linear with $r^2 = 0.9996$. This is a very unique and useful application of the ion beam splitter for measuring very large or very small isotope ratio. At natural abundance, carbon-13 is only ~ 1% of carbon-12, the count rate of $^{13}C^+$ is ~ 99 times less than the count rate of $^{12}C^+$. Therefore, we can use a smaller portion of the ion beam for measuring the more abundant isotope and a bigger portion of the ion beam for measuring the less abundant isotope. In this fashion, we sacrifice the count rate of the major isotope for improving the count rate of the minor isotope. The altered isotope ratio can easily be related to the actual ratio with a calibration curve. The ICP-TQMS is calibrated daily to correct for mass bias anyway. The linearity of the calibration curve is reproducible from day to day and from month to month although the slopes and intercepts may vary. The mean correlation square (r^2) of six calibration curves is 0.9996 ± 0.0002 ($\pm$ SD).

Background signal and drift

Background correction

The average background measured at m/z = 13 and m/z = 12 is about 300 counts per second (cps) and 4000 cps respectively irregardless of solvent used (0.7% HNO_3 or d-H_2O). The ^{13}C : ^{12}C ratios obtained by mass scanning are 0.0111 ± 0.0008 (n = 7) for 0.7% HNO_3, and 0.0111 ± 0.0003 (n = 7) for H_2O. The measured ratios are essentially the same as the carbon natural abundant ratio (0.0111). The m/z 12 and 13 backgrounds mainly come from the dissolved CO_2 gas in the solution and from the background CO_2 gas or organic gases in the argon supply, and to a lesser extent m/z 13 also from the $^{12}C^1H^+$ ions. Since the typical ion count rates are ~ 1.2 x 10^5 cps at m/z = 12 and ~ 3500 cps at m/z = 13, these are much higher than the background count rates. They are at least 30 times above the background for m/z = 12 and 10 times above the background for m/z = 13. These levels of background are small enough to be subtracted accurately. Therefore, background correction is applied to all ^{13}C : ^{12}C ratio measurements of amino acid, protein, oligosaccharide, and the daily ion beam splitter calibration curve.

The background count rate at m/z = 12 is obtained by using an average of 30 data points before the signal rises, or after the signal drops, or by using an average of data from both these regions as indicated in Figure 10a. The corrected count rate at m/z = 12 is equal to the average of 100 data points of the total count rate at m/z 12 minus the background count rate. The same computation is applied to correct the count rate at m/z = 13. The corrected ^{13}C : ^{12}C ratio is equal to the corrected count rate at m/z = 13 divided by the corrected count rate at m/z = 12 (Figure 10b).

Drift correction

Slow instrumental drift usually occurs in all ICP-MS devices and the individual count rate drifts more severely than the ratio. Drift in the twin quadrupole device complicates the isotope ratio measurements. After the calibration curve has been established at the beginning of the day, the ICP standard is analyzed periodically, and a normalization factor K is used to correct for drift during data processing. K is defined as the measured ^{13}C : ^{12}C ratio at later time t divided by the measured ^{13}C : ^{12}C ratio at initial time t = 0 when the calibration curve was constructed. Any point of those 8 points that contributed to the calibration curve can be used to establish the normalization factor K, however, the first point (the non-enriched glucose standard) is usually employed to acquire K. The measured ^{13}C : ^{12}C ratio (R_m) from protein or carbohydrate samples is then multiplied by this factor K to yield a new ^{13}C : ^{12}C ratio called R_m'. R_m' is used in place of R_m for the calculation of the actual ratio using the daily beam splitter calibration curve. The calculated ratios R and the corresponding calibration curves are then reported as the final results in this report.

Carbon isotope ratio measurements of amino acid and protein

The largest amino acid of all - tryptophan [95] and an easily obtained and well-characterized globular protein - myoglobin were chosen for this study [96-99]. Table 5 summarizes the results of carbon isotope ratio measurements of tryptophan and myoglobin from two different days. Each data point shown in Table 5 is an average of 10 units resulting from 100 collected data points (refer to Table 2). In most cases, the RSD% is only 1.5 times above the counting statistics RSD%. In tryptophan, the mean ratios from two different days

are 0.0109 ± 0.0004 (n = 3) and 0.0107 ± 0.0001 (n = 4), which agree with each other. These ratios are not significantly different from the natural abundance ratio ($^{13}C : {}^{12}C = 0.0111$). For myoglobin, the mean ratios from two separate days are 0.0120 ± 0.0002 (n = 4) and 0.0129 ± 0.0001 (n = 4). These values are significantly higher than the natural abundance ratio, and they do not agree with each other (Table 5). The elevated m/z 13 : m/z 12 ratio seen from myoglobin could not come from the background, because tryptophan was also analyzed on the same day, under the same ICP-TQMS operating conditions. It is also unlikely that the observed 16% increase in m/z 13 : m/z 12 ratio is the actual $^{13}C : {}^{12}C$ ratio. A plausible explanation for the elevated m/z 13 : m/z 12 ratio is spectral interference at m/z = 13 ($^{12}C^1H^+$).

Origin of $^{12}C^1H^+$ ion

A plausible CH^+ source is from myoglobin itself. A myoglobin molecule is at least 800 times more massive than a tryptophan molecule (Table 6). It is very possible that a globular protein having a three-dimensional structure may not dissociate completely during a few milliseconds transit through the ICP. Some of the undissociated CH could be ionized to form CH^+ as shown in equation 1. The first ionization potential (IP) of CH is just 0.62 eV below the first ionization potential of carbon (equation 2) [100]. If carbon is ~ 5% ionized in the ICP [2, 8], then at least 5% of the total undissociated CH is also ionized to CH^+.

Equation 1:	CH	$\rightarrow$	$CH^+ + e^-$	IE = 10.64 eV
Equation 2:	C	$\rightarrow$	$C^+ + e^-$	IE = 11.26 eV
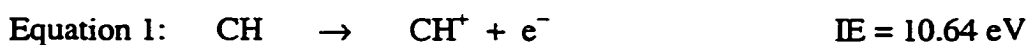
Another pathway that leads to the formation of CH^+ is through the attachment of H^+ to C neutral atom (equation 3), since carbon from myoglobin is only ~ 5% ionized in ICP, there are plenty of neutral C atoms available for H^+ to attach. But this requires equation 4 to take place. Although the first ionization potential of hydrogen is even higher than that of carbon, nevertheless, there are also plenty of H_2O molecules around to provide H atoms, and the bond dissociation energy of the hydrogen-oxygen bond of water is only ~ 5 eV [101].

Equation 3: $H^+ + C \rightarrow CH^+$

$-D_o(C-H^+) = -\{D_o(CH) + IE\ (H) - IE(CH)\}$

$= -\{3.465 + 13.60 - 10.64\}$

$= -6.42\ eV$

Equation 4: $H \rightarrow H^+ + e^-$ $IE = 13.60\ eV$

Equation 5: $H\text{-}OH \rightarrow H + OH$ $D_o(H\text{-}OH) = 5.16\ eV$
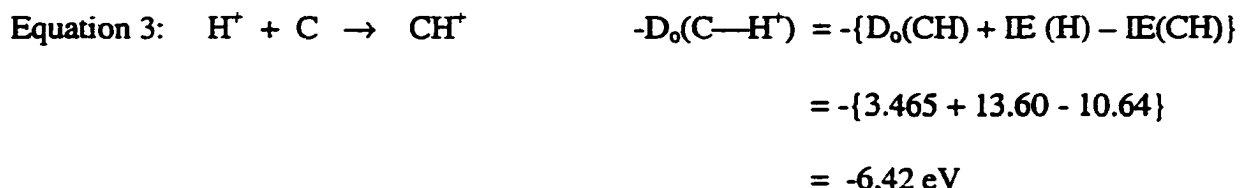
Theoretical calculation of $^{12}C^1H^+$: $^{12}C^+$ ratios arrived from 0.7% HNO_3, glucose, tryptophan, and myoglobin

The products of equation 1 and 3 can dissociate to form C^+ ion and H neutral atom as shown in equation 6, or to form C neutral atom and H^+ ion, the reverse of equation 3, but thermodynamically, equation 6 is more favorable:

Equation 6: $CH^+ \rightarrow C^+ + H$

$D_o(C^+-H) = D_o(CH) + IE\ (C) - IE\ (CH)$

$= 3.465 + 11.260 - 10.64$
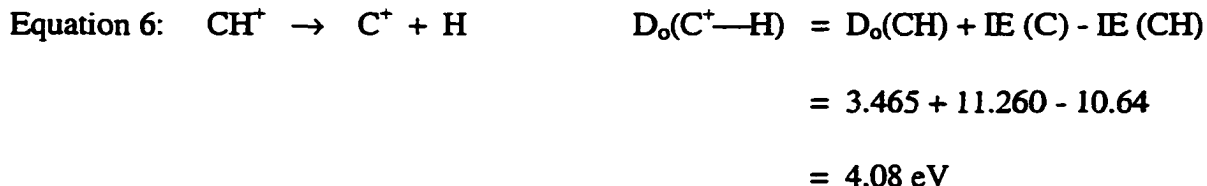
$= 4.08\ eV$

At local thermodynamic equilibrium, the dissociation constant K_d of CH^+ is related to the number density of CH^+, C^+, and H^+.

$$CH^+ \rightleftharpoons C^+ + H \qquad\qquad K_d(CH^+) = (n_H)\frac{n_{C^-}}{n_{CH^+}}$$

$$\log K_d(CH^+) = 1.5\log T_{gas} - 5040\, D_0/T_{gas}$$
$$+ \log(M_{C^-}\, M_H/M_{CH})$$
$$+ \log(Z_{C^-}\, Z_H/Z_{CH^+}) + 20.274$$

where D_0 is the bond dissociation energy of CH^+ (4.08 eV), M is the atomic or the molecular weight (g mol^{-1}), Z is the total partition function and T_{gas} is in K [100]. Since the necessary spectroscopic constants of CH^+ have been measured [100], the above equation can be substituted with the alternative equation as shown below, assuming that the electronic partition function of CH^+ equals the statistical weight of the ground electronic state [100]:

$$\log K_d = 0.5\log T_{gas} - 5040\, D_0/T_{gas}$$
$$+ \log(M_{C^-}\, M_H/M_{CH^+})$$
$$+ \log(Z_{C^-} Z_H)$$
$$+ \log(1 - 10^{-0.625\omega/T_{gas}})$$
$$+ \log(B/g) + 20.432$$

where ω is the vibrational constant (2739.7 cm^{-1}), B is the rotational constant (14.177 cm^{-1}), and g (1) is the statistical weight of the ground electronic state of CH^+ [100].

It is reasonable to assume that $n_H \approx 8 \times 10^{16}$ cm^{-3} in the plasma [102, 103]. If the ratio n_{C^-}/n_{CH^+} is measured, then K_d (CH^+) and T_{gas} can be calculated from the above equation. The ratio n_{C^-}/n_{CH^+} can be estimated from the experimental measured m/z 13 : m/z 12 ratio.

$$\frac{I(m/z\,13)}{I(m/z\,12)} = \frac{n\left(^{13}C^+\right)}{n\left(^{12}C^+\right)} + \frac{n\left(^{12}CH^+\right)}{n\left(^{12}C^+\right)} = \frac{^{13}C^+}{^{12}C^+} + \frac{^{12}C^1H^+}{^{12}C^+}$$

where $^{13}C^+ : ^{12}C^+$ is the natural abundance ratio 0.011/0.989, and the quantity $\left(^{12}C^1H^+/^{12}C^+\right)$ is approximately equal to n_{CH^-}/n_{C^-}.

The calculated n_{CH^-}/n_{C^-} ratios and the calculated T_{gas} values for 0.7% HNO$_3$, tryptophan, glucose, and myoglobin are summarized in Table 6. Based on the calculated T_{gas}, T_{gas} of 0.7% HNO$_3$ > T_{gas} of tryptophan > T_{gas} of glucose > T_{gas} of myoglobin, we can deduce that myoglobin is the most difficult atomized species, and tryptophan is the easiest atomized species. The $^{12}C^1H^+ / ^{12}C^+$ ratio is highest when myoglobin is the sample, therefore the relative error is the largest (Table 7). The calculated $^{12}C^1H^+ / ^{12}C^+$ ratio from 0.7% HNO$_3$ background is only ~ 8 x 10^{-6}, which corresponds to an insignificant error of < 0.07% in the carbon isotope ratio measurements. This supports our previous argument that the observed elevated m/z 13 : m/z 12 ratios of myglobin (Table 4) do not come from the background. It indeed comes from the analyte itself. The level of CH$^+$ however does appear to depend on the nature of the analyte. This is even more obvious when we compare the measured m/z 13 : m/z 12 values between glucose and tryptophan, in which the latter has a larger molecular mass and a stable aromatic ring [95]. Yet a significant relative error of 13% is found in ^{13}C : ^{12}C ratios from glucose, with little error from in tryptophan under the same ICP-MS operating conditions. The measured m/z 13 : m/z 12 ratio of myoglobin on this day (Table 7) is even higher than the measured m/z 13 : m/z 12 ratios on previous days (Table 5). This is an indication that $^{12}C^1H^+$ species is rather sensitive to the ICP-MS operating conditions from day to day. This might be the key to success in eliminating the $^{12}C^1H^+$ interference species.

Elimination of $^{12}C^1H^+$ interference species

There are several parameters we could manipulate to lessen the formation of $^{12}C^1H^+$ ions. Since protein molecules tend to absorb a lot of H_2O, each myoglobin molecule is hydrated with 74 H_2O molecules [104, 105]. Thereby, removing as much H_2O as possible before sending the myoglobin aerosols to the ICP can help to decrease the formation of $^{12}C^1H^+$ ions through the reduction of n_H in equation 5, 4, and 3 mentioned in the previous section. This can be done by increasing the heater temperature behind the ultrasonic nebulizer. Another parameter that can be manipulated is the aerosol gas flow rate. Lowering the aerosol gas flow rate shrinks the axial channel of the ICP and changes the locations of the analyte emission and ionization zones, therefore changing the sampling position. The new sampling position is now farther downstream from the tip of the initial radiation zone [106], and the protein molecules are dissociated more completely, thus help in reducing the abundance of $^{12}C^1H^+$ ions.

To test each parameter, the twin quadrupole mass spectrometer is operating in mass scanning mode. This offers an advantage of eliminating the calibration curve for the ion beam splitter, and the result can be obtained immediately. Another reason is related to our past experiences with this device. When a standard solution is nebulized, say lithium, with mass analyzers A and B both monitoring m/z 7 (^7Li), merely changing the aerosol gas flow rate can change the count rate of channel A and channel B, thus changing the ^7Li : ^7Li ratio. Since one of our test parameters is to adjust the aerosol gas flow rate, using only one quadrupole ensures that if any changes in the m/z 13 : m/z 12 ratios are indeed caused by the change of $^{12}C^1H^+$ count rate and not such an artifact. Standard glucose is used for the initial

testing to optimize the ICP-MS operating conditions such that the measured m/z 13 : m/z 12 ratio is the same as the natural abundance ratio. A second purpose of first using glucose is to conserve the protein solutions and preserve the sampler-skimmer cones because it usually takes 30 minutes or so to find such conditions.

A typical mass spectrum of carbon is shown in Figure 6. To obtain the true m/z 13 : m/z 12 ratio, the spectrum was first corrected for background using the count rate at m/z = 8, where there are no ions. The m/z 13 : m/z 12 ratio is then calculated by taking the ratio of the corrected areas under the peaks at these two m/z values. The area under the curve equals to the sum of the count rates that are enclosed by the curve.

$$\frac{m/z\ 13}{m/z\ 12} = \frac{\sum \text{corrected count rate of } m/z\ 13}{\sum \text{corrected count rate of } m/z\ 12}$$

The results are summarized in Table 7. In these tests, α-D-glucose was used and the heater temperature of the desolvater was increased to 160 °C (20 °C higher than normal). Merely decreasing the aerosol gas flow rate by ~ 5% decreases the relative error (RE) from ~13% to ~5% which is more than half. Further decreasing the aerosol gas flow rate by another ~ 3% decreases the RE% to < 1%. Decreasing the RF forward power while keeping the aerosol gas flow rate unchanged decreases the RE% by half. Lastly, changing the extraction voltage from –150 to –170 V does not influence the ^{13}C : ^{12}C ratio significantly. Clearly, the $^{12}C^1H^+$ species is most sensitive to the aerosol gas flow rate. Therefore, carefully adjusting this condition can eliminate $^{12}C^1H^+$ interference ions.

Using the best ICP-MS conditions for glucose to test for myoglobin, having both mass analyzers now operating in single ion monitoring modes, the effect of pH on ^{13}C : ^{12}C

ratio measurements of myoglobin are also investigated. The measured ^{13}C : ^{12}C ratios of

myoglobin in H_2O, 1.55 x 10^{-5} M HNO_3 (pH 4.81), and 1.55 x 10^{-3} M HNO_3 (pH 2.81) are

0.0113 ± 0.0003 (n = 5), 0.0112 ± 0.0005 (n = 3), and 0.0112 ± 0.0002 (n = 4) respectively.

It does not seem to matter what pH environment myoglobin is in, these solvent conditions

have no influence on ^{13}C : ^{12}C ratio measurements. The ^{13}C : ^{12}C ratio is also confirmed by

mass scanning and equals to 0.0112 which is in agreement with the values obtained by single

ion monitoring. The myoglobin result using H_2O as solvent was repeated approximately a

week later to assess the reproducibility of the method. The ^{13}C : ^{12}C values listed in Table 8

agree with the ^{13}C : ^{12}C values mentioned above. This proves that the optimization method is

reliable and reproducible. The RSD% of each ^{13}C : ^{12}C ratio measurement is either at or near

the RSD% calculated at shot noise limit (Table 8).

Carbon isotope ratio measurements of oligosaccharide

The operating conditions were first optimized with standard glucose solution until the

result from mass scanning showed that ^{13}C : ^{12}C is at natural abundance. Using the

conditions that work for glucose, carbon isotope ratio from β-cyclodextrin is measured

(Table 8). It is rather interesting that glucose is so much smaller than β-cyclodextrin and

myoglobin, and yet whatever ICP-TQMS condition works for glucose also works for β-

cyclodextrin and myoglobin. By observation, of the latter two, β-cyclodextrin is actually

more susceptible to $^{12}C^1H^+$ interference than myoglobin. The measured carbon isotopic

composition in β-cyclodextrin exhibits a natural abundance ratio. Again, the RSD% of

individual isotope ratio measurement is either near or at the RSD% expected from counting statistics.

In all of these measurements, the count rate of ^{13}C is no more than few thousand counts per second. There are two ways to enhance the count rate of ^{13}C artificially. One way is to increase the voltage of the detector that detects the minor isotope negatively; and another way is to shift the ion beam splitter off the central axis, so that most of the ion beam is sent to the channel that measures the minor isotope. These are in fact two unique features of this twin quadrupole device. The effect of detector voltages on the count rate of $^{13}C^+$ is shown in Table 9. As the detector A ($^{13}C^+$) voltage increases negatively with detector B ($^{12}C^+$) voltage unchanged (-2300 V), the count rate of $^{13}C^+$ increases, and the RSD% of the individual count rate measured at $^{13}C^+$ improves accordingly (from 4.72% to 3.63%). This is because at low count rate level (shot noise limiting regime), the noise level is proportional to the square root of the signal only; thus, there is a signal to noise enhancement advantage. However, the RSD% of ^{13}C : ^{12}C ratio remains about the same, and this is probably because the count rate of $^{13}C^+$ does not improve enough to influence the precision of the ratio significantly. The precision of the ratio is still limited by the total count of the minor isotope at shot noise limit. By simply changing the detector A voltage from -2300 to -2700 V, the count rate of ^{13}C nearly doubles. In this fashion, the resultant ^{13}C : ^{12}C ratio is also changed (Table 9). With the detector A voltage set at -2500 V, ^{13}C : ^{12}C ratio of β-cyclodextrin is determined. The results shown in Table 10 are already corrected for mass bias using the same optimization conditions that work for glucose. The mean ^{13}C : ^{12}C ratio reported in Table 10 (0.0112 ± 0.0002) (n = 5) is basically the same as the one shown in Table 8. Once

again, the precision of individual isotope ratio measurement is either close to or the same as the counting statistics limit.

A second way of artificially enhancing the count rate of the minor isotope (^{13}C) is by shifting the ion beam splitter off the central axis. The calibration curve now has a very steep slope as shown earlier in Figure 10. The idea is to send most of the ion beam through the channel that detects the minor isotope. Nevertheless, increasing the detector voltage is preferable than moving the splitter, because the latter is much more labor intensive and is irreversible. It involves venting the system, opening the chamber, and aligning the splitter. In addition, the count rate of the major isotope is sacrificed for the improvement of the count rate of the minor isotope.

OVERALL PERFORMANCE CHARACTERISTICS OF THE ICP-TQMS

A related question is whether this ICP-TQMS device can always measures isotope ratios with precision as good as expected from the counting statistics. To answer such a question, a long-term study was conducted over 5 months. During this time, the twin quadrupole device had performed a total of 267 isotope ratio measurements of carbon (^{13}C : ^{12}C, ^{12}C : ^{12}C) and a total of 124 isotope ratios measurements of lithium (^{6}Li : ^{7}Li, ^{7}Li : ^{7}Li). In the case of carbon, the results show that ~ 80 out of 100 times the precision of isotope ratio measurements of carbon is better than 2 times the precision expected from the counting statistics; 35 out of 100 times, the precision is as good as that expected from the counting statistics. For lithium, the ICP-TQMS performs a little bit better. Approximately 90% of the RSD% of isotope ratio measurements are within 2 times the RSD% calculated from the

counting statistics, and ~50% of the time the RSD% is as good as that expected from the counting statistics. Although we only investigated the RSD% of isotope ratio measurement of one easily ionized element and one difficult ionized element, in a very qualitative point of view, this does reflect the overall performance characteristics of this twin quadrupole device.

CONCLUSION

Theoretical calculation supports the premise that there are numerous collisions at the skimmer orifice as the gas passing through. A second supersonic expansion behind the skimmer is possible when the gases expand from first stage to second stage. Placing the first extraction lens deep inside the zone of silence of the second supersonic jet improves ion collection efficiency. The overall count rate from both channels has improved at least 19 times.

Carbon isotope ratio measurements of non-volatile organic compounds have also been demonstrated with our prototype inductively coupled plasma twin quadrupole device. At present, the precision is ~ 1 %RSD, which is sufficient for stable carbon isotope metabolic tracer studies. The ICP-TQMS system could be coupled with different protein separation techniques. For example, online high performance liquid chromatography (HPLC), size exclusion chromatography (SEC), isoelectric focusing (IEF), or capillary gel electrophoresis (CGE) could reduce the total analysis time. With the unique abilities of canceling flicker noise during isotope ratio measurement and artificially enhancing the count rate of the minor isotope, the ICP-TQMS could develop into an alternative method to GC-combustion-IRMS for rapid carbon isotope ratio determination in non-volatile bio-organic molecules.

ACKNOWLEDGEMENT

REFERENCES

1. Houk, R. S. *Acc. Chem. Res.* **1994,** *27,* 333.

2. Jarvis, K. E.; Gray, A. L.; Houk, R. S. *Handbook of ICP-MS*: Blackie, London, and Chapman and Hall, New York, **1992,** pp. 18, 22, 230.

3. Montaser, A.; Golightly D. W. (Eds.) *ICPs in Analytical Atomic spectrometry,* 2nd edn: VCH, London, **1992.**

4. Montaser, A. (Ed.) *Inductively Coupled Plasma Mass Spectrometry*: VCH, New York, **1996**

5. Evans, E. H.; Giglio, J. J.; Castillano, T. M.; Caruso, J. A. *Inductively Coupled and Microwave Induced Plasma Sources for Mass Spectrometry*: The Royal Society of Chemistry, Cambridge, UK, **1995,** Chap. 2 and pp. 29, 51, 89.

6.   Hieftje G. M.; Norman, L. A. *Int. J. Mass Spectrom. Ion Process*, **1992**, *118/119*, 519.

7.   Begley, I.; Sharp, B. L. *J. Anal. At. Spectrom.* **1994**, *9*, 171.

8.   Houk, R. S. *Anal. Chem.* **1986**, *58*, 97A-105A.

9.   Russ III, G. P. *"Isotope Ratio Measurements Using ICP-MS"*, *in Applications of ICP-MS*, Date, A. R.; Gray, A. L. (Eds): Blackie, London, **1989**, p.108.

10.   Janghorbani, M.; Ting, B. T. G. *"Stable Isotope Tracer Applications of ICP-MS"*, *in Applications of ICP-MS*, Date, A. R.; Gray, A. L. (Eds): Blackie, London, **1989**, Chap. 5.

11.   Ting, B. T. G.; Janghorbani, M. *Spectrochim. Acta, Part B*, **1987**, *42B*, 21.

12.   Serfass, R. E.; Thompson, J. J.; Houk, R. S. *Anal. Chim. Acta*, **1986**, *188*, 73.

13.   Furuta, N. *Anal. At. Spectrom.* **1991**, *6*, 199.

14.   Ketterer, M. E.; Peters, M. J.; Tisdale, P. J. *J. Anal. At. Spectrom.* **1991**, *6*, 439.

15.   Whittaker, P. G.; Barrett, J. F. R.; Williams, J. G. *J. Anal. At. Spectrom.* **1992**, *7*, 109.

16.   Walder, A. J.; Koller, D.; Reed, N. M.; Hutton, R. C.; Freedman, P. A. *J. Anal. At. Spectrom.* **1993**, *8*, 1037.

17.   Walder, A. J.; Furuta, N. *Anal. Sci.* (Japan) **1993**, *9*, 675.

18.   Walder, A. J.; Abell, I. D.; Platzner, I.; Freedman, P. A. *Spectrochim. Acta, Part B* **1993**, *48B*, 397.

19.   Esat, T. M. *Int. J. Mass Spectrom. Ion Processes* **1995**, *148*, 159.

20.   Swihart, G. H. *Rev. Mineral.* **1996**, *33*, 845.

21.   De Lacter, J. R.; Rosman, K. J. R.; Loss, R. D. *At. Energy Can. Ltd. AECL 1996* (AECL-11342), **1996**, *8*, 8.

22.   Hattori, K.; Menagh, D. and Cole, T. J. S. *Anal. Chem.* **1998**, *70*, 4100-4105.

23. Heumann, K. G. *At. Energy Can. Ltd., AECL 1996 (AECL-11342),* **1996,** 2, 2

24. Schwieters, J. B.; Bach, P. *At. Energy Can Ltd. AECL 1996 (AECL-11342),* **1996,** *49,* 49.

25. Warren, A. R.; Allen, L. A.; Pang, H. M.; Houk, R. S.; Janghorbani, M. *Appl. Spectrosc.* **1994,** *48,* 1360-1366.

26. Myers, S. A.; Tracy, D. H. *Spectrochim. Acta, Part B* **1983,** *38B,* 1227.

27. Belchamber, R. M.; Horlick, G. *Spectrochim. Acta, Part B* **1982,** *37B,* 1037.

28. Mermet, J. M.; Ivaldi, *J. Anal. At. Spectrom.* **1993,** *8,* 795.

29. Ivaldi, J. C.; Barnard, T. W. *Spectrochim. Acta, Part B* **1993,** *48B,* 1265.

30. Travis, J. C.; Winchester, M. R.; Salit, M. L.; Wythoff, B. J.; Scheeline, A. *Spectrochim. Acta, Part B* **1993,** *48B,* 691.

31. Winge, R. K.; Eckels, D. E.; DeKalb, E. L.; Fassel, V. A. *J. Anal. At. Spectrom.* **1988,** *3,* 849-855.

32. Allen, L. A.; Pang, H. M; Warren, A. R.; Houk, R. S. *J. Anal. At. Spectrom.* **1995,** *10,* 267-271.

33. Allen, L. A.; Leach, J. J.; Pang, H. M.; Houk, R. S. *J. Anal. At. Spectrom.* **1997,** *12,* 171-176.

34. Luong, E. T.; Du, Z. Y.; Houk, R. S. *Unpublished data,* **1998.**

35. Sugimoto, A. *Geochem. J.* **1996,** *30,* 195

36. Goni, M.A.; Eglinton, T.I. *Org. Geochem.* **1996,** *24,* (*6-7, Proceedings of the 17th International Meeting on Organic Geochemistry, Pt. 2, 1995*), 601.

37. Meier-Augenstein, W.; Watt, P. W.; Langhans, C. D. *J. Chromatogr. A.* **1996,** *752,* 233.

38. McRae, C.; Love, G. D.; Murray, I. P; Snape, C. E.; Fallick, A. E. *Anal. Commun.* **1996**, *33*, 331.

39. Henner, U.; Mosandl, A.; Hagenauer-Hener, U.; Dietrich, H. *Wein-Wiss.* **1995**, *50*, 113.

40. Aguilera, R.; Becchi, M.; Casabianca, H.; Hatton, C. K.; Catlin, D. H.; Starcevic, B.; Pope, H.G., Jr. *J. Mass Spectrom.* **1996**, *31*, 169.

41. Abramson, F. P.; Osborn, B. L.; Teffera, Y. *Anal. Chem.* **1996**, *68*, 1971-1972.

42. Popp, B. N.; Sansone, F. J.; Rust, T. M. *Anal. Chem.* **1995**, *67*, 405-411.

43. Sansone, F. J.; Popp, B. N.; Rust, T. M. *Anal. Chem.* **1997**, *69*, 40-44.

44. Matthew, D. E.; Hayes, J. M. *Anal. Chem.* **1978**, *50*, 1465-1473.

45. McKinney, C. R.; McCrea, J. M.; Epstein, S.; Allen, H. A.; Urey, H. C. *Rev. Sci. Instrum.* **1950**, *21*, 724.

46. Sweeley, C. C.; Elliott, W. H.; Fries, J.; Ryhage, R. *Anal. Chem.* **1966**, 38, 1549.

47. Freedman, K. H.; Gillyon, E. C. P. and Jumeau, E. *J. Am. Lab.* **1988**, *13*, 1123-1129.

48. Wong, W. W.; Clarke, L. L.; Johnson, G. A.; Llaurador, M.; Klein, P. D. *Anal. Chem.* **1992**, *64*, 354-358.

49. Silfer, J. A.; Engel, M. H.; Macko, S. A.; Jumeau, E. J. *Anal. Chem.* **1991**, *63*, 370-374.

50. Caimi, R. J.; Brenna, J. T. *Anal. Chem.* **1993**, *65*, 3497-3500.

51. Luke, A. H.; Schoeller, D. A. *Anal. Chem.* **1995**, *67*, 3086-3088.

52. Luong, E. T.; Houk, R. S. *Unpublished dat*, **1997**.

53. Lichtfouse, E.; Budzinska, H. *Analysis* **1995**, *28*, 364.

54. Routh, J.; Cifuentes, L. A. *Adv. Anal. Geochem.* **1995**, *2*, 283.

55. Brand, W. A. *J Mass Spectrom.* **1996**, *31*, 225

56. Gillson, G. R.; Douglas, D. J.; Fulford, J. E.; Halligan, K. W.; Tanner, S. D. *Anal. Chem.* **1988**, *60*, 1472.

57. Chambers, D. M.; Hieftje, G. M. *Spectrochim. Acta, Part B* **1991**, *46*, 761.

58. Chambers, D. M.; Poehlman, J.; Yang, P.; Hieftje, G. M. *Spectrochim. Acta, Part B* **1991**, *46*, 741.

59. Chambers, D. M.; Ross, B. S.; Hieftje, G. M. *Spectrochim. Acta, Part B* **1991**, *46*, 785.

60. Tanner, S. D. *Spectrochim. Acta, Part B* **1992**, *47*, 809.

61. Tanner, S. D.; Cousins, L. M.; Douglas, D. *J. Appl. Spectrosc.* **1994**, *48*, 1367.

62. Tanner, S. D.; Douglas, D. J.; French, J. B. *Appl. Spectrosc.* **1994**, *48*, 1373.

63. Chen, X.; Houk, R. S. *Spectrochim. Acta, Part B* **1995**,

64. Falk, H. *J. Anal. At. Spectrom.* **1992**, *7*, 255.

65. Taylor, H. E.; Garbarino, J. R. in *Inductively Coupled Plasmas in Analytical Atomic Spectrometry*, Montaser, A.; Golightly, D. W.: VCH, New York, **1992**, pp 651-677.

66. Douglas, D. J.; Kerr, L. A. *J. Anal. Atomic Spectrom.* **1988**, *3*, 749-752.

67. Vaughan, M. A.; Horlick, G. *Spectrochim. Acta, Part B* **1990**, *45B*, 1289-1299.

68. Hu, K.; Clemons, P. S.; Houk, R. S. *J. Am. Soc. Mass Spectrom.* **1993**, *4*, 16-27.

69. Hu, K. *Ph.D Thesis, Iowa State University.* **1992**, *chapter 3*, p100.

70. Chilton, R. *Unpublished data*, Chilton, **1993**.

71. Turner, P. J. Some observations on mass bias effects occurring in ICP-MS systems, in Holland, G. and Eaton, A. N. (eds.), *Applications of Plasma Source Mass Spectrometry*: The Royal Society of Chemistry, Cambridge, UK, 1991, p 71.

72. Douglas, D. J.; French, J. B. *J. Anal. At. Spectrom.* **1988**, *3*, 743.

73. Kantrowitz, A.; Grey, J. *Rev. Sci. Instrum.* **1951**, 22, 328.

74. Campargue, R. *J. Phys. Chem.* **1984**, 88, 4466.

75. Douglas, D. J.; Kerr, L. A. *J. Anal. At. Spectrom.* **1988**, 3, 749.

76. Hu, K. *Ph.D Thesis, Iowa State University,* **1992,** chapter 1, p18.

77. Niu, H.; Houk, R. S. *Spectrochim. Acta, Part B* **1996**, 51, 779-815.

78. Li, G.; Duan, Y.; Hieftje, G. M. *J. Mass Spectrom.* **1995**, 30, 841.

79. Chen, X.; Houk, R. S. *Spectrochim. Acta, Part B* **1996**, 516, 41.

80. Hobbs, S. E.; Olesik, J. W. *Appl. Spectrosc.* **1991**, 45, 1395.

81. Olivares, J. A.; Houk, R. S. *Anal. Chem.* **1985**, 57, 2674-2679.

82. Nagy, G. A.; Szilagyi, M. *Introduction to the Theory of Space-Charge Optics:* Halsted Press, New York, Macmillan and London, **1974**.

83. Szilagyi, M. *Electron and Ion Optics:* Plenum Press, New York, **1988**, p 313.

84. Humphries, S. *Charged Particle Beams:* John Wiley & Son, New York, **1990**, p 834.

85. Amad, M. H. and Houk, R. S. *J. Anal. At. Spectrom.* **1998**, 13, 223-228.

86. Niu, H. S.; Houk, R.S. *Spectrochim. Acta, Part B* **1994**, 49, 1283.

87. French, J. B. *Molecular Beam for Rarefied Gasdynamic Research:* NATO-AGARD Fluild Dynamics Panel, Paris, **1966**, p 6.

88. Douglas, D. J.; French, J. B. *J. Anal. Atomic Spectrom.* **1988**, 3, 743-747.

89. Ashkenas, H.; Sherman, F. S. *Rarefied Gas Dynamics, Fourth Symposium IV,* Volume 2: De Leeuw, J. H. (Ed), Academic Press, New York, **1966**, p 84.

90. Houk, R. S.; Lim, H. B. *Anal. Chem.* **1986**, 58, 3244.

91. Lim, H. B.; Houk, R. S.; Edelson, M. C.; Carney, *J. Anal. At. Spectrom.* **1989**, 4, 365.

92. Kawaguchi, H.; Asada, K.; Mizuike, A. *Mikrochim. Acta* **1988**, 3, 143.

93. Luan, S.; Pang, H. M.; Houk, R. S. *J. Anal. At. Spectrom.* **1996**, *11*, 247.

94. French, J. B. *Molecular Beam for Rarefied Gasdynamic Research*: NATO-AGARD Fluid Dynamics Panel, Paris, **1966**, p 22.

95. Darell, J.; Lodish, H.; Baltimore, D. *Molecular Cell Biology*: Scientific American Books, New York, New York, **1986**, p90.

96. Go, M. *Nature.* **1981**, *291*, 90.

97. Phillips, D. C.; Richards, F. M. *Altas of molecular structures in biology*: Clarendon Press, Oxford, **1973**.

98. Zubay, G. *Biochemistry*: Wm. C. Brown, Duguque, Iowa; Melbourne, Australia; Oxford, England. **1993**, p109.

99. Kagen, L. J. *Myoglobin; biochemical, physiological, and clinical aspects*: Columbia University Press, New York, **1973**.

100. Huber, K. P.; Herzberg, G. *Molecular Spectra and Molecular Structure IV. Constants of Diatomic Molecules*: Van Nostrand Reinhold, New York, **1979**.

101. Weast, R. C.; Astle, M. J. *CRC Hand Book of Chemistry and Physics*: CRC Press, Boca Raton, Florida, **1981-82**, F-192.

102. Chamber, D. M.; Poehlman, J.; Yang, P.; Hieftje, G. M. *Spectrochim. Acta Part B* **1991**, *46*, 741.

103. Olesik, J. W.; *Winter Conference on Plasma Spectrochemistry*, Cambridge, UK, January **1995**, Paper No. 15.

104. Sherwood, C.; Mauk, A. G.; Brayer, G. D. *J. Mol. Biol.* **1987**, *193*, 227.

105. Evans, S. V.; Brayer, G. D. *J. Mol. Biol.* **1990**, *213*, 885.

106. Koirtyohann, S. R.; Jones, J. S. and Yates, D. A. *Anal. Chem.* **1980**, *52*, 1965.

Table 1. Instrumental components of the ICP-TQMS

ICP

Plasma Therm generator

(now RF Plasma Products)

Model HFP-2000D

RF Plasma Products torch box

(modified in-house for horizontal operation

with home-made copper shielding box)

Ion extraction

Ames Laboratory construction

interface

Vacuum system*

Three stages differential pumping

Welded stainless steel

Ames Laboratory construction

Mass analyzers

VG Plasma Quad

Model SPX 300 with RF-only pre-filters

Model SPX 603 Controllers and RF Generators

Table 1. Instrumental components of the ICP-TQMS (cont.)

Detectors	ETP discrete dynodes
	Model AF 562A
Counting	EG & G ORTEC
electronics	Model 660 dual 5 kV bias supply
	Model 9302 amplifier / discriminator
	Model 994 dual counter / timer

*Details in reference 32

Table 2. ICP-MS general operating conditions

Radio frequency	27.12 MHz
Forward power	1.25 kW
Reflected power	< 5 W
Argon flow rate:	
Argon cooling gas	15 L / min
Nebulizer gas	0.9 L / min*
Auxiliary gas	1.1 L / min
Cetac U-5000 ultrasonic nebulizer:	
Desolvating system	140 °C
Condenser	4 °C
Solution uptake rate	1 mL / min
Differential pumping:	
First stage pressure	1.4 Torr
Second stage pressure	2×10^{-4} Torr
Third stage pressure	1.1×10^{-5} Torr

Table 2. ICP-MS general operating conditions (cont.)

Data collecting and processing:

Single ion monitoring mode	1.5 ms dwell time per data point, 10 point per unit, 10 units.
Mass scanning mode	1.5 ms dwell time per channel, 10 channels per m/z

*Selected on a daily basic to maximize the signal for $^{12}C^+$ and to minimize the signal for $^{12}CH^+$

Table 3. Effect of skimmer-first extraction lens separation on ion collection efficiency

Type of skimmer	X_s (cm)	X_e (cm)	X_{sk-e} (cm)	X_{m1} (cm)	X_s/X_{m1}	P_i (Torr)	P_1 (Torr)	P_2 (10^{-4} Torr)	X_{m2} (cm)	X_{sk-e}/X_{m2}	Total cps [Li]/ppm (10^5)	Factor of improvement
Home-made	1.06	5.81	4.75	1.65	0.64	5.40	1.51	5.3	5.48	0.86	2.2	1.0
		5.06	4.00							0.73	17.2	7.8
		4.56	3.50							0.64	31.5	14.3
Sciex 6000	1.06	5.81	4.75	1.72	0.63	5.40	1.40	1.9	9.08	0.52	10.6	4.8
	1.31	5.06	3.75		0.78	3.53			7.34	0.48	27.7	12.5
	1.46	4.56	3.10		0.86	2.85			6.59	0.47	42.0	19.1

X_s = sampler-skimmer separation

X_e = sampler-first extraction lens separation

X_{sk-e} = skimmer-first extraction lens separation

X_{m1} = onset of the 1st Mach disk measured from tip of sampler

P_i = impact pressure (see text)

P_1 = first stage pressure (~5% variation)

P_2 = second stage pressure (~15% variation)

X_{m2} = onset of the 2nd Mach disk measured from tip of skimmer

cps = count per second

Table 4. Carbon isotope ratio measurements of α-D-glucose

$^{13}C^+$ (cps)* ; RSD%	$^{12}C^+$ (cps) ; RSD%	$^{13}C^+ / {}^{12}C^+$; RSD%	Counting statistics RSD%
3372 ; 1.75%	188000 ; 2.62%	0.0180 ; 1.65%	1.42%
5079 ; 3.67%	269000 ; 4.40%	0.0189 ; 0.91%	1.16%
3860 ; 1.11%	165000 ; 1.26%	0.0233 ; 1.32%	1.33%
3350 ; 0.96%	197000 ; 1.76%	0.0171 ; 1.42%	1.42%
3230 ; 2.67%	87700 ; 5.51%	0.0338 ; 1.22%	1.52%

*cps = counts per second

Table 5. Carbon isotope ratio measurements of tryptophan and myoglobin

Calibration curve	Tryptophan $^{13}C^+ / {}^{12}C^+$; RSD%	Counting Statistics RSD%	Myoglobin $^{13}C^+ / {}^{12}C^+$; RSD%	Counting Statistics RSD%
y = 5.844x r² = 0.9994	0.0113 ; 2.94%	1.64%	0.0122 ; 1.63%	1.61%
	0.0107 ; 3.06%	1.68%	0.0118 ; 2.91%	1.64%
day 1	0.0107 ; 2.92%	1.67%	0.0117 ; 2.38%	1.70%
			0.0122 ; 3.13%	1.66%
mean ± SD	**0.0109 ± 0.0004**		**0.0120 ± 0.0002**	
y = 1.608x r² = 0.9993	0.0107 ; 2.31%	1.98%	0.0129 ; 2.54%	1.90%
	0.0108 ; 2.28%	1.97%	0.0127 ; 1.92%	1.77%
day 2	0.0107 ; 3.14%	1.97%	0.0130 ; 2.25%	1.62%
	0.0106 ; 2.82%	1.97%	0.0129 ; 1.32%	1.60%
mean ± SD	**0.0107 ± 0.0001**		**0.0129 ± 0.0001**	

Table 6. Theoretical calculations of T_{gas} for 0.7% HNO_3, tryptophan, glucose, and myoglobin

	Calculated K_d (CH^+)	Measured m/z 13 : m/z 12	T_{gas} (°K)	Calculated $^{12}C^1H^+$ / $^{12}C^+$	%RE
0.7% HNO_3	2.3×10^{21}	0.0111	~ 5600	7.6×10^{-6}	< 0.07%
Tryptophan	1.4×10^{21}	0.0113	~ 4200	1.8×10^{-4}	~ 1.6%
α-D-glucose	1.9×10^{19}	0.0126	~ 3500	1.5×10^{-3}	~ 13%
Myoglobin	8.3×10^{18}	0.0147	~ 3300	3.6×10^{-3}	~ 32%

Table 7. Effect of ICP-MS operating conditions on $^{13}C^+$ / $^{12}C^+$ ratio measurements of α-D-glucose

Extraction lens (V)	RF forward power (KW)	Aerosol gas flow rate (L / min)	$^{12}C^+$ 10^3 (cps) ; RSD%	$^{13}C^+$ / $^{12}C^+$ from mass scanning	Relative error %
-150	1.30	0.882	532 ; 3.6%	0.0126 ± 0.0002 (n = 7)	13.3%
-150	1.30	0.834	370 ; 3.3%	0.0117 ± 0.0003 (n = 6)	5.2%
-150	1.25	0.834	432 ; 2.5%	0.0114 ± 0.0003 (n = 7)	2.5%
-150	1.30	0.810	656 , 3.0%	0.0112 ± 0.0002 (n = 7)	0.7%
-170	1.30	0.810	1213 ; 3.8%	0.0111 ± 0.0003 (n = 5)	0.02%

Table 8. Carbon isotope ratio measurements of myoglobin and β-cyclodextrin

myoglobin $^{13}C^+/{}^{12}C^+$; RSD%	Counting statistics RSD%	β-cyclodextrin $^{13}C^+/{}^{12}C^+$; RSD%	Counting statistics RSD%
0.0110 ; 1.64%	1.65%	0.0115 ; 0.97%	1.40%
0.0107 ; 1.80%	1.65%	0.0111 ; 1.40%	1.66%
0.0114 ; 1.82%	1.66%	0.0110 ; 1.32%	1.48%
0.0104 ; 1.52%	1.66%	0.0112 ; 2.02%	1.40%
		0.0109 ; 1.88%	1.40%
0.0109 ± 0.0004*		**0.0111 ± 0.0002***	

Calibration curve: $y = 1.3802x + 0.0446$ $r^2 = 0.9996$

*mean ± SD

Table 9. Effect of detector voltage on count rate of $^{13}C^+$

Detector A voltage (V)	Quadrupole A $^{13}C^+$ (cps)* ; RSD%	Quadrupole B $^{12}C^+$ (cps) ; RSD%	$^{13}C^+ / {}^{12}C^+$; RSD%	Counting statistics RSD%
-2300	5080 ; 4.72%	269000 ; 4.40%	0.0189 ; 0.91%	1.16%
-2400	6070 ; 4.63%	278000 ; 4.10%	0.0218 ; 1.05%	1.06%
-2500	7260 ; 4.28%	282000 ; 4.28%	0.0258 ; 1.16%	0.97%
-2600	8240 ; 3.98%	275000 ; 4.69%	0.0300 ; 1.13%	0.91%
-2700	9620 ; 3.63%	280000 ; 4.38%	0.3439 ; 1.06%	0.85%

*Counts per second

Table 10. Carbon isotope ratio determination of β-cyclodextrin with detector A voltage set at -2500 V

$^{13}C^+$ (cps) ; RSD%	$^{12}C^+$ (cps) ; RSD%	$^{13}C^+ / {}^{12}C^+$; RSD%	Counting statistics RSD%
6720 ; 3.59%	300000 ; 2.91%	0.0113 ; 1.36%	1.01%
6800 ; 2.77%	304000 ; 3.41%	0.0111 ; 1.66%	1.00%
6950 ; 1.89%	310000 ; 1.54%	0.0110 ; 0.97%	0.99%
7040 ; 1.02%	310000 ; 1.75%	0.0113 ; 1.33%	0.98%
7040 ; 3.16%	308000 ; 2.23%	0.0114 ; 1.48%	0.98%
		0.0112 ± 0.0002*	

$y = 1.654x + 0.0049 \quad r^2 = 0.9997$

*mean ± SD

ICP

Sampler ——/\—— Ground

Skimmer ——/\—— Ground

Extraction lens ⌐| |⌐ -70 V

⌐| |⌐ -18.0

—— —— -2.14

Differential → pumping orifice, -26.9V

◼☐◼ ← Beam shift plates: Left -2.39 V

Right -1.14

Top -1.01

Bottom -1.01

Beam splitter

-72.0 -75.4

-207 -82.3

-62.8

-165 -168

-28 -25

0.36 -16

Quadrupole A   Quadrupole B
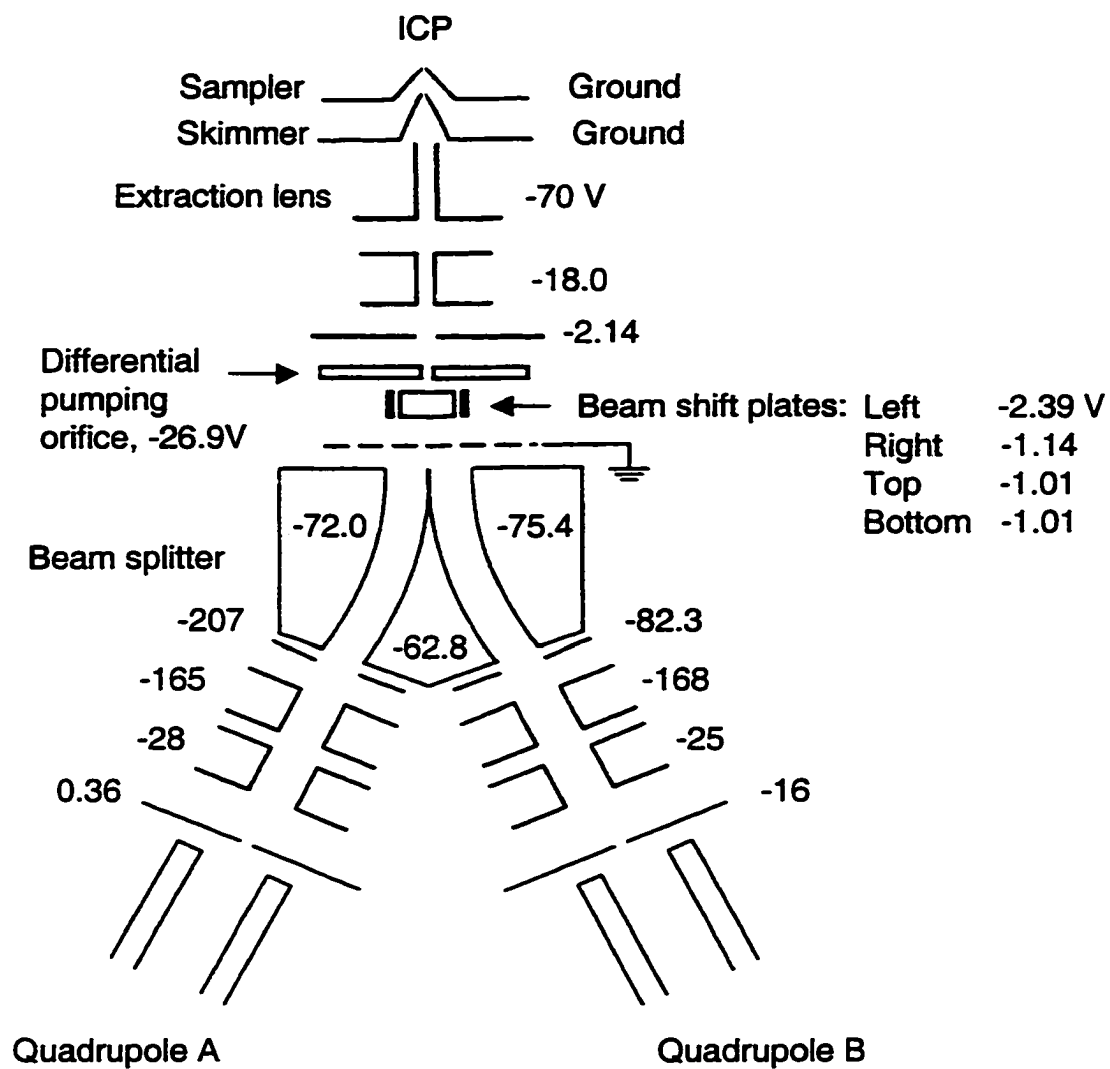
Figure 1. Schematic diagram of the twin quadrupole mass spectrometer.
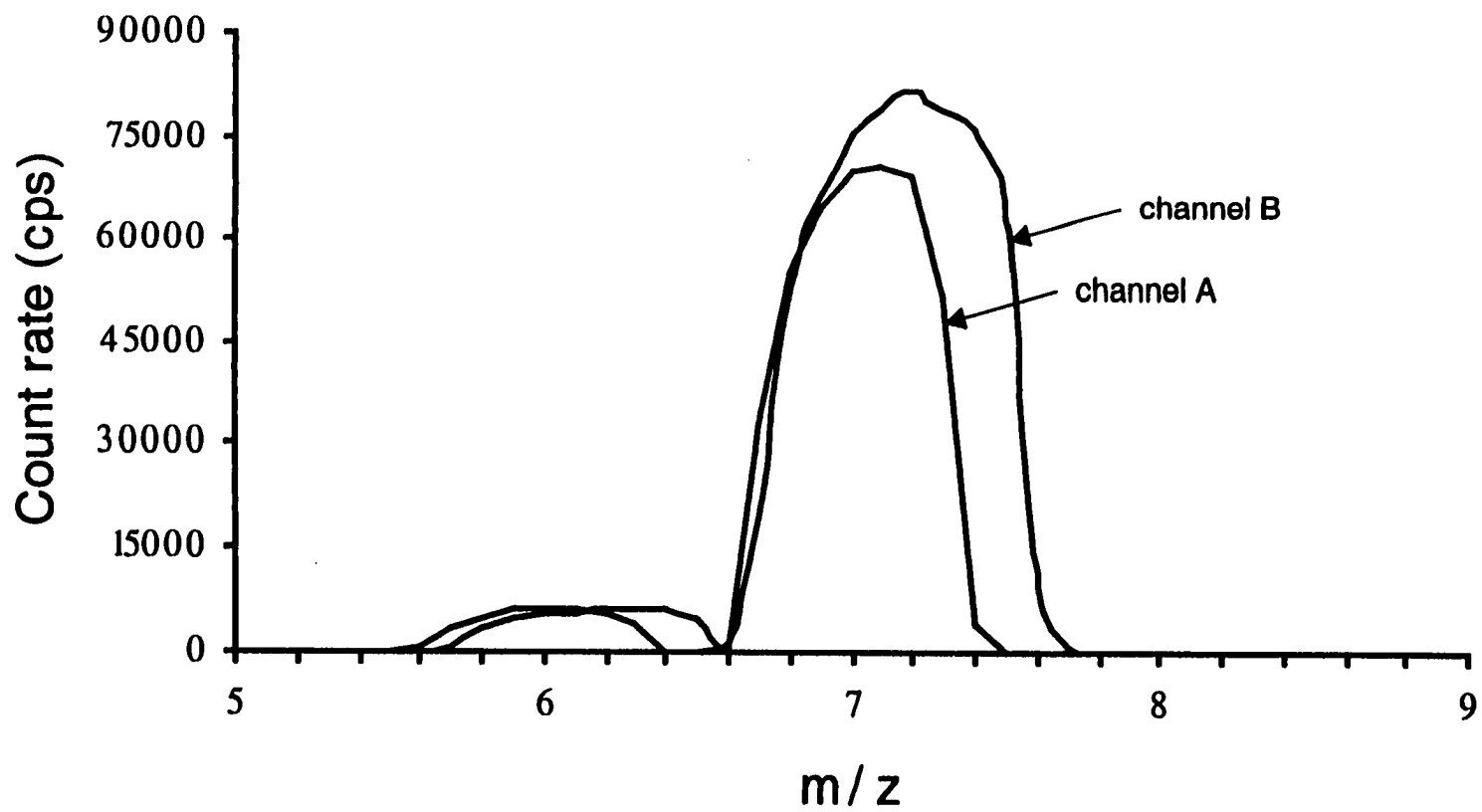
Figure 2. Low resolution mass spectrum of 0.2 ppm Li / H_2O.
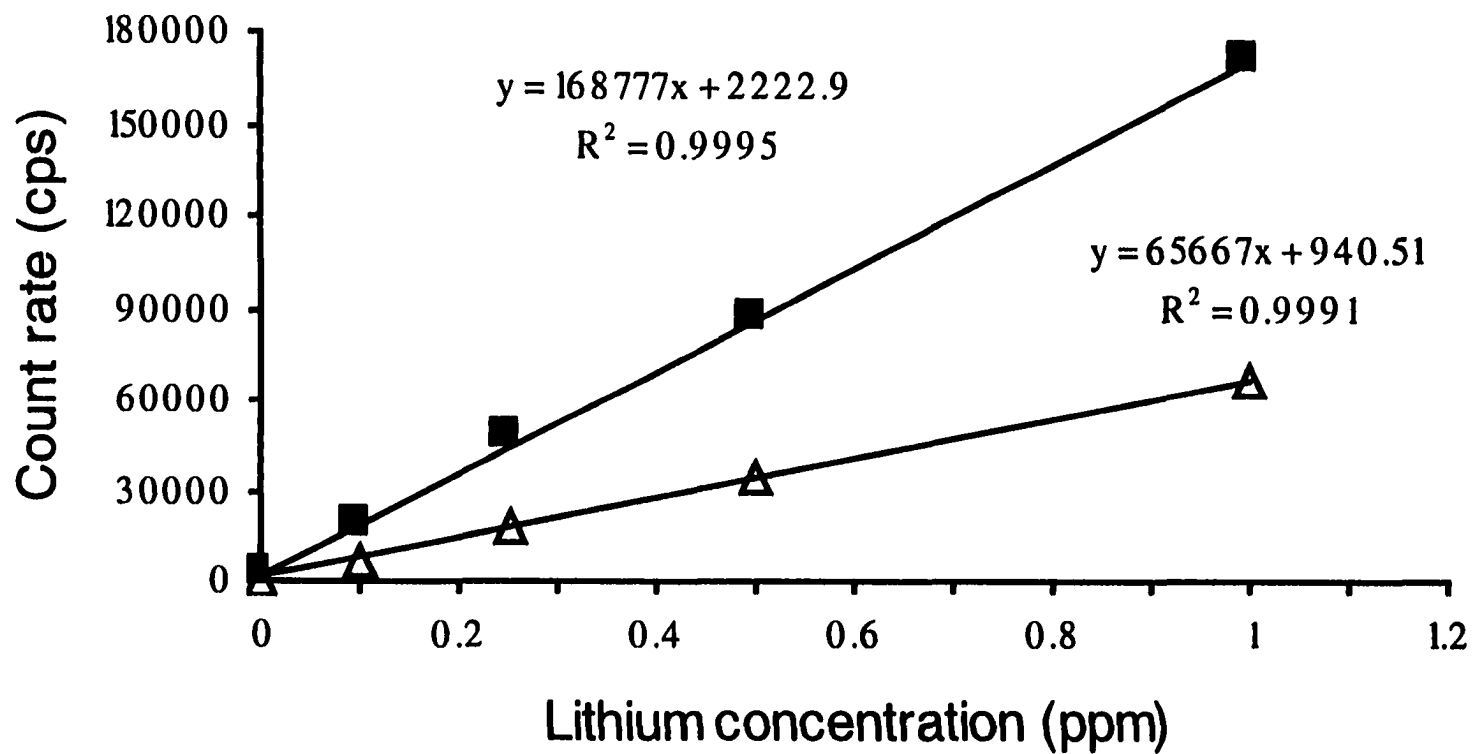
Figure 3. Lithium standard curves. Solvent is H_2O. Signals on channel A and B are monitored

simultaneously. On this day, channel B (top regression line) is approximately 3 times

more counts than channel A (bottom regression line).
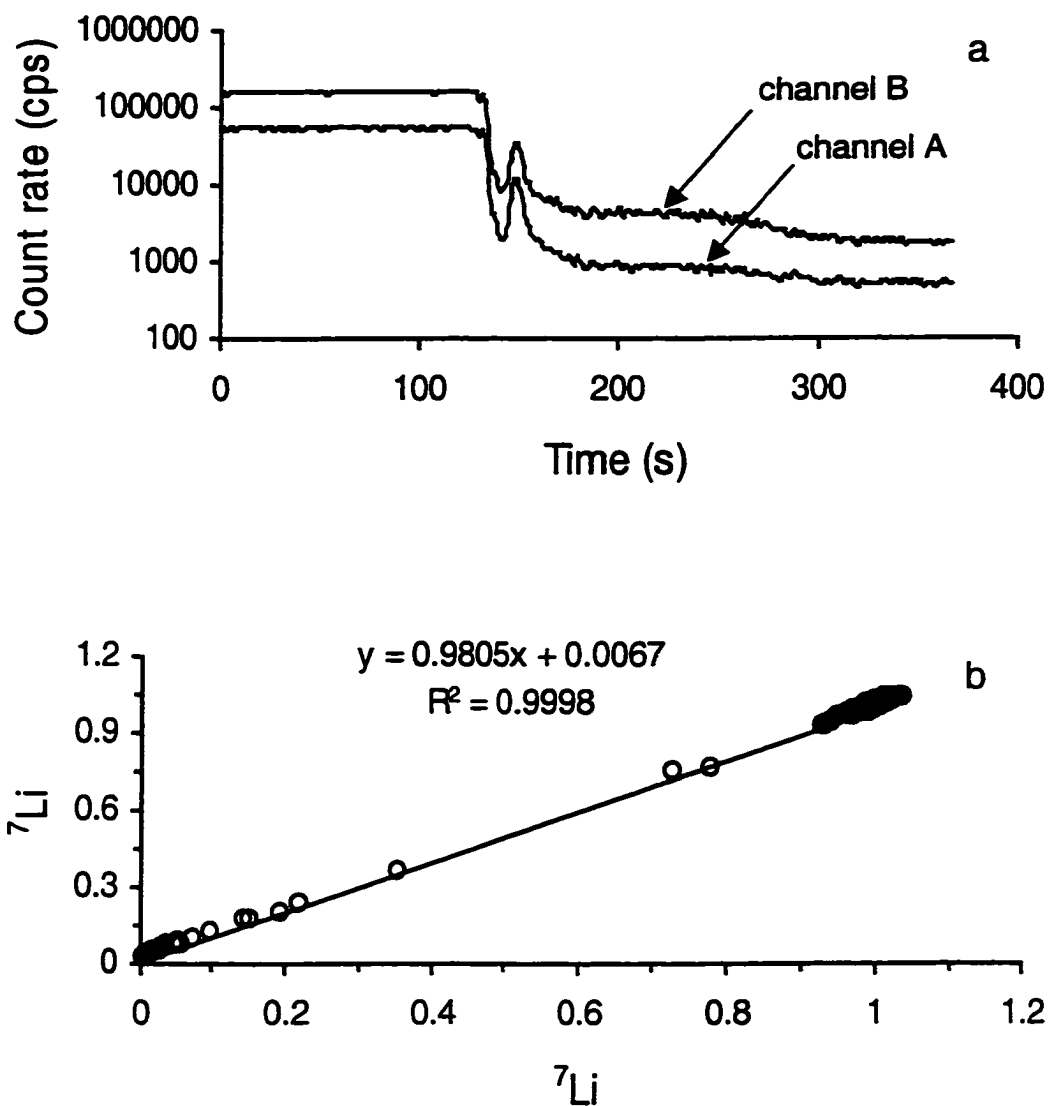
Figure 4. a) Rinse out curve of 1 ppm Li / H_2O with water. Count rates at

channel A and channel B were monitored simultaneously at m/z = 7. b)

Correlation plot of (a), a plot of normalized count rate of ^7Li at channel A

versus the normalized count rate of ^7Li at channel B.
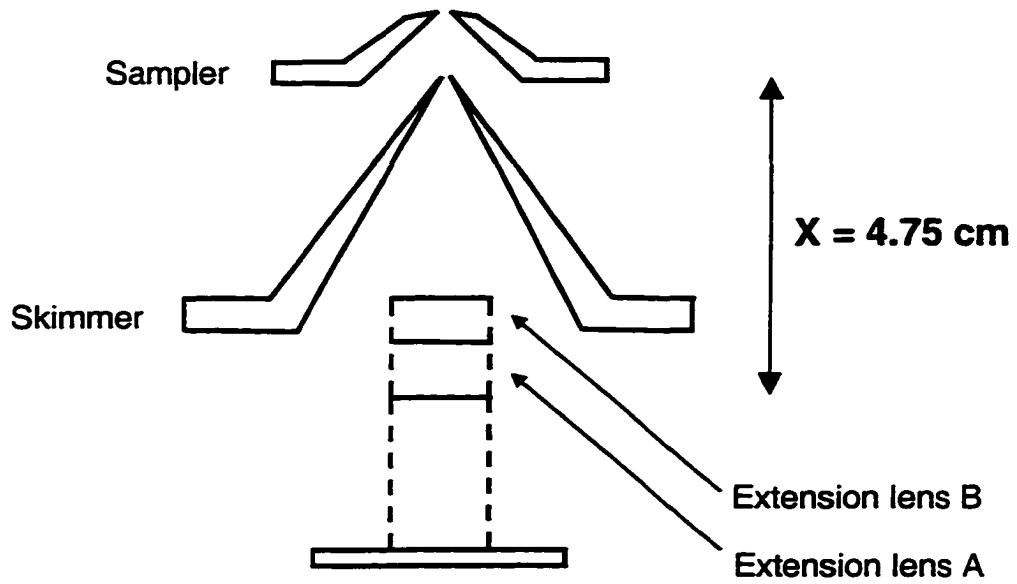
Figure 5. Schematic diagram of the ICP-MS interface, showing the relative position of sampler, skimmer, and the first extraction lens.
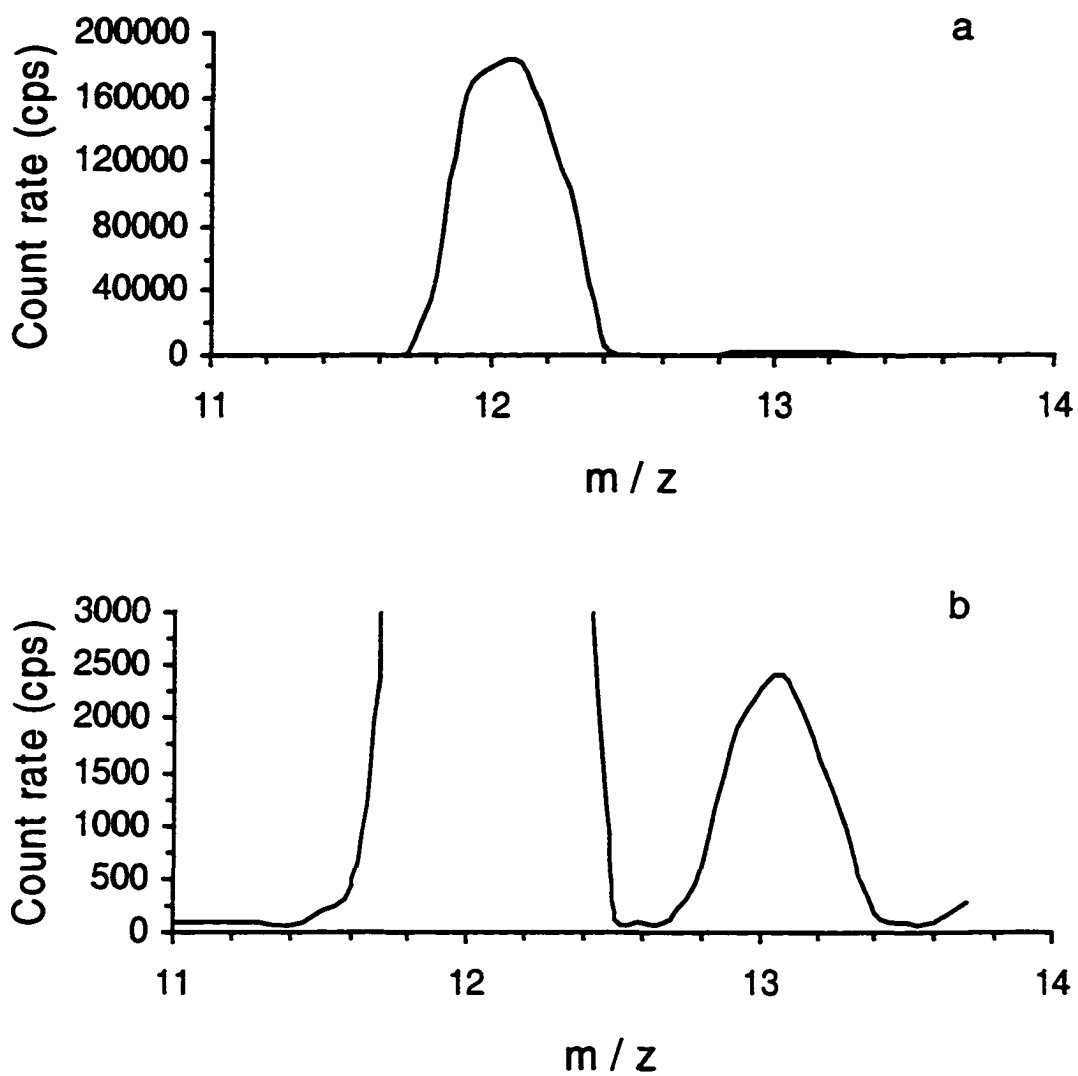
Figure 6. Low resolution mass spectra of 1000 ppm glucose in H_2O.

a) normal spectrum b) expanded spectrum.

$$y = 429.73x + 278.19$$
$$R^2 = 0.9997$$
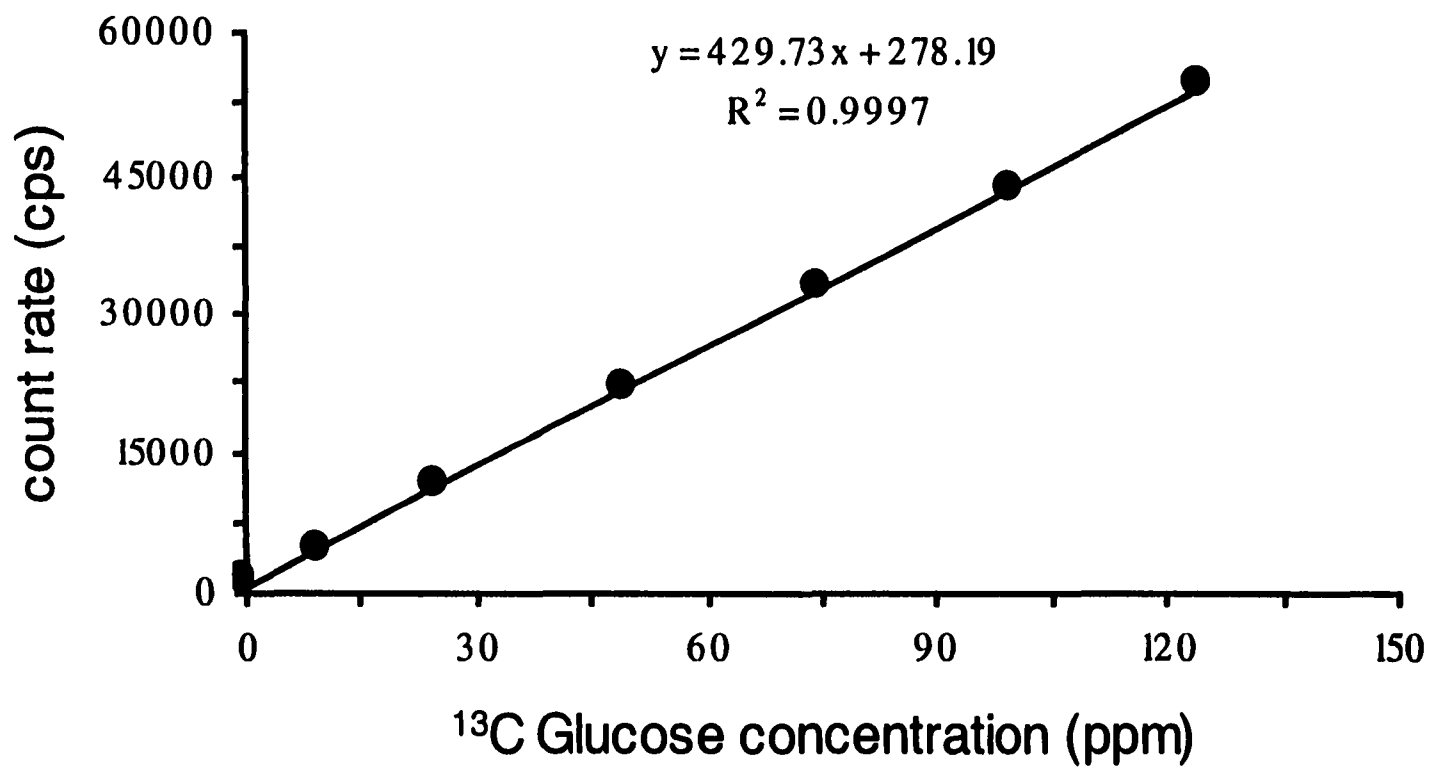
Figure 7. Carbon standard curve.
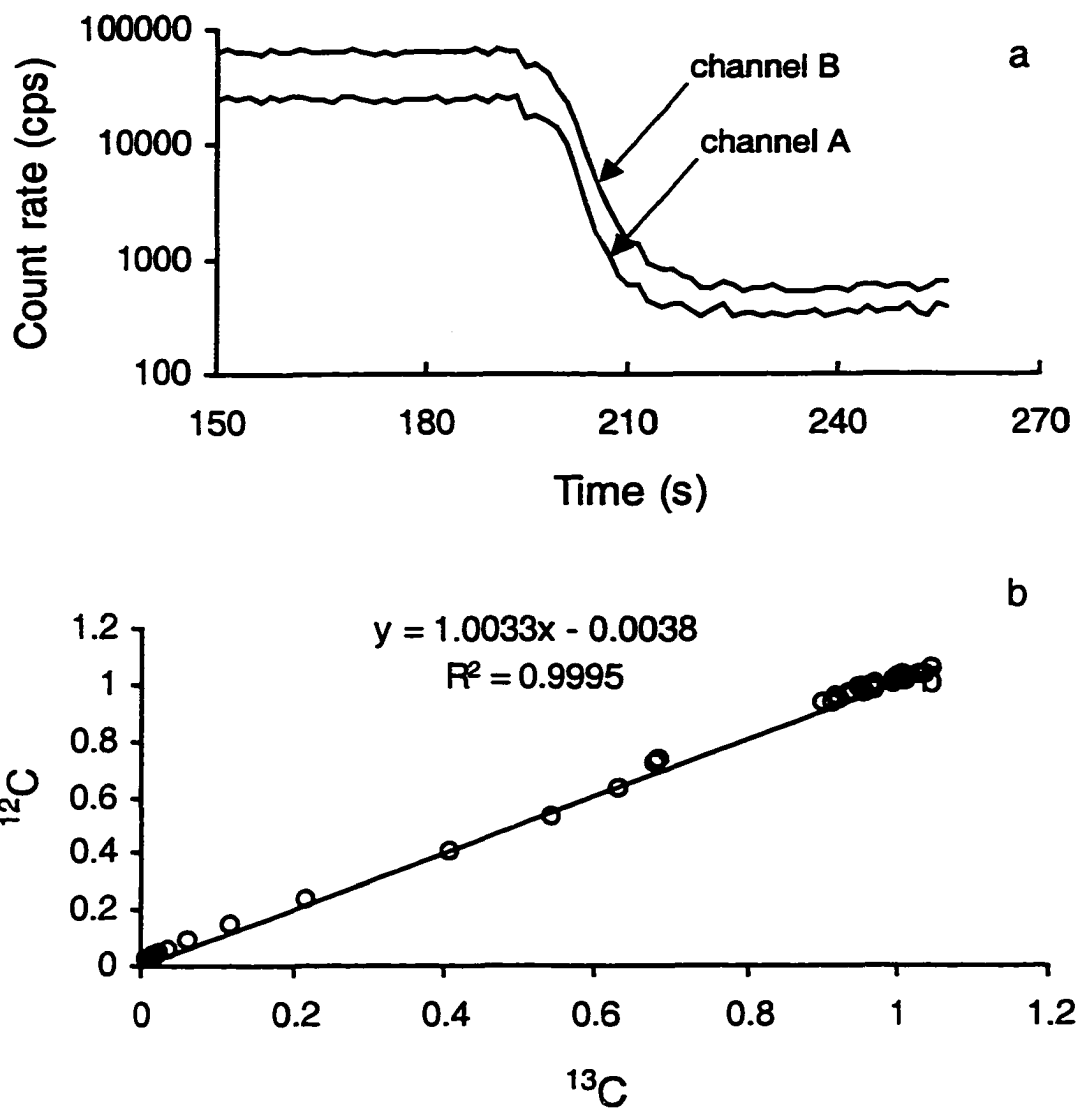
Figure 8. a) Rinse out curve of 500 ppm α-D-glucose / H_2O enriched with equal amount of ^{13}C-glucose. Count rates at channel A and channel B were monitored simultaneously at m/z = 13 and m/z = 12 respectively. b) Correlation plot of (a), a plot of normalized count rate of ^{12}C at channel B versus the normalized count rate of ^{13}C at channel A.
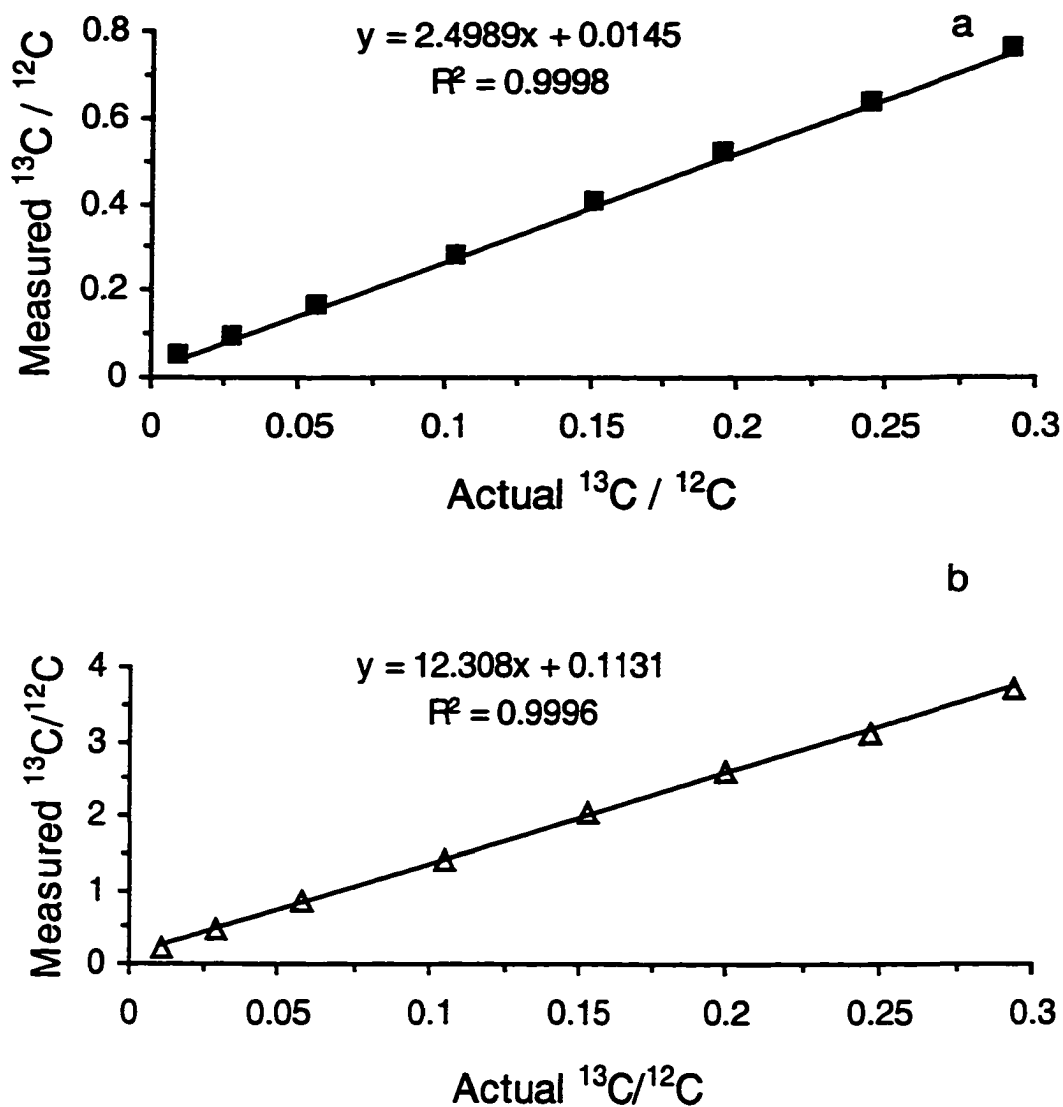
Figure 9. Calibration curve of the ICP-TQMS. Standard 1000 ppm α-D-glucose at natural abundance was spiked with different amount of ^{13}C-glucose. The x-axis represents the actual ^{13}C/^{12}C ratios after spiking. The y-axis is the measured ^{13}C/^{12}C ratios from the ICP-TQMS device. The uncertainty of the individual point is smaller than the symbol. a) split ratio is ~2.5. b) split ratio is ~ 12.
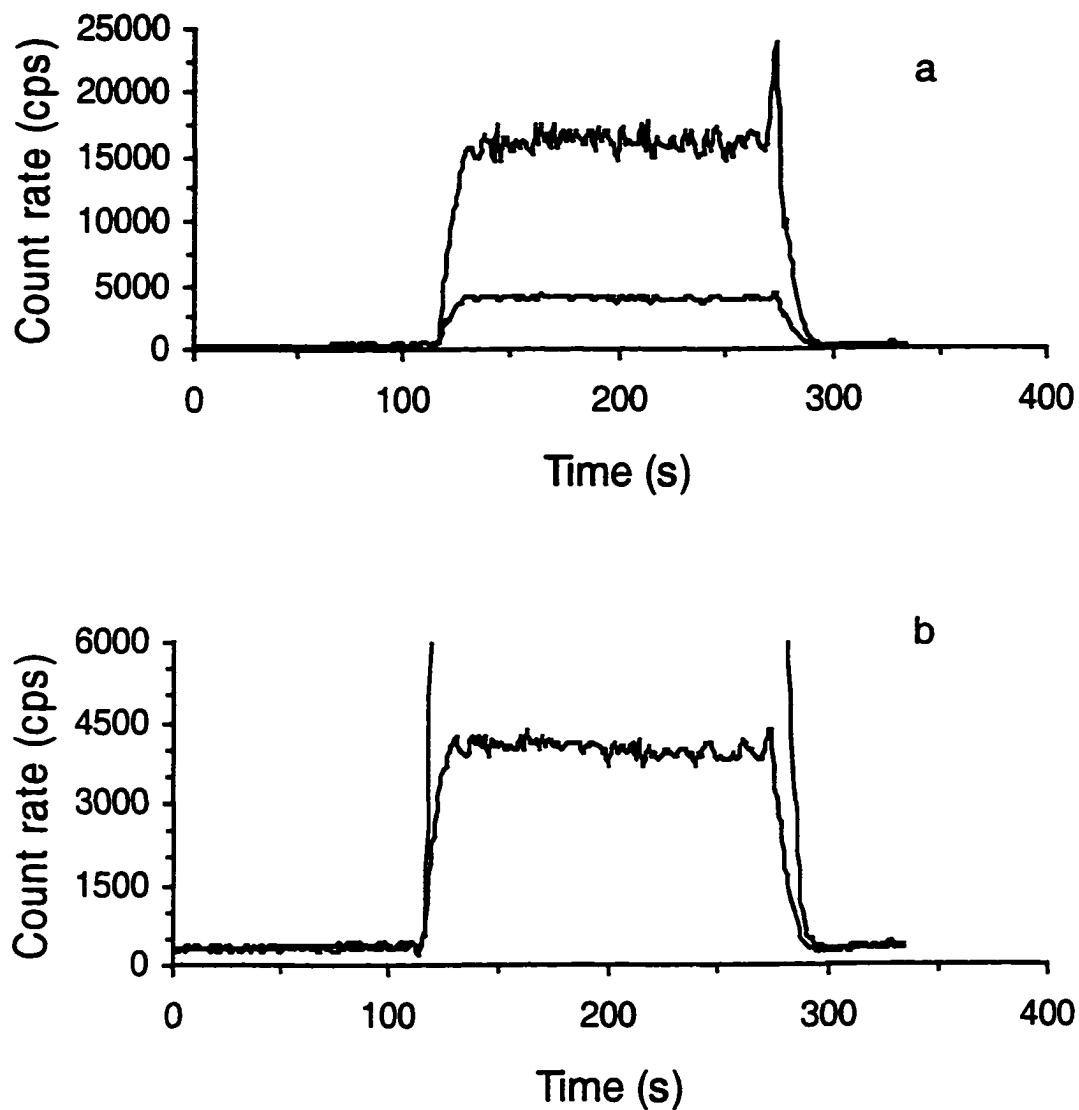
Figure 10. Illustration of background correction with a solution of 1000 ppm

α-D-glucose at natural abundance. a) plot on normal scale, top curve is monitored

at m/z = 12 on channel B (signal / background = 55), bottom curve is monitored at

m/z = 13 on channel A (signal / background = 12). b) plot on expanded scale

showing signal rises and falls at m/z = 13.

CHAPTER 4. METHODS FOR IMPROVING ION TRANSMISSION AND PRECISION DURING ISOTOPE RATIO MEASUREMENTS WITH THE INDUCTIVELY COUPLED PLASMA TWIN QUADRUPOLE MASS SPECTROMETER

A paper to be submitted to the Journal of the American Society of Mass Spectrometry

Elise T. Luong and R. S. Houk[1]

ABSTRACT

A second-generation ion beam splitter is designed for improving ion transmission efficiency for the inductively coupled plasma twin-quadrupole mass spectrometer. The original design of the ion beam splitter is also modified for this purpose. By simply cutting back and rounding off the razor like front edge of the current beam splitter, transmission of ions is improved by 5 times while maintaining the performance characteristics of the instrument as a whole. Isotope ratios for copper and argon are measured with relative standard deviation (RSD%) of 0.39% and 0.25% respectively, which are close to the limiting precision predicted by counting statistics (0.33% for copper, and 0.19% for argon). Effects of dwell time and total ion collection time on the precision of isotope ratio measurements are investigated thoroughly. The best combination of the two is found to be 9.0 and 45 seconds respectively.

---

[1] Corresponding author

Key words: Inductively coupled plasma mass spectrometry, twin-quadrupole mass spectrometer, ion beam splitter, signal improvement, isotope ratio.

INTRODUCTION

Since the original design and construction by Warren and co-workers in 1992 [1], the inductively coupled plasma twin quadrupole mass spectrometer (ICP-TQMS) has been used for precise elemental isotope ratio measurements of solution and solid samples [2-5].

The driving force for the development of this ICP-TQMS device is to provide a true simultaneous isotope ratio measurement by splitting the extracted ion beam into two parts prior to entering the two quadrupole mass analyzers. The component responsible for this splitting action is known as the ion beam splitter. This device is simply two toroidal electrostatic analyzers back to back [1]. Simultaneous measurement of two isotopes provides the advantage of canceling most, if not all, of the flicker noise from the ICP and the sample introduction system. Thus, when the ratio of the count rate of the two isotopes is calculated, the precision (relative standard deviation RSD%) is improved.

We have completed a long-term study using lithium (first ionization potential (IE) = 5.39 eV) with natural abundance ratio of ^{6}Li / ^{7}Li < 0.080, and carbon (IE = 11.26 eV) with natural abundance ratio of ^{13}C : ^{12}C = 0.011 [6, 7] to assess the reproducibly and feasibility of the ICP-TQMS device in precise isotope ratio measurements operating in a variety of conditions [8]. Over the five month interval, the ICP-TQMS had performed a total of 391 isotope ratio measurements of lithium and carbon (^{6}Li : ^{7}Li, ^{7}Li : ^{7}Li, ^{13}C : ^{12}C, ^{12}C : ^{12}C). The quotient of the precision of ratio measurement to the precision expected from counting

statistics (RSD% / CST%) is used to elucidate the overall performance characteristics of ICP-TQMS device. Most of the results have been previously described [5]. In short, ~ 80 out of 100 times, the precision (RSD%) of the isotope ratio measurement is within 2 times the precision expected from counting statistics. Approximately 40 out of 100 times, the precision is as good as that expected from counting statistics. This is by far the best benefit a twin quadrupole can provide over a single quadrupole instrument when very large or very small isotope ratio is measured.

Other attractive features include the ability to enhance the signal of minor isotope artificially either by increasing the detector voltage that detects the minor isotope, or by shifting the beam splitter offset from the central axis [5]. This unique ability is attributed to the twin quadrupole utilizing two detectors for ion detection whereas a single quadrupole operating on only one detector at a time. This is particularly useful when the count rates of two measured isotopes differ substantially. Offsetting the ion beam splitter ensures both detectors are operating within their linear dynamic range.

Despite the advantages offered by the ICP-TQMS, our home-built instrument does suffer from low sensitivity. Several causes have been identified. One of which is the ICP-TQMS is a home-built instrument which was constructed solely for research. The machining precision is hardly comparable to the commercial instrument. As expected, a commercial ICP-MS is usually much more sensitive than a home-built device. Furthermore, constructing a chamber which houses two quadrupoles requires even more precision than constructing a chamber for just one quadrupole. Another cause of low sensitivity is believed to be from the ion beam splitter itself. Splitting the ion beam into 2 parts means only 50% of the original beam are transmitted through each channel under ideal conditions. In practice, ions are

probably lost at the entrance to splitter and elsewhere. We believe that the current geometry of the splitter is responsible for the major loss of ions which were successful in making their ways through the beam shift plates but unsuccessful in transmitting through the splitter. This is evidenced by the marks left on each side of the wall of the central electrode. Further more, the splitter is actually a twin electrostatic analyzer (ESA), or a kinetic energy selector, which could contribute to some loss of ions during transmission. Ions extracted through skimmer are believed to have a kinetic energy spread from 2 to 10 eV [9-11]. Therefore, not all ions are transmitted through the ESA at any given electric field strength generated by the applied voltages to the ESA. Finally, the main factor that influences the sensitivity of an ICP-MS instrument comes from the ICP-MS interface, irregardless of whether it is a commercial or a home-built unit. The ICP-MS interface plays a major role in ion collection efficiency. In contrast to the outstanding ionization efficiency provided by the ICP, the ion extraction efficiency is radically poor. For every one million ions which are produced in the ICP, only a few ions successfully survive to the detector, resulting the overall ion collection efficiency approaches to ~ 5 x 10^{-6} [12]. In other words, the chance for an individual ion that created in the ICP but being detected is extremely low. The odds are therefore virtually the same as if the author wishes to win the lottery. Without the advanced development of the electron multiplier with gigantic detector gain (10^{8}), fast trace element concentration determination using ICP-MS would be difficult if not impossible. The low ion collection efficiency associated with the extraction process is mainly attributed to the substantial pressure difference from where the ions are made (760 Torr) to where the ions are detected (10^{-5} Torr). The major loss of ions at the ICP-MS interface during the ion extraction processes is at least caused by first, the rarefaction of the beam as it travels downstream from the

skimmer tip, and second, the space charge effects [13-24]. We have recently improved the ion extraction interface and the ion lenses arrangement behind the skimmer of our ICP-TQMS system for improving ion transmission, details of such results have been reported elsewhere [5].

This paper first describes a new design of a second-generation ion beam splitter for the ICP-TQMS instrument, then presents the initial test results of 5-fold signal improvement by simply cutting back and rounding of the razor like edge of the central electrode of the current splitter while maintaining the performance characteristics of the ICP-TQMS device. Finally, this paper presents the first detailed comprehensive results from thorough investigations of the effects of dwell time and total ion collection time as well as their influences on the precision of isotope ratio measurements of the ICP-TQMS system.

EXPERIMENTAL

Instrumentation

The ICP-TQMS system used in the present work has been described previously [1]. The second-generation ion beam splitter was designed by the authors. The current splitter was modified by the Ames Laboratory Machine Shop (Ames, Iowa, U.S.A.). The instrumental components and general operating conditions of the device are listed in Table 1 and Table 2 respectively. A CETAC U-5000 ultrasonic nebulizer (USN) with desolvating system and condenser was supplied by CETAC Technologies (Omaha, Nebraska, U.S.A.), and was used for generating aerosols from solution samples. The water circulator with cooling mechanism connected to the USN was also supplied by CETAC Technologies. The

peristaltic pump used to pump solution samples to the USN was provided by Rainin Instrument (Woburn, Massachusetts, U.S.A.). An oscilloscope, Model 2221A used to monitor the background noise amplitude of the ICP-TQMS was obtained from Tektronix (Beaverton, Oregon, U.S.A.).

Materials and reagents

Double layer tubing (formulation SE 200) composed of Tygon on the exterior wall and thin Teflon in the interior wall was used for the transit of dried aerosols from the USN to the ICP torch, and was purchased from Norton Performance Plastic (Akron, Ohio, U.S.A.). A Millipore Laboratory Water System (Bedford, Massachusetts, U.S.A.) furnished the laboratory with a milli-Q low organics pyrogen-free system, consisting of one super-C carboncartridge, two ion-exchange cartridges; two organex-Q cartridges, which supplied 18 $M\Omega$ de-ionized water (H_2O). Standard stock and working solutions were stored in 15-mL or 50-mL polypropylene tubes that were provided by Fisher Scientific (Pittsburgh, Pennsylvania, U.S.A.).

Argon gas with 99.996% purity was supplied by Air Products (Des Moines, Iowa, U.S.A.). Ultrex II ultra-pure concentrated nitric acid was purchased from J. T. Baker (Phillipsburg, New Jersey, U.S.A.). Copper and cobalt working solutions were diluted from the stock 1000 ppm ICP standards, which were supplied by Spex CertiPrep (Metuchen, New Jersey, U.S.A.). All working solutions were prepared prior to use by diluting aliquots of the stock solutions with 0.7% HNO_3.

RESULTS AND DISCUSSION

Second generation ion beam splitter design

Goals

The new splitter is designed to alleviate the following problems with the old splitter [Figure 1]:

1. The high potential field generated in front of the sharp edge of the central electrode is one of the causes for poor ion transmission. Positive ions created in the plasma are extracted through the sampler and skimmer. Many ions are lost between this region. Some where behind the skimmer, the majority of ions are further lost by space charge effects, the remaining ions were then refocused by a series of ion lenses onto the central axis. Near the entrance of the splitter, the supposedly refocused ion beam is probably defocused again and deflected by the high potential field near the sharp edge. The deflected ions are either lost to space or immediately strike the wall. Some ions will struggle through the entrance of the ESA and eventually make their way to the quadrupoles. Others will soon be lost to the wall shortly after entering the ESA because of too great an injection angle or by the reason that was discussed in the introduction section. The best way to improve signal is to minimize the loss of ions along their flight path.

2. Unwanted photons. With the current ICP-TQMS configuration, there is some light escaping from the plasma to the detectors causing a higher background on all masses than is anticipated, even though the inner surface of the three electrodes are coated with graphite.

Dimension

Our original plan was to design a new splitter, which consisted of two 30 degree ESA's such that the channels (flight path inside the two electrostatic analyzers) extend all the way to the quadrupole entrances to eliminate most of the ion lenses in these space [Figure 1 of Chapter 3]. However, the chamber that houses the two quadrupoles already has a defined shape and the distance from the exit of the ESA to the entrance of the quadrupole is quite large (> 9 cm). Therefore the intended design would cause the ions to be injected to the quadrupoles at an angle, and would make the precision worse. Constructing a whole new chamber can solve the problem; however, this requires substantial investments. Therefore, we keep the dimension and shape of the new splitter the same as the original one [1].

Features

Figure 2 shows a three-dimensional drawing of the second-generation ion beam splitter. There are five distinct modifications over the current splitter.

1. The three electrodes of the new splitter have hollowed bodies, instead of solid stainless steel blocks. The four toroidal inner surfaces of the three electrodes of the old splitter are replaced with four planar surfaces that are made of stainless steel mesh (not shown in the drawing). Each steel mesh is positioned by four beveled support screen flashings. This is analogous to glass supported within a picture frame. The flashing design facilitates the task of testing different meshes. The grid of meshes accomplishes two jobs at once. The grid of the meshes is chosen to be small enough to form a relatively uniform

electric field across the area between the central and side electrode for transmitting ions while the porous structure of the meshes allows stray light to escape out of the splitter.

2. The central electrode of the new splitter is recessed several centimeters from the front entrance, and the frontal edge is round rather than razor like. The front parts of the left and right electrode serve as beam shift plates, and the back part of the electrode is part of the ESA. The ion beam is split gradually in this design instead of abruptly in the older design.

3. The central electrode actually consists of two half electrodes called the central left and central right electrode. In the older design, the central electrode consisted of one piece. Usually, the voltage of the central electrode is kept constant while changing the voltage of the left and right electrodes to obtain different electric field strengths for each channel. In contrast to the original design, the new design has the voltage of the left and right electrode set equally while changing the central left and central right electrode to alter the electric field strengths within each ESA.

4. The new design has three top plates in comparison with the older design, which has only one plate. This design allows the ion beam to be deflected upward or downward independently before and after the beam is split as well as from the left and right channels.

5. An additional ion lens is placed in front of the entrance of the splitter to keep the ion beam in focus.

Modified ion beam splitter

To evaluate the idea of having the central electrode receded as seen from Figure 3, we modified the current beam splitter by cutting the central electrode 9.5 mm back from the

frontal plane and rounding off the sharp edge as shown in Figure 3. Signal enhancement is obtained by comparing the total count rate monitored at m/z 40 (Ar^+), and 41 (ArH^+) on both channels A and B during a continuous nebulization of a 0.7% HNO_3 solution at a 1 mL / min flow rate before and after modifying the beam splitter. In addition, we also compared the Cu signal before and after the splitter was cut using a 1 ppm Cu / 0.7%HNO_3 solution at the same liquid flow rate. Other general ICP-TQMS operating conditions are listed in Table 2.

Signal improvement

Table 3 summarizes the results obtained from using the modified ion beam splitter. Comparing the count rate obtained from 11-4-98 (right before the splitter was modified) and 1-14-99 (right after the splitter was modified), there is an approximately 4-fold signal enhancement measuring at m/z 40 (Ar^+), and ~ 5-fold signal improvement measuring at m/z = 41 (ArH^+). The signal enhancement is attributed to two factors. First, the razor like sharp frontal edge is no longer present. The rounder edge does not generate as intense potential field as the sharp edge, causing fewer ions to be deflected before they are split Thus more ions are transmitted through the ESA. Second, the ion beam is split less abruptly when the central electrode is receded from the front. Even receding the edge as little as 9.5 mm makes a significant improvement for ion transmission. If we were to compare the count rates of $^{63}Cu^+$ and $^{65}Cu^+$ measured on 2-3-99 (shortly after the splitter was modified) with the count rates measured 18 months before (5-20-97) using the same sampler, skimmer, and detectors (without correcting for aging), we still observe more than a 2-fold signal enhancement.

Isotope ratio measurements

This experiment is to demonstrate that the modified ion beam splitter provides equally precise isotope ratio measurements as the original splitter. All precision (relative standard deviation in percent, RSD%) from isotope ratio measurements are to be compared with the theoretical precision obtained at the shot noise limiting case (CST%). The method of calculating the RSD% of isotope ratio measurement at counting statistics has been described in reference 1. In short, the counting statistics RSD% of the ratio depends mainly on the total count of the less abundant isotope, and the total count is equal to the count rate multiplied by dwell time. Each ratio measurement listed in Table 4 is an average of 30 data points, and the dwell time for each point is 1.5 seconds. Therefore, the total data collection time per each ratio measurement is 45 seconds.

The split ratio of the ICP-TQMS system is optimized approximately to unity for isotope ratio measurements of $^{40}Ar^+ : ^{40}Ar^+$ and $^{41}ArH^+ : ^{41}ArH^+$, meaning the ion beam is split nearly equally to each channel as seen from the results listed in Table 4. The measured ratios for $^{40}Ar^+ : ^{40}Ar^+$ and $^{41}ArH^+ : ^{41}ArH^+$ are 1.2615 and 1.2599. These values are essentially the same and the measured RSD%'s are 0.25% and 1.36% for $^{40}Ar^+ : ^{40}Ar^+$ and $^{41}ArH^+ : ^{41}ArH^+$ respectively, which are very close to the RSD% expected from counting statistics (0.19% and 1.16%) in both cases.

One unique feature of this ICP-TQMS device is that both channels A and B need not be approximately the same count rate during isotope ratio measurement to obtain good RSD%. This is illustrated with the copper isotope ratio measurements. The results are summarized in Table 4. At first, we optimized the split ratio of the ICP-TQMS system to approximately 3 to

1, meaning 75% of the beam is sent through channel A, and 25% of the beam is sent through channel B. Both channels are monitoring at m/z = 63 simultaneously. The measured ^{63}Cu : ^{63}Cu ratio is 3.3383 with an RSD% of 0.39%. This is very close to the counting statistics RSD% (0.33%). Later, without changing the ICP-TQMS operating conditions or changing any ion lenses voltages, quadrupole A is switched to m/z = 65 while quadrupole B is kept at m/z = 63. In this fashion, the measured ^{65}Cu : ^{63}Cu ratio is close to unity (0.9455) because their natural abundance ratio is 0.4451 [6, 7]. If the ion beam were split equally, the measured ^{65}Cu : ^{63}Cu would not be unity. In the past, we measured the ^{6}Li : ^{7}Li and ^{13}C : ^{12}C ratios with the original splitter operating at split ratio as great as 15 :1 and 58 : 1 [5]. The precision of such measurements is still as good as the precision obtained from counting statistics. We later challenged our ICP-TQMS device to measure an isotope ratio at a new split ratio of 132 : 1, causing the split beam to be extremely asymmetric as shown in Figure 4. Under this circumstance, the measured ^{63}Cu : ^{63}Cu ratio is 132.11 with RSD% of 1.15%, which is essentially the same as the counting statistics RSD% (1.27%). The success of such performance is attributed to both ion signals being measured simultaneously with two detectors, and most of the flicker noise is cancelled out by taking the ratio of the two signals.

Effect of dwell time on precision during isotope ratio measurements

Whether the ICP-MS is a single quadrupole or double quadrupole instrument, the detector dwell time and total ion collection time have profound influences on the precision of isotope ratio measurements. The effect of dwell time and total ion collection time on the precision of isotope ratio measurement in our ICP-TQMS system was investigated

extensively. We utilized the readily available Ar^+ ions from the argon plasma with both quadrupoles at m/z 40 and the beam splitter operating at a split ratio ~ 2 to 1. The results are summarized in Table 5a. $^{40}Ar^+$: $^{40}Ar^+$ ratios are measured while varying the dwell time per measurement. Except for measurement number 5, each $^{40}Ar^+$: $^{40}Ar^+$ measurement is an average of 30 data points and the dwell time is either 1.5, 2.0. 3.0, or 5.0 seconds. The total data collection time for measurement 1 to 5 is therefore from 45 to 180 seconds. When the dwell time and total ion collection time increases, the measured RSD% decreases from 0.28% (measurement number 1) to a minimum of 0.20% (measurement number 3) then increases again to 0.34% (measurement number 5). Statistical calculations utilizing the F-test at 95% confidence level for comparing the measured RSD% of 0.28% and 0.20% indicate that there is a difference in precision between the two methods. However, if we perform the same F-test for comparing their measured RSD% to the counting statistic RSD% (CST%) ratios, there is no significant difference between 1.4 and 1.5 statistically. On the contrary, the measured RSD% of measurement 3 and 4 (0.20% and 0.23%) poses no significant difference statistically but their measured RSD% to CST% ratios (1.5 and 2.3) are now showing significant difference using the same statistical test. This is because the counting statistics RSD% always decreases as the dwell time increases. What appears to be more precise (smaller measured RSD% value) at first glance is not necessarily "more precise" with respect to the precision obtained at the shot noise limiting case (CST%). This is even more obvious if we compare the methods of measurement 1 and 5. The precision of the former case appears to be only 1.2 (0.34 / 0.28) times worse than the later case, in fact, statistically, there is no significant difference between the precision of these two methods. But, if we compare their measured RSD% to the CST% ratios, the precision of measurement

number 5 is now at least 3 times (4.4 / 1.4) worse than the precision of measurement number 1, and statistically, there is a significant difference between these two methods even at the 99% confidence level. All other comparisons are summarized in Table 5a and 5b.

To gain a deeper understanding of the relationship between dwell time and total ion collection time of our ICP-TQMS system, we measured the $^{40}Ar^+$ count rates on both quadrupoles with dwell time of 1.5, 2.0, 3.0, 5.0 and 9.0 seconds per data point with varying total ion collection times. The measured RSD% of the $^{40}Ar^+$: $^{40}Ar^+$ isotope ratio measurements are compared with the counting statistics RSD% obtained from each individual case. The reciprocal measured RSD% for all cases is plotted in Figure 5 as a function of the total ion collection time. In all cases, the precision is poorer as the total ion collection time increases. The best-measured RSD% for all five different dwell times happens at the shortest total ion collection time, which is 45 seconds in the present study. Up to the total ion collection time of 110 seconds, the precision decreases as the dwell time per data point decreases at any given total ion collection time. Beyond 110 seconds, the precision for all dwell times still decreases but no longer follows the same trend. Except for dwell time of 1.5 seconds which is distinctively poorer than other dwell times, there is no significant difference in the measured RSD% for dwell times of 2.0, 3.0 5.0 and 9.0 seconds at any given total ion collection time. At the total ion collection time of 45 seconds there is a clear advantage of dwelling a data point for 9 seconds as seen from Figure 6. The measured RSD% is at least 3 times better than dwelling the data point for just 1.5 seconds.

In fact, the measured RSD% should always be compared with the counting statistics RSD% (CST%). Figure 6 is a plot of the ratios of CST% / RSD% for all dwell times as a function of total ion collection time. In general, the CST% / RSD% decreases as the total ion

collection time increases. Except for the dwell time of 9.0 seconds, the order of decreasing CST%/RSD% at a given total ion collection time is 2.0 > 3.0 > 5.0 > 1.5 seconds which does not follow the same order as depicted in Figure 6 for total ion collection time up to 110 seconds. At dwell time of 9.0 seconds, the CST% / RSD% ratio falls sharply beyond the total ion collection time of 90 seconds, and the 9.0s line intersects all other lines quickly. When the total ion collection time increases to ~ 130 seconds, the 9.0s line shows the poorest precision of all with respect to the counting statistics RSD%. Details of the statistical comparison of all dwell times at a given total ion collection time at 45 seconds and 150 seconds from Figure 6 and 7 are summarized in Table 6a, 6b, and Table 7a, 7b respectively. Again, in many cases, what appears to be significantly different when comparing the measured RSD% values turns out to be insignificant if comparing the CST% / RSD% ratios and vice versa using the statistical F-test at a 95% confidence level.

The general conclusion from this section is that keeping the total ion collection time low, preferably no longer than 50 seconds can enhance the precision in both ion signals and isotope ratio measurements as long as the dwell time per data point is longer than 1.5 seconds.

Effect of power sources on the precision of isotope ratio measurements

We have demonstrated in several papers (including this one) that simultaneous measurements of two ion signals with two quadrupole mass spectrometers can cancel most of the flicker noise when the ratio is taken. However, can the precision be further improved if the two quadrupole mass spectrometers and two detectors were supplied by the same power

source? In the following experiment, a high voltage divider is used to divide the power output from a single power supply to the two detectors mounted behind the two quadrupole mass spectrometers. Three different dwell times (2.0, 5.0 and 9.5 seconds) and two different total ion collection times (60 and 200 seconds) were investigated with the two detectors powered by two sources or by just one source. The experimental results are summarized in Table 8. Irregardless of what the total ion collection time is, short (60s) or long (200s), using the same power source improves precision most noticeably with low dwell times (2.0s). The measured RSD% improves nearly 2 times (from 1.53% to 0.82%) at a total ion collection time of 200 seconds, and improves 1.5 times (from 0.89% to 0.59%) at a total ion collection time of 60 seconds. But for other dwell times (5.0 or 9.5s), irregardless of the total ion collection time, statistical F-test does not indicate that there is a significant difference in the measured RSD% using one power source or two power sources.

CONCLUSION

We have demonstrated several options to improve the performance of our ICP-TQMS. The modified ion beam splitter shows a ~ 5 times signal enhancement while maintaining the general performance characteristics of the device. The second-generation ion beam splitter once constructed would solve some of the current problems such as high background and low count rate and continue to improve the ion transmission efficiency. Lastly, reducing the total data collection time to no longer than 50 seconds would improve the precision of isotope ratio measurements.

ACKNOWLEDGMENT

REFERENCES

1. Warren, A. R.; Allen, L. A.; Pang, H. M.; Houk, R. S.; Janghorbani, M. *Appl. Spectrosc.* **1994**, *48*, 1360-1366.

2. Allen, L. A.; Pang, H. M; Warren, A. R.; Houk, R. S. *J. Anal. At. Spectrom.* **1995**, *10*, 267-271.

3. Allen, L. A.; Leach, J. J.; Pang, H. M.; Houk, R. S. *J. Anal. At. Spectrom.* **1997**, *12*, 171-176.

4. Leach, J. J.; Houk, R. S. *J. Anal. At. Spectrom* **1998**, submitted.

5. Luong, E. T.; Houk, R. S. *J. Am. Soc. Mass Spectrom.* **1999**, in process.

6. Bievre, P. D.; Barnes, I. L. *Int. J. Mass Spectrom. Ion Processes.* **1985**, *65*, 211-230.

7. Weast, R. C.; Astle, M. J. *CRC Hand Book of Chemistry and Physics*: CRC Press, Boca Raton, Florida, **1981-82**, F-192.

8. Luong, E. T.; Houk R. S. *Unpublished data.* **1998**.

9. Fulford, J. E.; Douglas, D. J. *Appl. Spectrosc.* **1986**, *40*, 971-974.

10. Tanner, S. D. *J. Anal. At. Spectrom.* **1993**, *8*, 891-897.

11. Montaser, A. (Ed.). *Inductively Couple Plasma Mass Spectrometry*: Wiley-VCH, New York, **1998**, Chapter 8.

12. Begley, I.; Sharp, B. L. *J. Anal. At. Spectrom.* **1994**, *9*, 171.

13. Gillson, G. R.; Douglas, D. J.; Fulford, J. E.; Halligan, K. W.; Tanner, S. D. *Anal. Chem.* **1988**, *60*, 1472.

14. Tanner, S. D. *Spectrochim. Acta, Part B* **1992**, *47*, 809.

15. Tanner, S. D.; Cousins, L. M.; Douglas, D. J. *Appl. Spectrosc.* **1994**, *48*, 1367.

16. Tanner, S. D.; Douglas, D. J.; French, J. B. *Appl. Spectrosc.* **1994**, *48*, 1373.

17. Hobbs, S. E.; Olesik, J. W. *Appl. Spectrosc.* **1991**, *45*, 1395.

18. Olivares, J. A.; Houk, R. S. *Anal. Chem.* **1985**, *57*, 2674-2679.

19. Niu, H.; Houk, R. S. *Spectrochim. Acta, Part B* **1996**, *51*, 779-815.

20. Li, G.; Duan, Y.; Hieftje, G. M. *J. Mass Spectrom.* **1995**, *30*, 841.

21. Chen, X.; Houk, R. S. *Spectrochim. Acta, Part B* **1996**, *516*, 41.

22. Nagy, G. A.; Szilagyi, M. *Introduction to the Theory of Space-Charge Optics*: Halsted Press, New York, Macmillan and London, **1974**.

23. Szilagyi, M. *Electron and Ion Optics*: Plenum Press, New York, **1988**, p 313.

24. Humphries, S. *Charged Particle Beams*: John Wiley & Son, New York, **1990**, p 834.

Table 1. Instrumental components of the ICP-TQMS

ICP	Plasma Therm generator
	(now RF Plasma Products)
	Model HFP-2000D
	RF Plasma Products torch box
	(modified in-house for horizontal operation
	with home-made copper shielding box)
Ion extraction	Ames Laboratory construction
interface	Sampler: 1.1 mm ID. Skimmer: 1.1 mm ID
Vacuum system*	Three stages differential pumping
	Welded stainless steel
	Ames Laboratory construction
Mass analyzers	VG Plasma Quad
	Model SPX 300 with RF-only pre-filters
	Model SPX 603 Controllers and RF Generators

Table 1. Instrumental components of the ICP-TQMS (cont.)

Detectors	ETP discrete dynodes
	Model AF 562A
Counting	EG & G ORTEC
electronics	Model 660 dual 5 kV bias supply
	Model 9302 amplifier / discriminator
	Model 994 dual counter / timer

*Details in reference 1

Table 2. ICP-TQMS general operating conditions

Radio frequency	27.12 MHz
Forward power	1.25 kW
Reflected power	< 5 W
Argon flow rate:	
Argon cooling gas	15 L / min
Aerosol gas	0.9 L / min
Auxiliary gas	1.1 L / min
CETAC U-5000 ultrasonic nebulizer:	
Desolvating system	140 °C
Condenser	4 °C
Solution uptake rate	1 mL / min
Differential pumping:	
First stage pressure	1.4 Torr
Second stage pressure	6×10^{-4} Torr
Third stage pressure	1.1×10^{-5} Torr
Data collecting and processing	See Text

Table 3. Comparison of ion collection efficiency between the original

and the modified ion beam splitter

	Total count rate ($\times 10^5$ cps)		Factor of improvement
	11-14-98	1-14-99	
$^{40}Ar^+$	8.5	33	3.9
$^{40}ArH^+$	0.66	3.3	5.0
	5-20-97	2-3-99	
$^{63}Cu^+$	2.4	5.5	2.3
$^{65}Cu^+$	1.0	2.3	2.3

Table 4. Isotope ratio measurements using the modified ion beam splitter

	Measured ratio	RSD%	CST%	RSD% / CST%
$^{40}Ar^+ : {}^{40}Ar^+$	1.2615	0.25	0.19	1.3
$^{40}Ar^1H^+ : {}^{40}Ar^1H^+$	1.2599	1.36	1.16	1.2
$^{63}Cu^+ : {}^{63}Cu^+$	3.3383[a]	0.39	0.33	1.2
$^{65}Cu^+ : {}^{63}Cu^+$	0.9455[a]	0.59	0.40	1.4
$^{63}Cu^+ : {}^{63}Cu^+$	132.11[b]	1.15	1.27	0.9
$^{65}Cu^+ : {}^{63}Cu^+$	37.157[b]	1.66	1.25	1.3

[a]split ratio – 3 : 1

[b]split ratio – 132 : 1

Table 5a. Effects of dwell time and total ion collection time on precision in isotope ratio measurements

Measurement	$^{40}Ar^+ : ^{40}Ar^+$	RSD%	CST%	RSD%/ CST%	dt (s)	Total (s)	pts
1	1.703	0.28	0.20	1.4	1.5	45	30
2	1.811	0.22	0.16	1.4	2.0	60	30
3	1.762	0.20	0.13	1.5	3.0	90	30
4	1.743	0.23	0.10	2.3	5.0	150	30
5	1.721	0.34	0.077	4.4	9.0	180	20

RSD% = measured relative standard deviation in percent

CST% = relative standard deviation in percent calculated at shot noise limit (counting statistics)

RSD% / CST% = ratio of measured RSD% to counting statistics RSD%

dt = dwell time per data point in seconds

Total = total ion collection time in seconds

pts = number of data point collected per measurement

Table 5b. Statistical results from F-test for the precision listed in Table 5a

	1.4	1.4	1.5	2.3	4.4	RSD/CST
0.28		n	n	yY	yY	1.4
0.22	n		n	yY	yY	1.4
0.20	yN	n		yN	yY	1.5
0.23	n	n	n		yY	2.3
0.34	n	yN	yY	yN		4.4
RSD%	0.28	0.22	0.20	0.23	0.34	

n or N = there is no significant difference in precision between the two methods

y or Y = there is significant difference in precision between the two methods

Small letter (n or y) = F-test at 95% confidence level

Capital letter (N or Y) = F-test at 99% confidence level

Table 6a. Effects of dwell time on precision in isotope ratio measurements with fixed total ion collection time at 45 seconds

Dwell time (s)	$^{40}Ar^+ : {}^{40}Ar^+$	RSD%	CST%	RSD%/CST%	pts
1.5	1.703	0.28	0.19	1.4	30
2.0	1.810	0.19	0.16	1.2	22
3.0	1.761	0.15	0.13	1.2	15
5.0	1.741	0.14	0.10	1.4	9
9.0	1.725	0.086	0.077	1.1	5

Table 6b. Statistical results from F-test for the precision listed in Table 6a

	1.4	1.2	1.2	1.4	1.1	RSD/CST
0.28		n	n	n	n	1.4
0.19	yN		n	n	n	1.2
0.15	yY	n		n	n	1.2
0.14	yN	n	n		n	1.4
0.086	yN	n	n	n		1.1
RSD%	0.28	0.19	0.15	0.14	0.086	

Table 7a. Effects of dwell time on precision in isotope ratio measurements with fixed total ion collection time at 150 seconds

Dwell time (s)	$^{40}Ar^+ : ^{40}Ar^+$	RSD%	CST%	RSD/ CST	pts
1.5	1.701	0.52	0.20	2.6	100
2.0	1.809	0.26	0.16	1.6	75
3.0	1.770	0.27	0.13	2.1	50
5.0	1.743	0.23	0.10	2.3	30
9.0	1.722	0.32	0.077	4.2	17

Table 7b. Statistical results from F-test for the precision listed in Table 7a

	2.6	1.6	2.1	2.3	4.2	RSD/CST
0.52		yY	n	n	yY	2.6
0.26	yY		yN	yN	yY	1.6
0.27	yY	n		n	yY	2.1
0.23	yY	n	n		yY	2.3
0.32	yN	n	n	n		4.2
RSD%	0.52	0.26	0.27	0.23	0.32	

Table 8. Effects of power sources on the precision of isotope ratio measurements

Total (s)	Power source	dt (s)	$^{40}Ar^+:^{40}Ar^+$	RSD%	CST%	RSD/CST
60 s	Two	2	4.40	0.89 [a]	0.24	3.7 [aa]
		5	4.29	0.44 [b]	0.16	2.8 [bb]
		9.5	4.31	0.44 [c]	0.11	4.0 [cc]
	One	2	8.20	0.59 [a']	0.28	2.1 [aa']
		5	8.31	0.42 [b']	0.18	2.3 [bb']
		9.5	8.29	0.24 [c']	0.13	1.8 [cc']
200 s	Two	2	4.39	1.53 [d]	0.24	6.4 [dd]
		5	4.29	0.72 [e]	0.16	4.5 [ee]
		9.5	4.30	0.82 [f]	0.11	7.3 [ff]
	One	2	8.21	0.82 [d']	0.28	2.9 [dd']
		5	8.33	0.81 [e']	0.18	4.5 [ee']
		9.5	8.33	0.87 [f']	0.13	6.7 [ff']

b and b', c and c', bb and bb', cc and cc', e and e', f and f', ee and ee', and ff and ff' show no significance differences between the two methods from F-test at 95% confidence level.

a and a', and aa and aa' show significant differences between the two methods from F-test at 95% confidence level, but show no significant difference at the 99% confidence level.

d and d', and dd and dd' show significant differences between the two methods from F-test at both 95% and 99% confidence level.
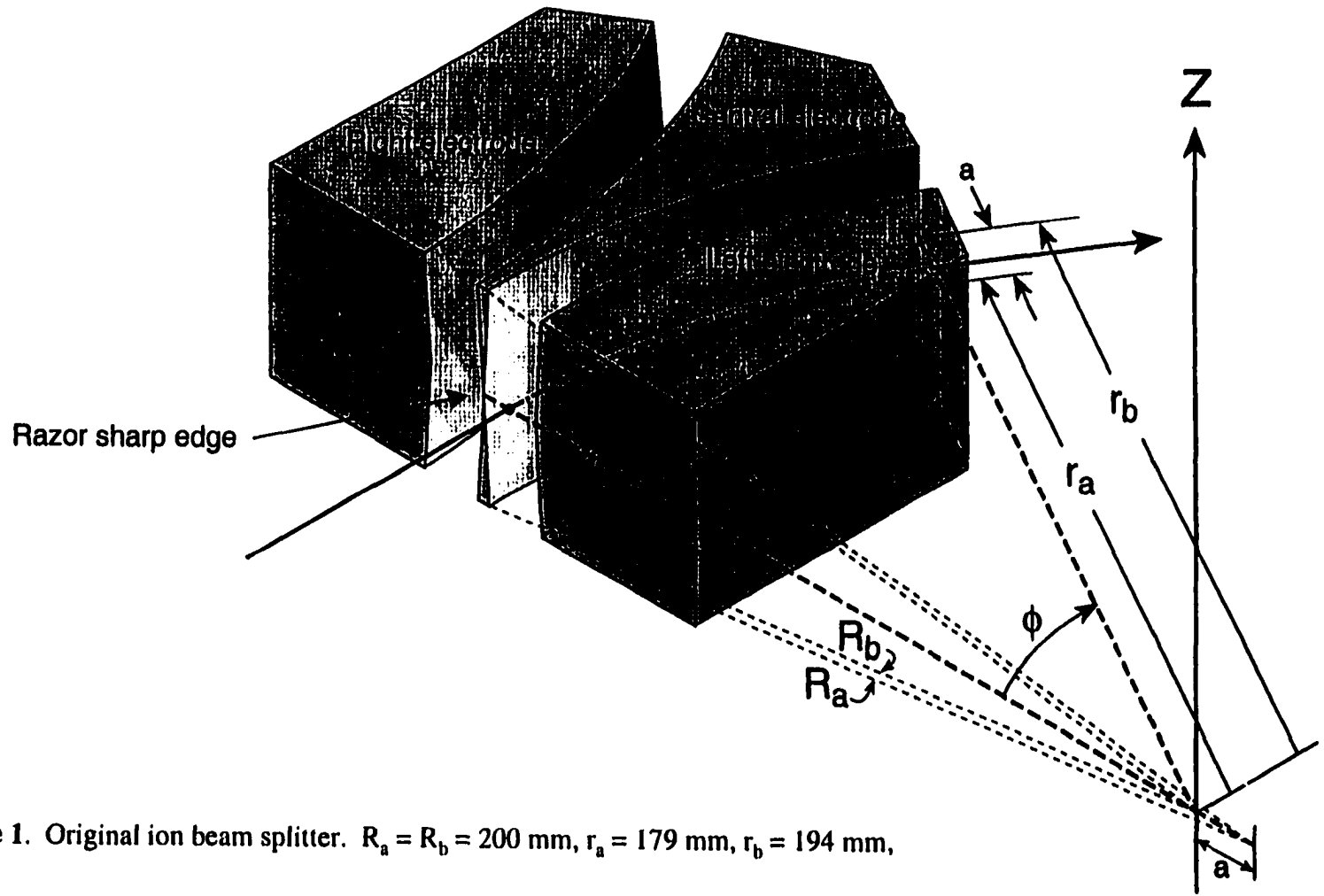
Figure 1. Original ion beam splitter. $R_a = R_b = 200$ mm, $r_a = 179$ mm, $r_b = 194$ mm, $a = 15$ mm, $\phi = 30°$ [1].
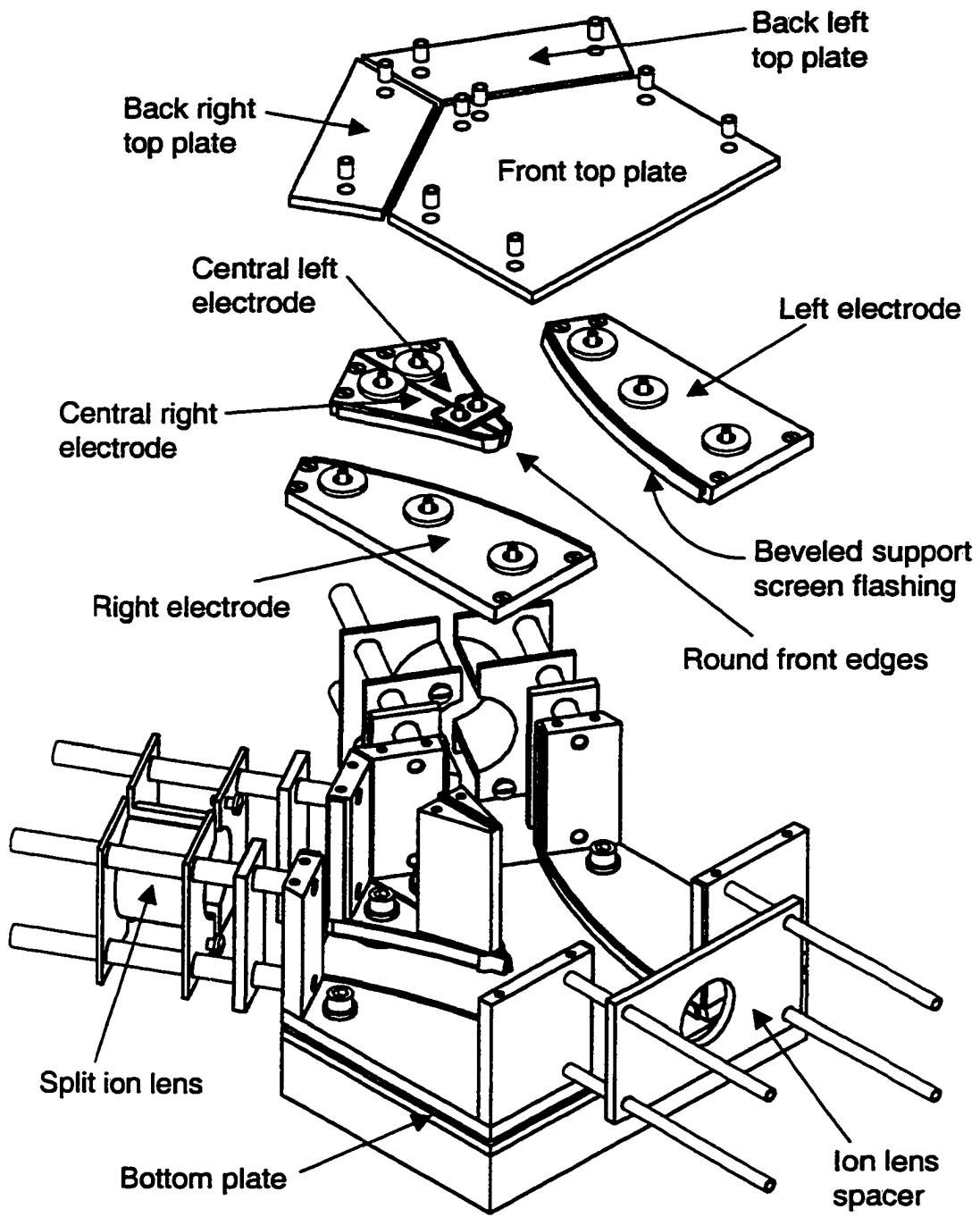
Figure 2. A design of the second-generation ion beam splitter.
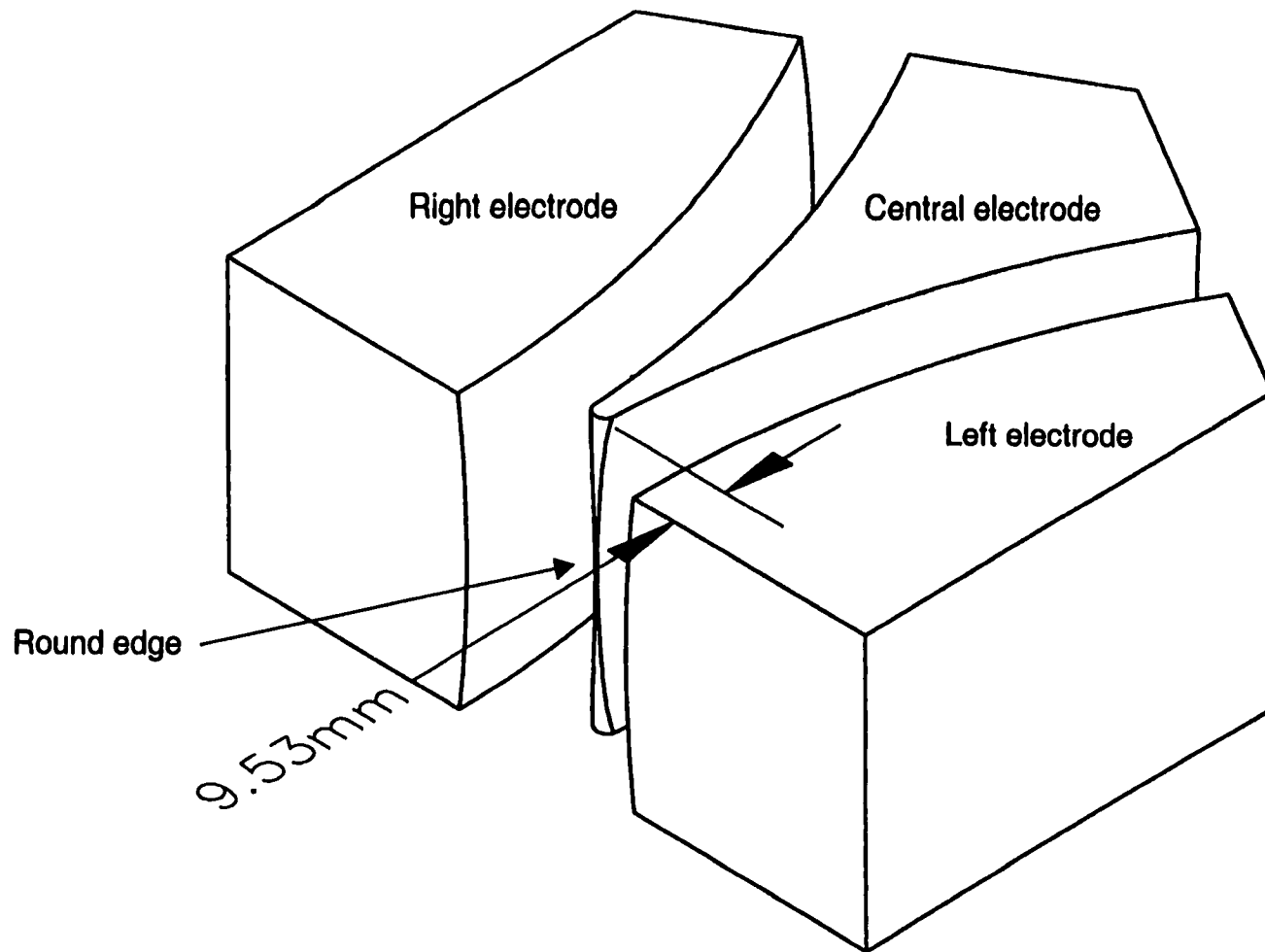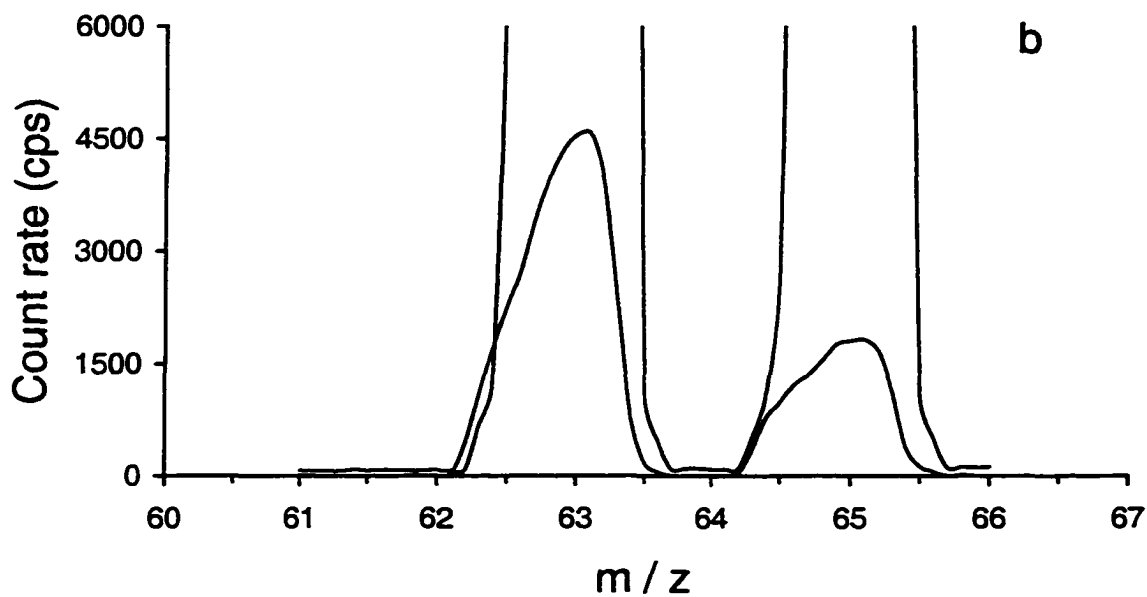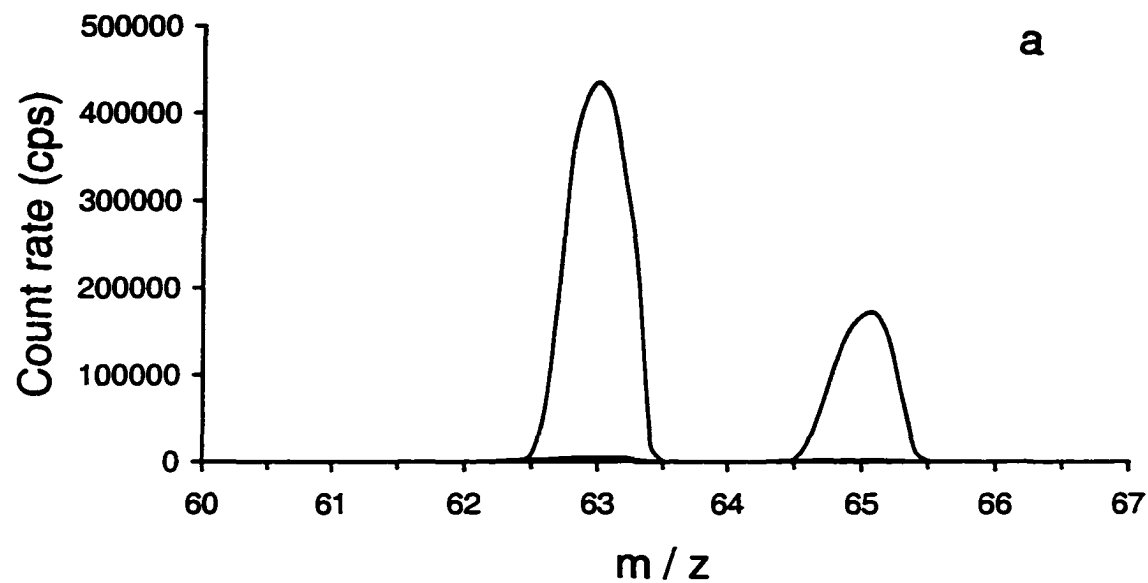
Figure 3. Modified ion beam splitter.

Figure 4. Low resolution mass spectra of copper showing two stable isotopes

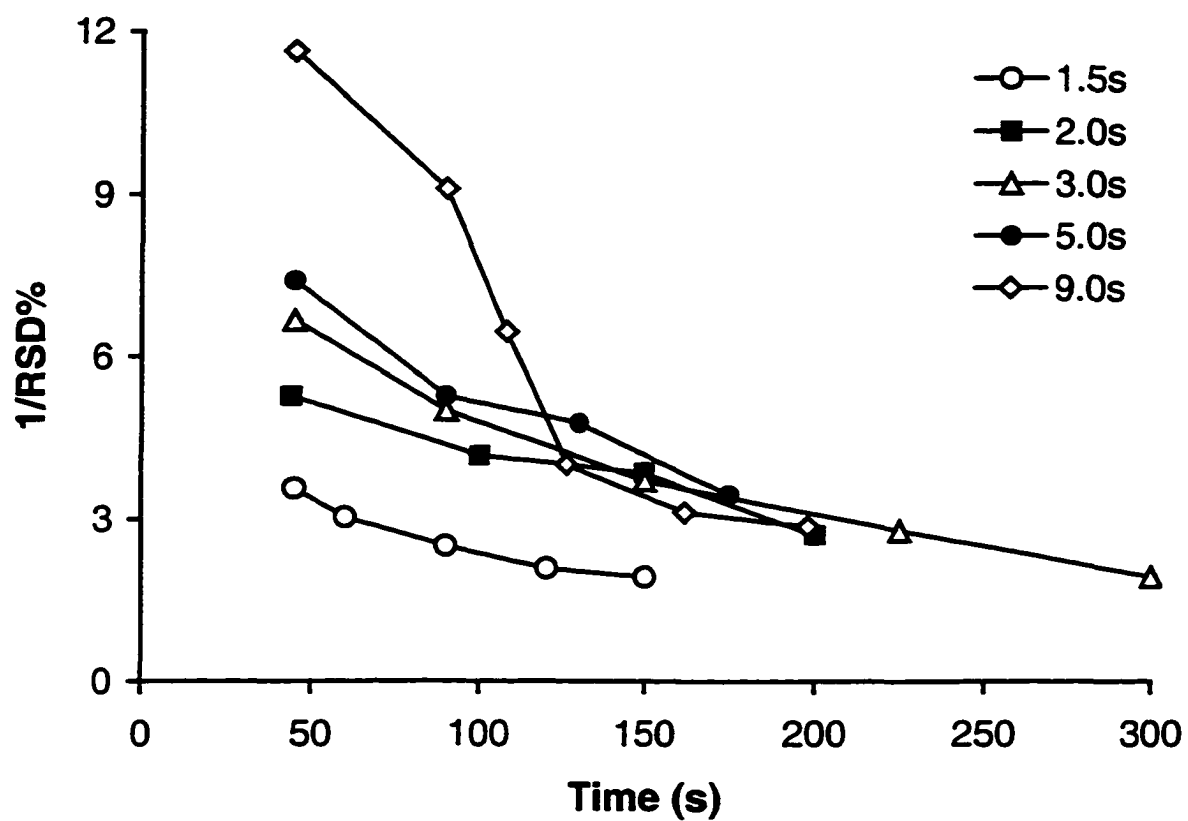^{63}Cu and ^{65}Cu. Split ratio ~ 132 : 1. a) Normal scale. b) Expanded scale.

Figure 5. Plot of reciprocal RSD% as a function of total ion collection time. The dwell time of each data point is 1.5. 2.0. 3.0. 5.0. or 9.0 seconds.
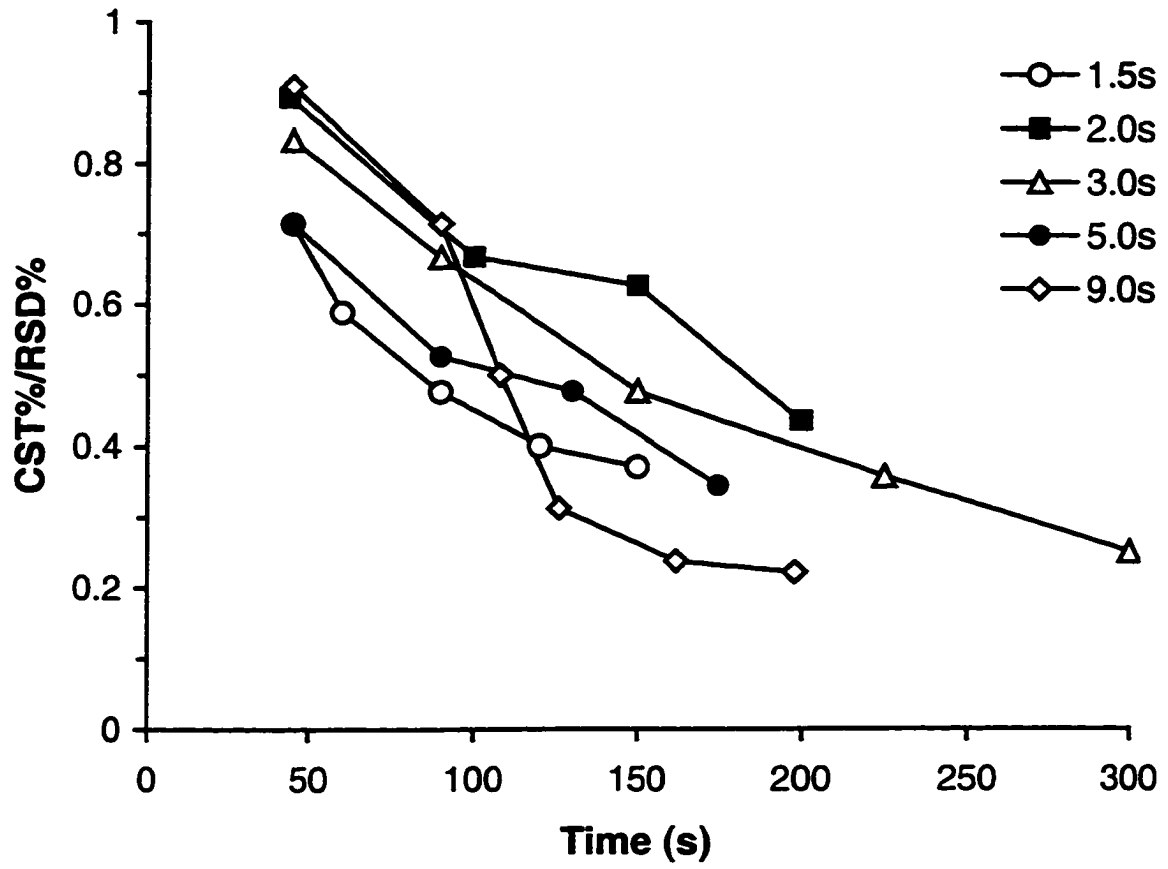
Figure 6. Plot of the ratio of precision expected from counting statistics to precision

of isotope ratio measurement (CST%/RSD%) as a function of total ion collection

time. The dwell time of each data point is 1.5, 2.0, 3.0, 5.0, or 9.0 seconds.

CHAPTER 5. GENERAL CONCLUSIONS

Methods for quantitative determination of ultra-trace level of molybdenum (Mo) in biological samples are limited because of the high solute content of matrices and the resultant spectral and non-spectral intereferences. Chromatographic isolation of Mo from the million-fold more concentrated sodium, chloride, sulfate, phosphate, etc. in aliquots of blood plasma is successfully accomplished using anion exchange microcolumns of alumina (made in house) with Mo uptake from 0.01 moles L^{-1} HNO_3 and elution with 3.75 moles L^{-1} NH_4OH. Sensitive and selective inductively coupled plasma mass spectrometry (ICP-MS) with isotope dilution is utilized for accurate ultra-trace concentration determination of Mo in the purified blood samples. This new level of detection and quantification has re-opened the door for many scientists in the field of biology, biochemistry, and clinical nutrition for their studies of molybdenum metabolism, functions, and distribution in plants, animals, and microorganisms.

Inductively coupled plasma with a twin quadrupole mass spectrometer (ICP-TQMS) has been demonstrated for high precision carbon isotope ratio measurements in amino acids, proteins, and carbohydrates. The ICP-TQMS system could also measure carbon ratio from gaseous or solid samples with proper sample introduction techniques. Carbon isotopic analysis is an important tool in geology [1], environmental science [2], biology [3], and medicine [4]. In biological and medical studies, analysis of isotopic ^{13}C / ^{12}C ratios enable the study of metabolic pathways in living systems. At present, either the radioactive tracer ^{14}C or stable ^{13}C isotope is used for such studies. The used of ^{13}C as a tracer for diagnostic purposes is a rapidly growing field [5]. Study using radioactive tracer is rapidly declined due to potentially harmful radiation effects and problems of radioactive waste disposal. In

geological studies, such as the sedimentation of carbonates, or in atmospheric studies, such as polar ice core and oceanic isotope ratio measurements, measuring $^{13}CO_2/$ $^{12}CO_2$ ratios enable the determination of the cycle of CO_2 production and absorption throughout history. In comparison with the current well-established gas chromatography combustion isotope ratio mass spectrometry (GC-combustion-IRMS) for determination of carbon isotope ratios from non-volatile organic compounds, the ICP-TQMS system is attractive for its speed in analyses, less severe memory effect, no isotopic fractionation, and no need for ^{17}O correction. The ICP twin quadrupole mass spectrometer utilizes two detectors for ion detection. This design greatly facilitates the task in simultaneous measurements of two isotopes or two ions with very large small or very large ratios (can be as great as 1 to 132).

The original ICP-TQMS interface design has been modified with a new skimmer interface. The combination of the new interface and the new arrangement of the ion optics result in a substantial improvement of signal to noise ratio. Further improvement of the system can be achieved with a new ion beam splitter design. Precision in isotope ratio measurement can further be improved by changing the dwell time and total ion collection time.

Overcoming instrumental drift and reaching for ultra-high precision in isotope ratio measurements with the current ICP-TQMS device continues to be a challenge. The greatest challenge is perhaps the utilization of as many ions as possible that are created in the ICP. This requires substantial modification of the ICP-MS instrument as a whole.

References

1. Quade, J. and Cerling, T. E. *Science.* **1990**, *250*, 1549.

2. Quay, P. D.; Tilbrook, B. and Wong, D. S. *Ibid.* **1992**, *256*, 74.

3. Chapman, T. E.; Berger, R.; Reijngoud, D. J. and Okken, A, Eds. *Stable isotopes in Paediatric Nutritional and Metabolic Research*, Ingercept Ltd., Andover, United Kingdom, **1991**.

4. Graham D. *Lancet i*, **1987**, 1174.

5. Krumbiegel P. *Stable Isotope Pharmaceuticals For Clinical Reseach and Diagnosis*, Fischer, Jena, Germany, **1991**.

.

ACKNOWLEDGEMENTS

I would like to thank my major professor, Dr. R. S. Houk whom I came to Iowa State University to study mass spectrometry with. I express deep appreciation for his support, guidance, knowledge, and assistance through out these years.

I would like to thank Drs. James S. Fritz, Patricia A. Thiel, Dennis C. Johnson, Mark S. Gordon, John G. Verkade, and Robert E. Serfass for being on my committee. I am grateful to Dr. Serfass for the joint research on the molybdenum project.

I would like to thank all of Dr. Houk's group members, both past and present. In particular, I would like to thank Xiaoshan Chen and Lloyd Allen for their helpful advice. I thank Zhiyang Du, Jin Wang, Towhid Hasan, Ma'an Amad, and Dave Aeschliman for assisting me in lifting heavy components. I would also like to thank Yan Zhai in our group, Liyu Yang and Jing Wei in Lee's group, Hongdong Tan in Yeung's group, Jei Li in Fritz's group, Douglas English, Kaustuv Das, and Kyle Ashby in Petrich's group, Dmitri Fedorov in Gordon's group, Yanhua Lu in Kraus' group, Janese O'Brien and Jing Ni in Porter's group, Joseph Burnett in the Department of Chemistry, Chengwei Wu and Yuexia Liang in the Center for Designing Foods to Improve Nutrition, and Di Wang in the Department of Physics for their kindness and eternal friendship. I wish Geoffrey Kent and Bing Guan, the two new group members well in their graduate studies.
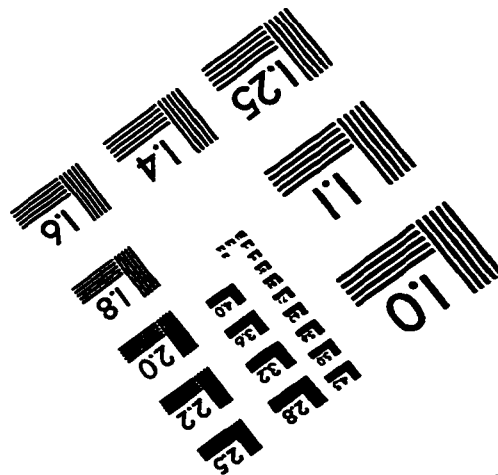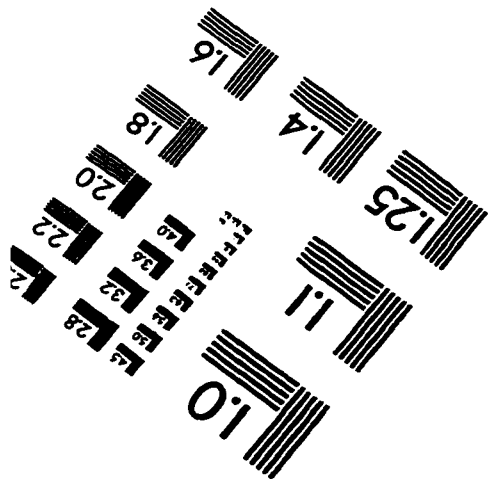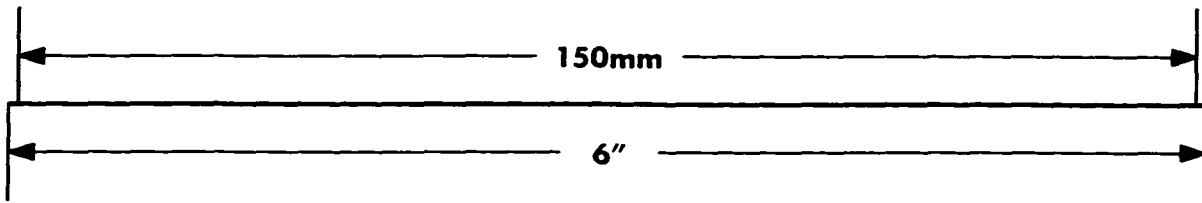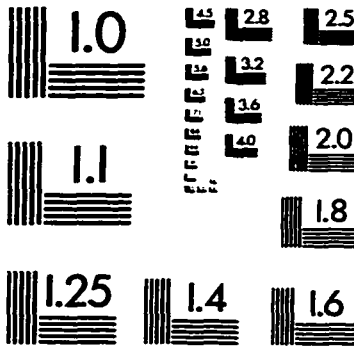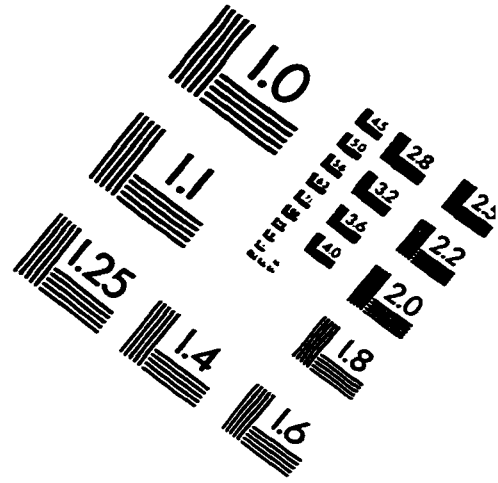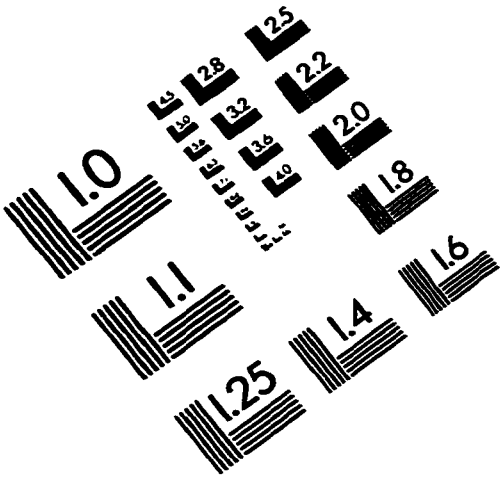
I certainly do not forget to thank all nurses and doctor, Jan Ahrens, Vickie Hahn, Karen Burk, Carol Mack, and Dr. Steven Sheldahl in the Ames Laboratory Occupational Medicine for keeping me healthy and happy.

Special thanks go to Maria Lukawski, the librarian who constantly assists me in finding reference materials.

I owe deep gratitude to my husband Alexandre Smirnov, and my parents Kieu Lu and Nhung Quoc Luong for their unconditional love and immense emotional support. I am also grateful to my brother Tri Quyen Luong, who traveled by bus all the way from Marietta Georgia to Ames Iowa to help me settle in my apartment five years ago.

IMAGE EVALUATION
TEST TARGET (QA-3)

150mm

6"